3D muscle architecture in the triceps surae muscle: 3D ultrasound methods and maps of fascicle orientation and curvature

by

Manku Rana

B.Sc., Panjab University, 2006

THESIS SUBMITTED IN PARTIAL FULFILLMENT
OF THE REQUIREMENTS FOR THE DEGREE OF
DOCTOR OF PHILOSOPHY

in the
Department of Biomedical Physiology and Kinesiology
Faculty of Science

SIMON FRASER UNIVERSITY

Spring 2012

Approval

Name: **Manku Rana**

Degree: **Doctor of Philosophy (Biomedical Physiology and Kinesiology)**

Title of Thesis: ***3D muscle architecture in the triceps surae muscle: 3D ultrasound methods and maps of fascicle orientation and curvature***

Examining Committee:

Chair: Will Couples, Professor

James Wakeling
Senior Supervisor
Associate Professor

Ghassan Hamarneh
Supervisor
Associate Professor

Max Donelan
Supervisor
Associate Professor

Nilima Nigam
Internal Examiner
Associate Professor
Department of Mathematics

Dinesh Pai
External Examiner
Professor, Department of Computer Science
University of British Columbia

Date Defended/Approved: March13, 2012

Partial Copyright Licence

SFU SIMON FRASER UNIVERSITY
THINKING OF THE WORLD

STATEMENT OF ETHICS APPROVAL

The author, whose name appears on the title page of this work, has obtained, for the research described in this work, either:

(a) Human research ethics approval from the Simon Fraser University Office of Research Ethics,

or

(b) Advance approval of the animal care protocol from the University Animal Care Committee of Simon Fraser University;

or has conducted the research

(c) as a co-investigator, collaborator or research assistant in a research project approved in advance,

or

(d) as a member of a course approved in advance for minimal risk human research, by the Office of Research Ethics.

A copy of the approval letter has been filed at the Theses Office of the University Library at the time of submission of this thesis or project.

The original application for approval and letter of approval are filed with the relevant offices. Inquiries may be directed to those authorities.

Simon Fraser University Library
Simon Fraser University
Burnaby, BC, Canada

Last update: Spring 2010

Abstract

Muscle fascicle architecture is an important parameter affecting the mechanical function of skeletal muscle. Most previous studies on fascicle architecture have been in 2D and the importance of 3rd dimension has not been much explored. The 3D orientation of the whole muscle may be regionalized in the muscle and can change with the contraction state of the muscle. Fascicles are arranged as sheets in muscles and the sheets' arrangement may change when the muscle bulges during contraction. With the muscle bulging, fascicle sheets may deform and affect the 3D fascicle orientations which will further influence the force generated by the muscle. In this thesis methods were developed and validated to study the in-vivo muscle fascicle architecture in 3D using B-mode ultrasound and optical tracking systems. Images were obtained from multiple scans of the muscles with scan times less than two minutes and analyzed for fascicle orientations, fascicle curvatures, fascicle sheet orientations and fascicle sheet curvatures. The 3D architecture information further was used to study the effect of ultrasound probe orientation and position on the measured 2D fascicle orientations. The orientation and curvature values of the fascicles and the fascicle sheets were quantified in the soleus and the gastrocnemii muscles in six male subjects for three torque levels (0%, 30% and 60% of MVC) and four ankle angles (-15°, 0°, 15° and 30° of planter flexion). The probe orientation and position was more critical in soleus than the gastrocnemii muscle due to more complex fascicle arrangement. Fascicle orientations and curvature values were regionalized across the muscles and changed with the change in ankle angle and relative torque level ($p<0.01$). The change in fascicle arrangement may be in response to the intramuscular pressure, and these changes can alter the mechanical output. The 3D information obtained in this thesis will be useful to understand the force generation of muscle and also to understand the change in muscle function with diseases affecting the muscle architecture.

Keywords: regionalization, torque, muscle length, intramuscular pressure

Acknowledgements

I would like to thank Dr. James Wakeling for believing in me and giving me the opportunity to work in his lab. His continual support, encouragement and patience to answer all the questions made my degree a complete learning experience. He was very encouraging towards the opportunities outside the lab, that gave me the exposure to learn beyond my project work. I would also like to thank him for the wonderful time I had while being a teaching assistant for his course and the coffee times spent in Nature's Garden.

I am very thankful to Dr. Ghasaan Hamarneh for being my co-supervisor and helping me to develop the computational methods in my thesis.

A special thanks to Dr. Sabrina Lee, Hadi Rahemi and Oliver Blake for the discussing the ideas, help with trouble shooting my problems and proof reading my work. Thanks to Hadi Rahemi for helping with my experimental set up, Avleen Randhawa for data collection and Ana Namburete and Taylor Dick for image digitisation.

Many thanks to Susie Nugent for her help in all these years, from applying to the program to arranging the defense day. She answered all the questions with a smile and helped to plan for deadlines in a timely fashion.

I feel fortunate to have met Dr. Parveen Bawa and work with her. I would like to thank her for introducing me to Dr. James Wakleing and giving me the basics in physiology after not studying it since grade 10.

Finally, I thank my family and friends for showing their love, support and patience over the last few years. My parents always inspired and encouraged me, without them I would not have made this far in life. Very thanks to my husband Ashish Dasaur who showed his love and support and patiently waited for me while I finished my thesis.

Table of Contents

List of Tables

List of Figures

List of Acronyms

α	Orientation of wavelet
β	Pennation angle
β	Arbitrary constant for multiscale vessel enhancement
β_c	Polar angle for normal to fascicle curve
β_{cf}	Pennation angle for fascicle projected in constant fascicle plane
β_f	Pennation angle for fascicle without any projection
β_{vf}	Pennation angle for fascicle projected in variable fascicle plane
c	Arbitrary constant for multiscale vessel enhancement
d	Damping factor
φ_c	Azimuthal angle for normal to fascicle curve
φ_{fsc}	Azimuthal angle for normal to fascicle sheet curve
φ_f	Azimuthal angle for fascicle orientation
φ_{fp}	Azimuthal angle for normal to fascicle plane

$G(x,y)$	Amplitude of wavelet at (x,y)
k	Half-width of wavelet
κ_c	Fascicle curvature
κ_{fsc}	Fascicle sheet curvature
L_f	Fascicle Length
L_t	Muscle thickness
λ	Wavelength for anisotropic wavelets
λ_1 and λ_2	Eigenvalues of hessian matrix for vesselness response
Δp	Pressure difference across a curved fascicle
P	Scale between pixels in ultrasound image to the actual distance
o	Offset for wavelets
Δr_f	Fascicle thickness
s	Scale for multiscale vesselness enhancement filtering
S	Frobenius norm of hessian matrix

σ	Spread of gaussian distribution
σ_f	Fascicle stress
θ	Orientation of grid for radon transform
$V(s)$	Vesselness response
w_c	Weight factor for convolution
w_d	Weight factor for distance from voxel center

1. Introduction

Muscle architecture is an important determinant of the mechanical function of muscle. Most of the in-vivo studies on muscle architecture have been done using 2D ultrasound imaging and not much work has been done on 3D architecture. In this thesis ultrasonography in used to study in-vivo muscle architecture in 3D and to study the importance of the third dimension.

1.1. Introduction to muscle architecture and mechanics

Muscles are the prime movers of the body and joint movements are determined by the action of the muscles crossing the joints (Powell et al., 1984; Wickiewicz et al., 1983). The mechanical function of muscle depends on its architectural parameters such as fascicle length, velocity, pennation angle and curvature. Muscle fascicles are bundles of muscle fibers, which are the muscle cells that can actively develop force. Along with their activation level, the force generated by muscle fibers depends on the fiber length and the velocity. The force generated by the fibers is sum of the force generated by sarcomeres active in parallel (active force) and the force generated by the passive components in those fibers. Passive forces increase with the increase in muscle length but the active force has a maximum at an optimal length and is reduced at lengths that are longer or shorter than optimal (Gordon et al., 1966). Along with the muscle fiber length, shortening velocity is an important parameter affecting the force generated by the fibers. Forces are the greatest for lengthening relative torques and the muscle absorbs work when it is stretched as opposed to generating work when it shortens (Flitney and Hirst, 1978). The force generated by muscles decreases at higher shortening velocities, decreasing to zero force at the maximum unloaded shortening velocity, which is an intrinsic property of the fiber (Hill, 1938). The force and the power diminish at very high shortening velocities of the fibers, and so it is important that the fiber shortening velocities do not approach the maximum unloaded shortening velocity.

In pennate muscles the fascicles are oriented at an angle (pennation angle) that is oblique to the line of action of the muscle are considered to generate greater force than fusiform muscle (fibers parallel to the line of action of muscle) because more fibers can be packed in the same volume of muscle (Alexander, 1968). Pennation angle is defined as the angle of line of action of muscle, however, because it is difficult to determine the line of action of muscle is measured with respect to the muscle aponeurosis (Fukunaga et al., 1997a; Maganaris et al., 1998b; Narici et al., 1996a). However, the increased force does not act along the line of action of the muscle and so only a component of the fiber force acts along the force generation axis of muscle (Azizi et al., 2008; Wakeling et al., 2011). An important property of pennate muscle is that the fascicles can rotate during muscle contraction. The fiber rotation uncouples the shortening velocity of muscle fibers from the shortening velocity of muscle belly (Wakeling et al., 2011). The ratio of the muscle belly shortening velocity to the muscle fiber shortening velocity is called muscle gearing. For fusiform muscle this ratio is 1. For pennate muscles, if the pennation angle were unable to change, this ratio would be less than one as the fibers will have to shorten more for a given shortening of the muscle belly. However, due to rotation of the fascicles, an increase in pennation actually occurs during relative torque and the fascicles shorten at a lower velocity than that of the muscle belly, resulting in a gearing ratio greater than 1 (Azizi et al., 2008; Wakeling et al., 2011). For very fast relative torques, muscle gearing can result in the fascicles maintaining relatively lower shortening velocities that facilitates high force and power production.

1.2. Regionalization of muscle properties

Regional variations in muscle activation patterns (English, 1984; Hoffer et al., 1987), fiber type (English and Letbetter, 1982; Wang and Kernell, 2000), fascicle strain (Ahn et al., 2003; Soman et al., 2005), work done by muscle (Higham et al., 2008) and fascicle orientation (Herring et al., 1979; Ritruechai et al., 2008) have been shown in different species. Regionalization of activation patterns and fiber type composition has a functional significance. Higham and co-workers (2008) showed a relation between the fiber recruitment and muscle stretch that was regionalized in the medial gastrocnemius of the guinea fowl. As muscle architecture is related to muscle function it is possible that the regionalization of muscle architecture also has functional significance. Regions of muscle having different neuronal control

(called neuromuscular compartments) are functionally important for different mechanical tasks. Regionalization of architecture in a muscle may facilitate these muscle compartments to perform different mechanical tasks.

Some muscles have complex architecture to achieve the desired muscle function. For instance, in the axial muscle of fish the fast and slow muscle fibers are anatomically separated with the slow fibers being parallel to the long axis of the fish and the fast fibers being curved (forming a partial helix) at an angle relative to the long axis of the body of the fish (Alexander, 1969). The complex fish muscle architecture maintains optimal strain rates for the fast and slow muscle fibers during different types of swimming behaviour in order for them to generate high power. Fast muscle fibers are activated during the startle response of the fish. The helical orientation of the fast muscle fibers allow them to shorten at lower strain rates than those that would have been required if they had the same orientation and position as the slow fibers, allowing the sarcomeres to shorten at their optimal velocity for generating high power (Rome et al., 1988). As another example, the regional variation of muscle fascicle orientation in pig masseter muscle has been shown to be correlated to the activation of the muscle segments during different phases of chewing. The timing of activation is managed so as to use the orientation properties of muscle fascicles to change the direction of pull by the muscle fascicles and hence obtain different force directions during different phases of the task (Herring et al., 1979).

In man, it has been shown that regional variations in activation occur in the gastrocnemii and soleus (Wakeling, 2009); the different compartments of these muscles are shown to be recruited differently based on the mechanical demand of the task performed. It is important to quantify the architectural properties in these regions and study the regional changes in architecture during muscle relative torques in order to understand the functional significance of the regional activations. Regional variations in the architecture of the rectus femoris, in the human quadriceps, have previously been shown using 2D ultrasound (Blazevich et al., 2006). This thesis describes novel in-vivo methods (explained in chapter 2 and chapter 3) to quantify the regionalization of muscle fascicle orientations in 3D (chapter 4).

1.3. Muscle fascicle curvature and fascicle plane deformation

Along with fascicle orientation, fascicle curvature is an important determinant of muscle architecture (Otten, 1988; van Leeuwen and Spoor, 1992). Curved fascicles have been considered to develop pressure on their concave side (Muramatsu et al., 2002; van Leeuwen and Spoor, 1992). For isometrically contracting muscles the pressure developed by the aponeurosis is balanced by the pressure developed by the curved fascicles for mechanical stability within the muscle model (Van Leeuwen and Spoor, 1992). The pressure developed in a muscle during relative torque depends on the curvature of the fascicles and increases with increase in fascicle curvature. Regional differences in intramuscular pressure exist (Sejersted et al., 1984) that may be reflected in regional changes in curvature.

Fascicle curvature results in longer fascicle lengths than linear fascicle lengths that would be estimated for a given pennation angle and muscle thickness. Differences in length of 6% have been reported between linear and curved estimates of muscle fascicles in 2D studies (Muramatsu et al., 2002). It is important to study the organization of fascicle curvature in muscle to understand its effect on muscle function and its use in muscle modelling. Fascicle curvature has been qualitatively (Fukunaga et al., 1997a; Kawakami et al., 1998; Maganaris et al., 1998c) described in previous studies. Muramatsu and co-workers (2002) have shown that fascicle curvature depends both on the relative torque state and the length of the medial gastrocnemius muscle. They found increased curvature in fascicles with maximum voluntary relative torque (MVC) when compared to resting muscle, and the curvature became larger with increased plantar flexion of the ankle. Savelberg and co-workers (2001) have shown from an in-situ preparation in rat muscles that during relative torques the fascicles do not just shorten along their longitudinal axis but are also displaced laterally. Asymmetrical displacement of fascicles results in helical deformations in the muscle fascicles. The 3D quantification of curvature has not been explored and the fascicles in human muscle may be curved in three dimensions, with non-planar changes in curvature occurring during relative torques.

Muscle bulging is an important factor affecting the muscle architecture and hence the muscle function. During relative torques the changes in muscle volume are very small (Baskin and Paolini, 1967) and so when a muscle belly shortens during relative torque, an increase in the

muscle cross-sectional area is expected to keep the volume changes minimal. The increase in cross-sectional area is achieved in the form of muscle bulging. Bulging along the fascicle plane results in a change in depth (Maganaris et al., 1998c), on the other hand a bulge can be perpendicular to the fascicle planes and instead would change the width of the muscle. The change in depth along the fascicle plane is related to the fascicle length, curvature and pennation angle which can alter the force generation by the muscle. Differential bulging of muscle in the two directions (depth and width) can result in different gearing ratios during muscle shortening and hence may facilitate the relative torque of muscle during different activities (Azizi et al, 2008). Maganaris and co-workers (1998 c) have shown a change in muscle depth in the lateral gastrocnemius and no change in the medial gastrocnemius during isometric relative torques. Depth change along the fascicle plane will result in a rotation of fascicles and a change in pennation angle, whereas bulging in the perpendicular direction may not affect the pennation angle, but can alter the alignment of fascicle planes in the muscle. In the previous 2D ultrasound studies, muscle fascicles are assumed to be arranged in planes (Benard et al., 2009; Kawakami et al., 1998; Maganaris et al., 1998c). However, the planar arrangement may not be possible due to the shape of the muscle. Sejerested and co-workers (1984) observed curved fascicle sheets in the vastus lateralis of human cadavers and have suggested the arrangement of fascicle sheets in an onion-like arrangement. This thesis reports development of methods to study the fascicles' arrangement as sheets within the muscle (chapter 4 and chapter 5). The non-planar sheet arrangement arises from 3D curving of fascicles in muscle. Further, the change in architecture during muscle bulging may not be uniform across the whole muscle. We expect bulging to be regionalized across the muscle and this may result in differences to the deformation of fascicle sheets and their alignment relative to each other.

It is important to study the muscle architecture in three dimensions to understand the changes in muscle architecture during muscle bulging and relate it to the muscle function. Some studies have reported muscle architecture and changes in depth but it is still not understood how the muscle architecture changes in three dimensions during relative torque and how muscle bulging changes the structure and function of a muscle. Fascicle sheet arrangement and the change in this arrangement with different relative torque states are quantified in chapter 4 and 5.

1.4. Techniques for studying muscle architecture

Muscle architecture has interested researchers for centuries (Benninghoff and Rollhauser, 1952; Haughton, 1873; Stenosis, 1667) however, most of the quantitative work on muscle architecture has been done in the last two decades. Much of the earlier information on skeletal muscle architecture was obtained from cadaver studies (Huijing, 1985), but to understand muscle function, it is important to study in-vivo muscle architecture as the properties of cadaver muscle are different from living muscle that can be activated. The cadaveric studies have been used to measure pennation angles and fascicle lengths in 2D dissected planes (Friederich and Brand, 1990; Wickiewicz et al., 1983), and also to obtain 3D architectural information (Agur et al., 2003). It has been shown that the information obtained from cadaver muscle does not match with a relaxed or contracted state of muscle (Martin et al., 2001). In-vivo studies in animals on muscle dynamics typically use sonomicrometry crystals to investigate the fascicle length and thus strains and strain rates (Ahn et al., 2003; Hoffer et al., 1989; Roberts et al., 1997). Sonomicrometry provides local 1D measured of length and fascicle lengths are calculated using the assumption that they are straight and not curved.

During the last two decades, brightness mode (B-mode) ultrasonography has been used to study muscle architecture (Kawakami et al., 1993; Kuno and Fukunaga, 1995) in two dimensions. Muscle fascicle architecture can be quantified non-invasively using B-mode ultrasound for both dynamic and isometric relative torques (Fukunaga et al., 1997a; Fukunaga et al., 1997b; Ito et al., 1998; Kawakami et al., 1998; Maganaris et al., 1998c). Typically, a few fascicles are digitized manually from each ultrasound image in a process that is both time-consuming and subjective. A few studies have developed automated methods to track the changes in contractile lengths (Loram et al., 2006) and distinct features (Darby et al., 2011) in ultrasound images. Automated methods were developed to study the 2D architecture from in-vivo ultrasound images (chapter 2; Rana et al., 2009). A challenge faced with 2D ultrasound is that due to the size of the probe, it does not scan the whole muscle. Most of the studies have used manual digitization to quantify the muscle fascicle length and pennation angle in the muscle belly (Fukunaga et al., 1997a; Hodges et al., 2003; Maganaris et al., 1998c). Also, due to the planar nature of 2D ultrasound images it cannot be used to quantify muscle bulging out of the image plane.

A few studies have used ultrasound to study 3D muscle architecture (Barber et al., 2009; Fry et al., 2003; Fry et al., 2004; Hiblar et al., 2003; Kurihara et al., 2005; Malaiya et al., 2007). 3D ultrasound uses 2D images from the ultrasound and 3D position information related to each image to reconstruct the shape of the muscle (Fry et al., 2003; Hiblar et al., 2003; Kurihara et al., 2005) and to determine muscle volume (Barber et al., 2009). Fry and co-workers (2003) used 3D methods to construct three dimensional images of the muscle in localized regions in space and suggested that muscle architecture is visible in such reconstructions. Hiblar and co-workers (2003) studied the orientation of muscle in three dimensions; however, the variation in their data was too large (coefficients of variation 30-40%) to study the change in muscle fascicle orientations. Kurihara and co-workers (2005) studied muscle fascicle length using 3D ultrasound. They reconstructed 3D images using software, identified fascicles by visual inspection of the 3D reconstruction (Tomtec3D, Tomtec, Germany) and reported fascicle length as the mean length of three fascicles in the belly of the muscle.

Diffusion tensor magnetic resonance imaging (DT-MRI) has been used for muscle–fiber tracking in 3D (Damon et al., 2002; Heemskerk et al., 2011; Kan et al., 2008; Lansdown et al., 2007; Levin et al., 2011). DT-MRI involves collecting magnetic resonance images and computer-based image analysis for tracking the fibers. DT-MRI detects the co-efficient of diffusion of water motion along the applied gradient axis. By combining the diffusion along the applied gradients, diffusion tensors can be obtained along any direction (Mori and Zang, 2006). For elongated structures, such as fibers, the diffusion coefficient of water is greater along the direction of the fiber than perpendicular to it (Farr and Allisy-Roberts, 1998; Hashemi and Bradley, 1997). This information can be combined across neighboring pixels to reconstruct the fiber trajectory. The reported scan times in recent studies are at least 15 minutes (Budzik J.F., 2007; Heemskerk et al., 2009) and most of the work has been done on passive muscles as active muscle relative torques cannot be obtained for the required scan times. Also it is difficult to study contracting muscle with DT-MRI because the technique is sensitive to soft tissue motion that invariably occurs during these long scan durations (Bishop et al., 2009) . One notable exception is the study by Deux and co-workers (2008) that used a scan time of 2 minutes 30 seconds and that related diffusion co-efficients with the relative torque state of muscle (rest, passive lengthening and active relative torque). However, they reported that their diffusion co-efficients may not relate to the direction of the fascicles, as they found a loss of parallelism of

fibers observed in 3D. Diffusion anisotropy determines the fascicle orientation using these techniques, and they reported a loss of diffusion anisotropy during the contracted state.

DT-MRI studies have been very qualitative; the technique is very sensitive to tissue motion and has been mostly used to study architecture in passive muscle. Ultrasound is less expensive than MRI to use, real-time acquisitions are possible and it is easier to operate than DT-MRI. The faster acquisition times using ultrasonography makes the testing of different relative torque states possible.

The purpose of this thesis was to develop methods to study muscle fascicle architecture in 3D using B-mode ultrasound and use these methods to study changes in muscle architecture in passive and contracting states.

1.5. Outline of this thesis

Chapters 2 and 3 present the methods to quantify the muscle fascicle architecture in 2D and 3D, respectively. Muscle fascicle orientations and fascicle plane orientations are studied for different ankle angles and relative torque states in chapter 4, and the effect of 2D ultrasound scan orientation on measured pennation angle is discussed. Muscle fascicle curvature and the fascicle sheet curvature are presented in chapter 5. Finally, chapter 6 integrates the information from chapters 4 and 5, describes the effect of 3D fascicle architecture on muscle function, compares these findings with previous 2D knowledge and presents the importance of the 3rd dimension on architecture and function.

Chapter 2 is based on a paper by Rana, Hamarneh and Wakeling (2009). Chapter 3 is based on a paper by Rana and Wakeling (2011). Chapter 5 uses ideas for calculating curvatures that have previously been published in a 2D context by Namburete, Rana and Wakeling (2011).

2. Automated tracking of muscle fascicle orientation in B-mode ultrasound images

2.1. Introduction

Pennation angle, is one of the main factors that determine the function of a muscle (Fukunaga et al., 1997a; Lieber and Fridén, 2000). For a given shortening velocity of the whole muscle belly, more pennate muscles will tend to have a smaller fascicle shortening velocity than less pennate muscle (Lieber and Fridén, 2000). Furthermore, greater pennation results in more fascicles being packed in parallel for a given muscle volume; this leads to a greater force production. However, this force is more oblique to the line of action of the muscle belly. Muscles in humans range from fascicles nearly parallel to the muscles' line of action, such as the Sartorius, to highly pennate muscles such as the short head of the biceps femoris with a pennation angle of 23°. The pennation angle changes during muscle relative torques with the fascicles rotating to greater pennation angles as the relative torque intensity increases. Differences of up to 12°-27° in pennation angle between resting and maximally contracted human muscles have been reported (Herbert and Gandevia, 1995; Maganaris et al., 1998c; Narici et al., 1996b). An architectural gear ratio, AGR, has been defined as ratio of muscle belly velocity to muscle fascicle velocity (Azizi et al. 2008; Wakeling et al. 2011) and this changes as the fascicles rotate. Changes in the shape of the muscle belly that occur with different muscle forces can cause changes in AGR and rotation and this predisposes the muscle to favor high force - low velocity relative torques or high velocity - low force relative torques (Azizi et al., 2008). Being able to quantify muscle architecture during dynamic relative torques is an important part of determining the function of the muscle.

Muscle fascicle architecture can be quantified non-invasively using B-mode ultrasound for both isometric situations (Blazevich et al., 2006; Fukunaga et al., 1997a; Fukunaga et al., 1997b; Ito et al., 1998; Kawakami et al., 1998; Maganaris et al., 1998c) and during dynamic

relative torques (Darby et al., 2011; Ichinose et al., 2000; Ishikawa et al., 2003; Kawakami et al., 2002; Kurokawa et al., 2001; Loram et al., 2006; Muraoka et al., 2001; Wakeling et al., 2011; Wakeling et al., 2006). Typically, the fascicles have been digitized manually in a process that is both time-consuming and subjective. An automated technique based on Lucas –Kanade algorithm was developed to track displacement of gastrocnemius aponeurosis and free tendon (Magnusson et al., 2003). An automated method based on spatial cross correlation for automating the tracking of features frame by frame was developed to track changes in contractile length of muscle fascicles (Loram et al., 2006). This latter method needed an initial manual digization step to identify the features or fascicles of interest, and then it followed the position of these features over a series of successive frames. The method is most robust when successive frames are most similar, as is the case for low amplitude relative torques and small changes in pennation. With substantial changes in pennation angle that occur with large joint movements and muscle relative torques, the local features within the ultrasound image change in shape and may even disappear from the ultrasound plane and this can result in error in the measurement. A recent method based on Kanade-Lucas-Tomasi methods and active shape models was tracks the distinctive features within ultrasound image sequences to quantify movement in different regions of the image and relate it to the activation of the muscle regions (Darby et al., 2011). However, this method does not relate to the fascicle length, shape or orientation.

The purpose of this study was to develop an automated method to quantify the orientation of the fascicles within a muscle from isolated ultrasound images, and to resolve the orientations to localized regions in the images.

2.2. Methods

2.2.1. Methods Overview

B-mode ultrasound images contain information on the muscle fascicle orientation as well as noise. A multistage process was used to determine the fascicle orientation (Figure 2.1): initial multiscale vessel enhancement filtering enhanced fascicle structure (which is vessel-like or tubular) and decreased the noise level. Fascicle orientation was then determined by two alternate methods: (a) radon transform was used to quantify the dominant orientation in the image and (b)

an ultrasound-specific wavelet analysis quantified the local orientation around each pixel. The two methods were validated against synthetic images with known orientation and also with real ultrasound images that were additionally digitized manually by ten people.

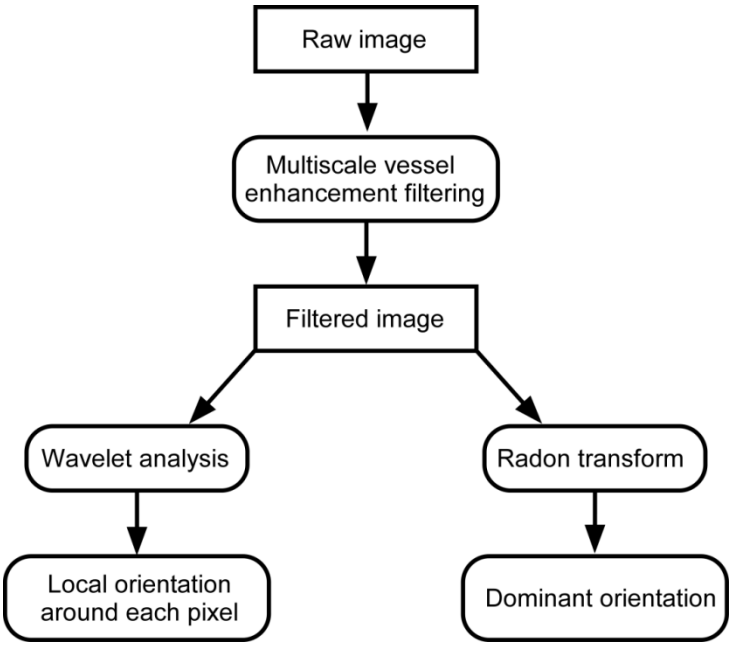

Figure 2.1 The sequence of methods used to determine fascicle orientation.

2.2.2. Multiscale Vessel Enhancement Filtering

Muscle fascicles appear dark in the image and connective tissue between the fascicles appears as bright, vessel-like tubular structures that parallel the fascicles. Multi-scale vessel enhancement filtering was used to enhance these vessel-like structures (Frangi et al., 1998). This method enhances the tubular structures in the image and is capable of resolving tubular structures of different radii.

The ultrasound images were 512×512 pixels, representing 5x5 cms of muscle region. The image was initially convolved with a series of four 13 x 13 pixel Gaussian kernels in which each kernel had a normalized Gaussian distribution of pixel intensities centered within the kernel. The standard deviations (2, 3, 4 and 5) for these Gaussian distributions were chosen based on diameter of the tubular structures in the image. If the standard deviation is greater than the diameter there is over-blurring of the image, and if it is lesser it picks more noise. The Hessian

matrix of these convolved images provides second-order information that is related to the vessel direction. For an ideal tubular structure, the eigenvalues λ_1 and λ_2 of the Hessian matrix obey the following rules:

$$|\lambda_1| >> |\lambda_2|$$

$$|\lambda_2| = 0$$

The eigenvector in the direction of the smallest eigenvalue represents the local vessel direction. The vesselness response $V(s)$ for each scale was determined as:

$$V(s) = \begin{cases} 0, & if\ \lambda_2 > 0 \\ exp\left(\frac{-R^2}{2\beta^2}\right)\left(1 - exp\left(\frac{-S}{2c^2}\right)\right), & if\ \lambda_2 \leq 0 \end{cases}$$

where $R = \frac{|\lambda_1|}{|\lambda_2|}$ and is a measure of 'line-like' structures; and $S = \sqrt{\sum_{i \leq 2} \lambda_i^2}$ is the Frobenius norm of the Hessian matrix. β and c are arbitrary constants both set to 0.5 according to Frangi et al. (1998). The whole process was repeated at each pixel for different scales and the filtered image taken as the maximum vesselness response at each pixel across the four scales (Figure 2.2).

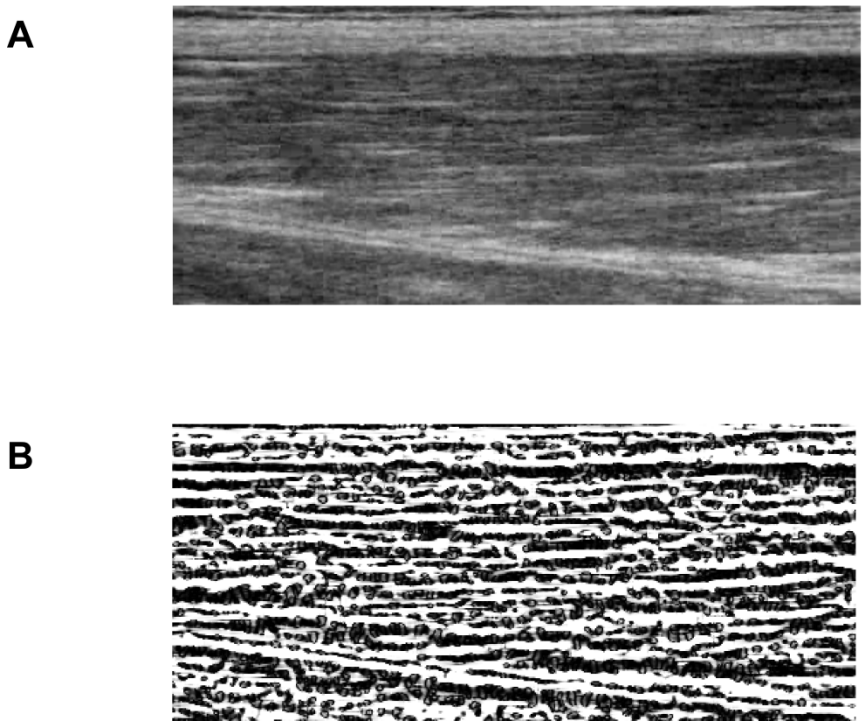

Figure 2.2 Ultrasound image from vastus lateralis (A) and image obtained after multiscale vessel enhancement filtering (B).

2.2.3. Anisotropic Wavelet Analysis

Muscle fascicle orientation at each pixel was obtained by using anisotropic wavelet analysis. A wavelet kernel was constructed based on a modified Mortlet wavelet that was extended into 3D and given polarization with a major orientation α (Figure 2.3). The kernel was $2k+1$ pixels in both the x and y directions. At any pixel the amplitude of the wavelet $G(x, y)$ was given by:

$$G(x,y) = exp\left(\frac{x^2+y^2}{-dk}\right) Cos\left(\frac{2\pi(xCos\alpha - ySin\alpha)}{\lambda}\right) + o,$$

where d is the damping of the wavelet, k is the half-width of the wavelet, λ is the wavelength and o is a linear offset. The damping was set at $d = 2.5622$ to (A) provide decay of the wavelet by the edges of the kernel (with $k = 19$) and (B) to satisfy the wavelet condition of zero integral (for $\alpha = 0$ and $o = 0$). However, due to pixilation artifacts, a non-zero value for o must be introduced for non-zero angles α in order to maintain a zero integral. The value for o

never exceeded 0.0004 % of the maximum value for the wavelet, and so this offset correction made a negligible difference to the results. For each pixel, the wavelet used for the convolution has it spatial wavelength, λ, to match the selected scale in the multiscale filtering. Four sizes of wavelets were used with λ equaling 10, 13, 16, and 19 pixels.

The filtered image was convolved with a set of wavelet kernels at different orientations α. The wavelet with orientation α resulted in the greatest convolution for a given region in the image identified that region as having a muscle fascicle orientation of α.

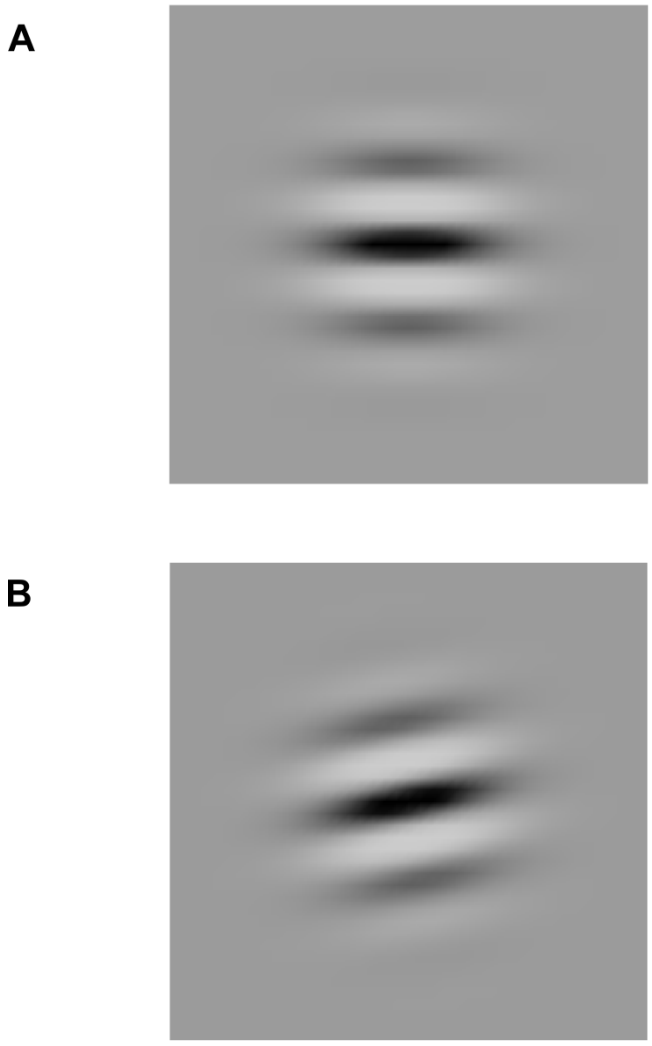

Figure 2.3 ***Anisotropic wavelets for determining fascicle orientation within ultrasound images. Wavelets were calculated using the above equation and from a 39×39 pixel grid. Wavelet grids in this illustration were obtained by interpolation of data are shown for orientation*** $\alpha = 0^o$ ***(A) and*** $\alpha = 10^o$ ***(B).***

2.2.4. Radon Transform

Radon transforms can be used to determine the predominant orientation in a repeated structure such as the muscle fascicles in an ultrasound image. The radon transform projects a grid of parallel lines, one pixel apart, across the image and calculates the integral of the image intensities along each line (Khouzani and Zadeh, 2005).The orientation θ of the grid is varied, and when θ approaches the dominant orientation of structures within the image then the radon

transform has greatest variability across the image (Figure 2.4); this variability was quantified by its variance or kurtosis. Variance was used for synthetic images, as has been used earlier by Khauzani and Zadeh (2005) and Kurtosis was used for real ultrasound images because kurtosis was more robust than variance for real images. Higher kurtosis indicates that more of the variance is due to infrequent extreme deviations, as opposed to frequent modestly-sized deviations. Since the real images have discontinuous line-like structures at unequal distances relative to each other (as opposed to uniformly distributed continuous lines in the synthetic images) the measure of kurtosis is more sensitive to fascicle orientation in the ultrasound images than the variance. The dominant fascicle orientation was taken as the angle θ at which the radon transform of the filtered image had the greatest variance (synthetic grids) or kurtosis (ultrasound images).

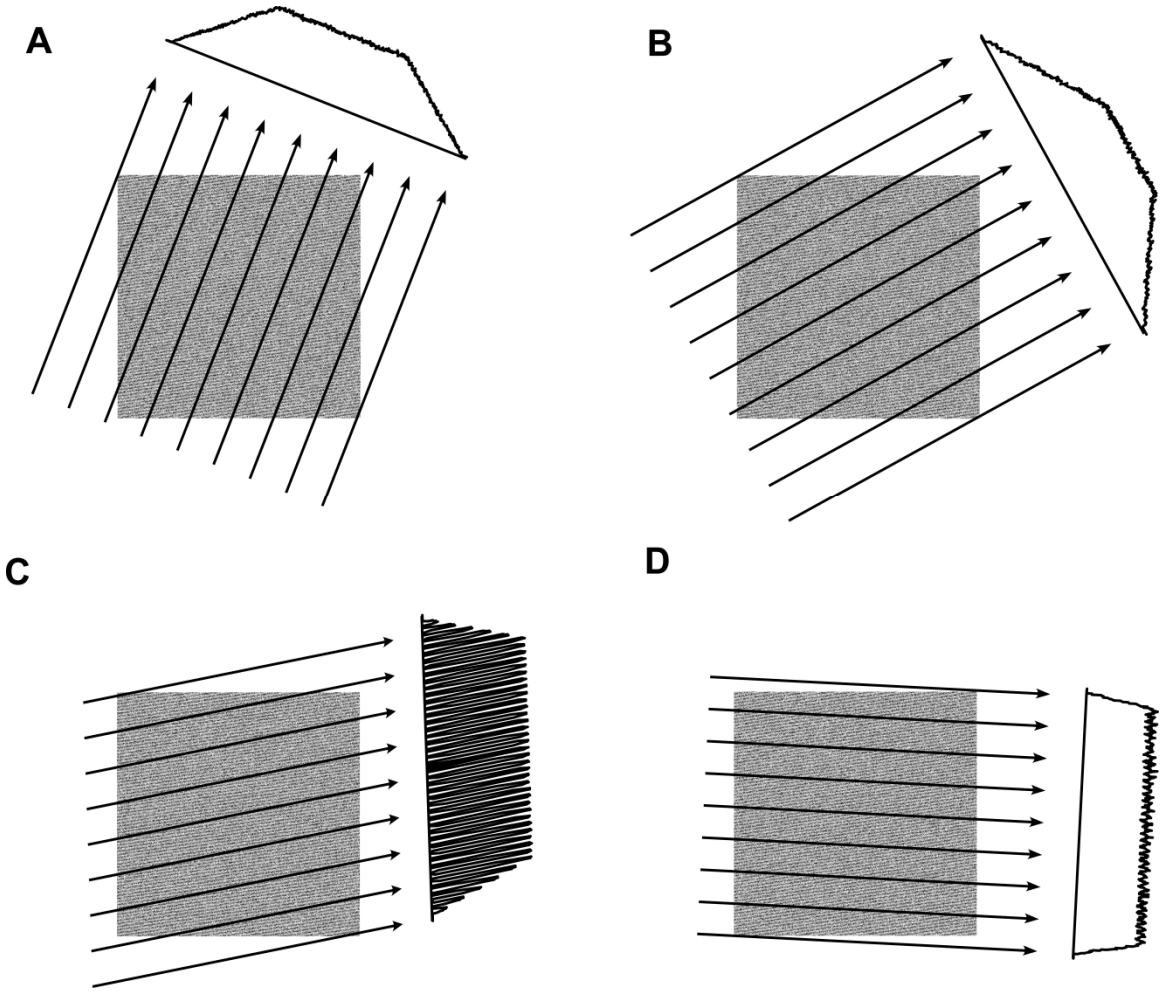

Figure 2.4 ***An illustration of radon transform at four different angles θ on synthetic grids (A-D). The arrows represent the projection through the gird, the projected intensity plots on the right represent the result of the radon transform. The radon transform shoes the greatest variance when theta approaches angle in the grid.***

2.2.5. Validation

The use of wavelet and radon transforms for ultrasound images was validated using both synthetic and real images. Synthetic images were grids of parallel lines at a known orientation that had sinusoidal changes in intensity across (or perpendicular to) the lines, these grids were combined with random noise (Figure 2.5). A contrast to noise ratio (CNR) was defined as the ratio of the absolute difference in intensity between bright and dark regions of the image to the sum of noise from those respective regions. For images with distributed pixel intensities the difference in intensity between bright and dark regions was taken as the difference between the mean pixel intensities (I) from the brightest and darkest 50% of the pixels. The noise from each region was quantified by the standard deviation (σ) of the image pixels in each region.

$$\mathrm{CNR} = \frac{I_{Bright} - I_{Dark}}{\sigma_{Bright} + \sigma_{Dark}}$$

The two methods were tested for synthetic grids at a fixed angle of 10° and different noise levels and then at fixed noise level (CNR =1.0) but different angles.

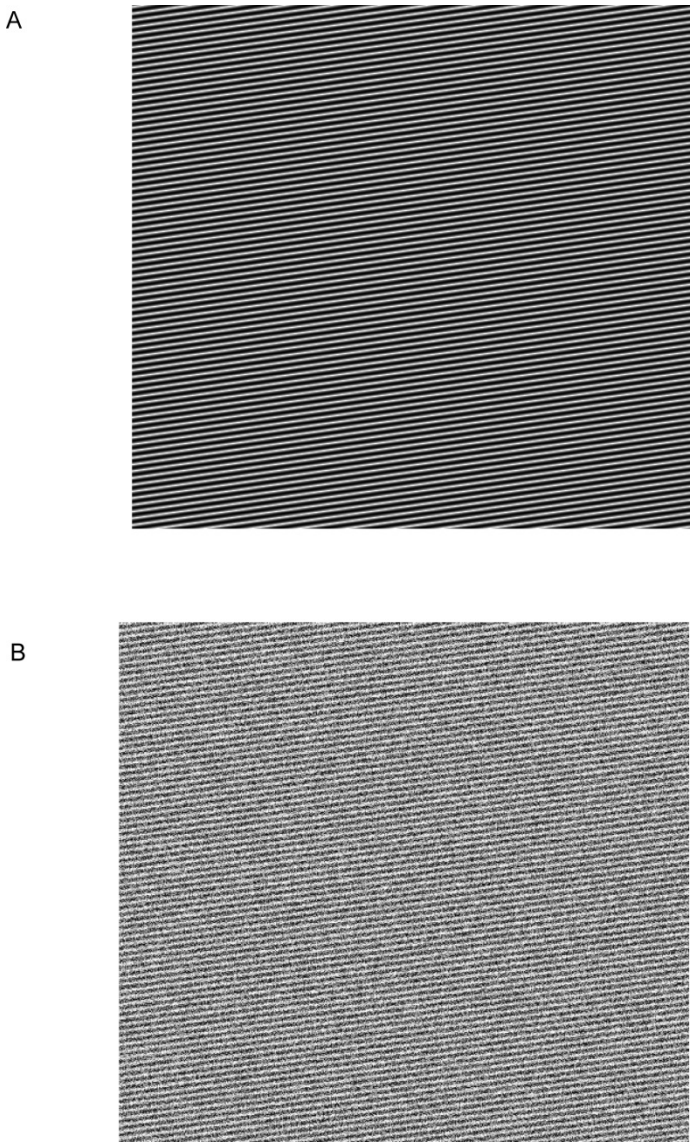

Figure 2.5 Synthetic images used for validation at an orientation of 10° with no added noise (A) and with added noise at CNR=0.79 (B).

To validate the methods against real images, B-mode ultrasound images (Echoblaster, Telemed; LT) were recorded at 45 Hz from the distal part of the left vastus lateralis of a subject during cycling on a stationary ergometer. A linear-array probe (128 elements at 7 MHz) was secured to the skin with elasticated bandages and aligned to a plane in which the muscle fascicles were situated. Bitmap images were extracted for each frame from the ultrasound sequence. The subject provided informed consent for this procedure in accordance with the Research Ethics procedures at Simon Fraser University. 60 ultrasound images from the ultrasound sequence were

manually digitized by 10 different researchers. The ultrasound sequence and the pedal position data were synchronized in time to relate the ultrasound images with the crank angle. The top dead center of pedal position was considered as 0° crank angle. Each person digitized the sequence twice, and only the second set of measurements were used to allow for a training effect in visualizing the fascicles. From each image a fascicle was identified that spanned from superficial to deep aponeuroses, and two points were digitized on the fascicle close to the aponeuroses. The angle between these points on the fascicle and the x-axis was calculated. A region of interest was identified for each image within the aponeuroses that contained only the muscle fascicles, and this fascicle direction was quantified by the mean α from the wavelet analysis and the dominant orientation θ from the radon transform (Figure 2.6). The orientations obtained by the above three methods were fit with respect to the crank angle using Fourier series to compare the respective results.

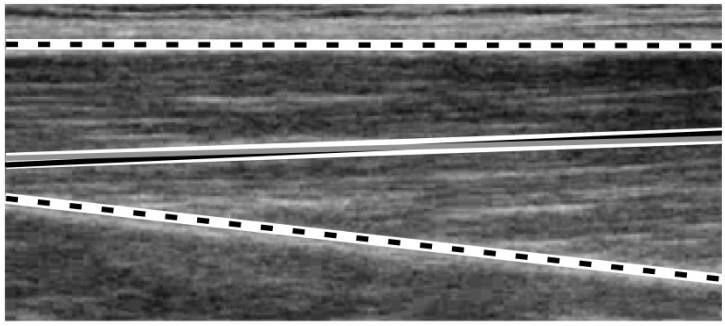

Figure 2.6 ***Ultrasound image from vastus lateralis. The aponeuroses are indicated by dashed lines. The mean fascicle orientations are shown by solid black and grey lines from the radon and wavelet transform, respectively. Each line is shown against a white relief for clarity.***

2.3. Results

The images after multiscale vessel enhancement filtering are shown in Figure 2.2B. It is clear that this method enhances the fascicle structure in the image and is capable of enhancing fascicles of different diameters. Both the wavelet analysis and radon transform methods were able to accurately identify the fascicle orientation in the synthetic images (Figure 2.6) with a C.N.R. of 0.8. The least squares linear regression was obtained for the calculated orientations

against the actual orientations for these two methods both had slopes not significantly different from unity ($r^2 > 0.99$). The mean absolute error for the radon transform across the range of 0° to 90° was 0.058°and the mean error for the wavelet transform across this range was 0.02°. These error values are small enough for practical applications.

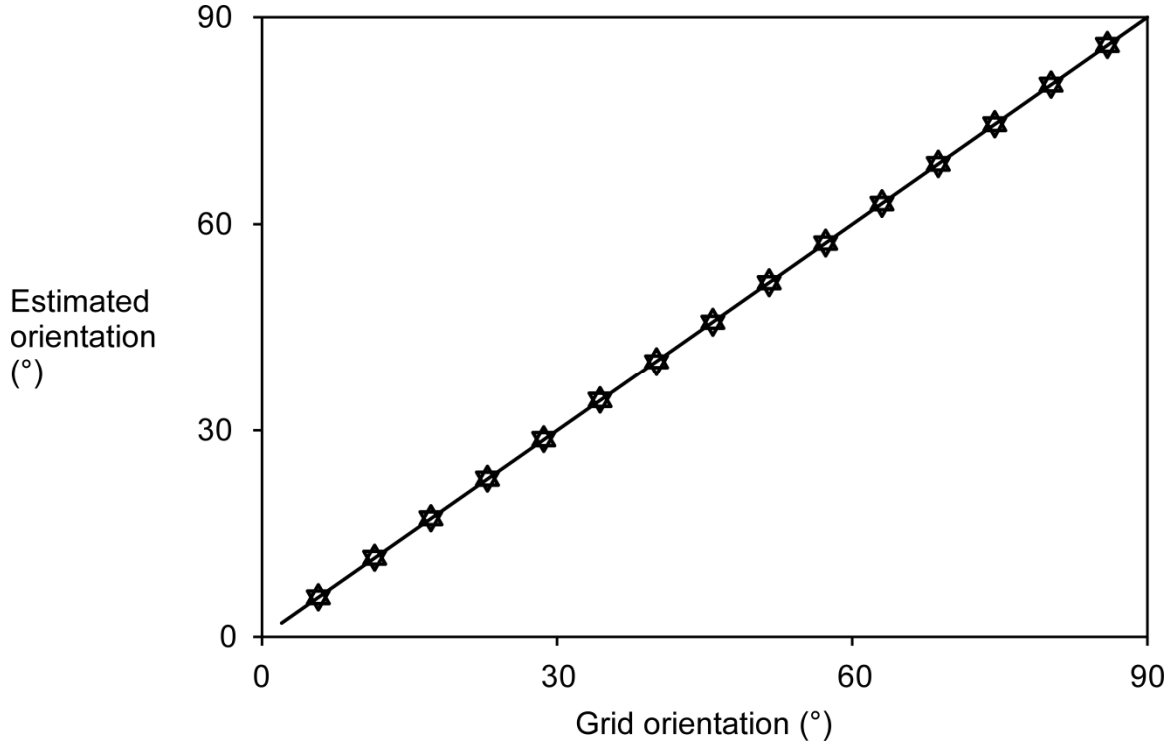

Figure 2.7 ***Estimated orientation from the simulated grids calculated for a range of angles using CNR=0.8.Angles calculated using the wavelet transform are shown by triangles with apex at top, and angles calculated using the radon transform are show by triangles with apex at their bottom. The line shows the ideal result.***

When the level of noise increased in the synthetic images there was an increase in the error of the estimate of orientation (Figure 2.8). The errors for both the radon transform and wavelet analysis were less than 0.02° for C.N.R. greater than 0.8. The C.N.R.s for the ultrasound images for the vastus lateralis were in the range 0.85-1.34.

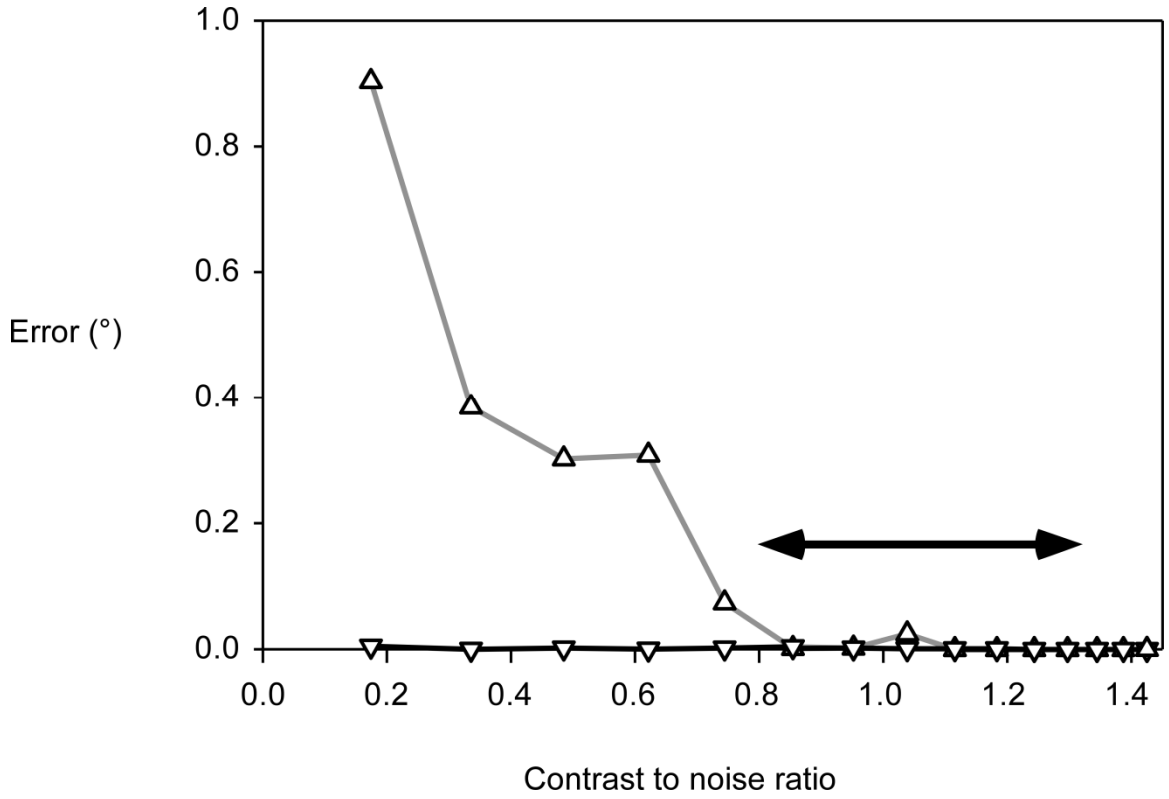

Figure 2.8 ***Errors in the estimated orientations from the simulated grids calculated for a range of CNR at fixed orientation of 8.6°.Angles calculated using the wavelet transform are shown by grey line and triangles with the apex at top, and angles calculated by radon transform are shown by black line and the triangles with apex at their bottom. The arrows show the range of contrast to noise ratios observed in ultrasound images from the vastus lateralis.***

The ultrasound images showed that the fascicle orientations changed in a cyclical fashion during each pedal cycle. The greatest fascicle angles occurred at the bottom of the pedal cycle when the knee was most extended, with a short vastus lateralis length. Manual digitization showed that the mean fascicle angles, relative to the x-axis (horizontal axis) on each image, varied between 2.0° and 3.5° and this corresponded to pennation angles of 8.6° to 9.5° that were relative to the deep aponeurosis. Considerable variability occurred in the fascicle orientations that were manually digitized by the 10 researchers (Figure 2.9). The standard deviation for the fascicle orientations for each frame had a mean value of 1.41° (range 0.46° to 2.83°).

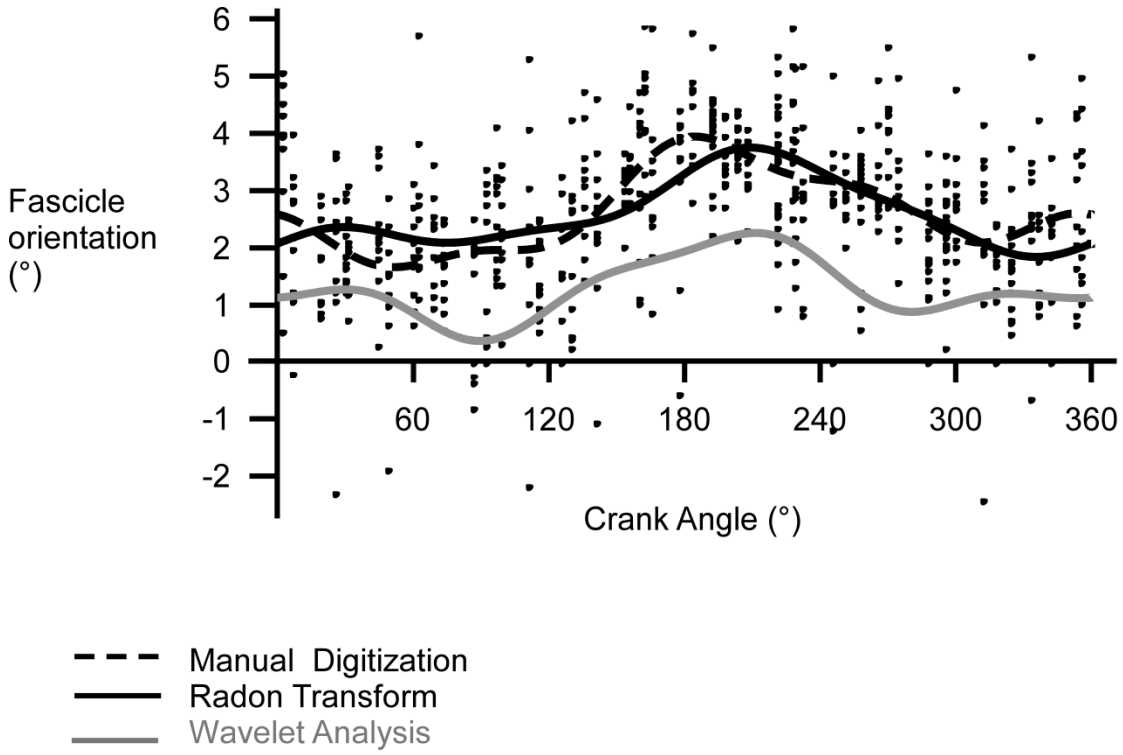

Figure 2.9 ***Muscle fascicle orientations in vastus lateralis during cycling. Orientations are relative to the ultrasound probe (skin) surface. Points show the orientations determined from manual digitization by 10 researchers. Lines show the orientations determined using Fourier series from the manually digitized points (dashed black line), radon transform (solid black line) and wavelet transform (solid grey line)***

The results from the wavelet analysis and radon transform on the ultrasound images can be visualized in Figure 2.6. Lines have been drawn that have an orientation determined from the radon transform or mean wavelet value, and pass through the centre of the muscle. The wavelet transform resulted in orientations at lesser angles than for the radon transform. The mean orientation α from the wavelet analysis was significantly different from the mean fascicle orientation that was manually digitized from each ultrasound frame (two-tailed, matched pair, t-test; $p<0.001$) with the mean difference being -1.35° this difference was less than the standard deviation of the manually digitized values for each frame of 1.41° (Figure 2.9). There was no significant difference between the dominant orientation θ from the radon transform and the manually digitized values from each ultrasound frame (two-tailed, matched pair, t-test; $p=0.773$).

2.4. Discussion

The combination of multi-scale vessel enhancement with either wavelet analysis or radon transform has resulted in methods that will automatically detect the orientation of fascicular structures within an image. Both methods had accuracy better than 0.02° for levels of noise typical of those in ultrasound images (Figure 2.8) with the wavelet transform performing slightly better than the radon transform. When the methods were applied to an actual ultrasound sequence the radon transform identified orientations with a closer match to the manual values than the wavelet analysis (Figure 2.9). This in itself does not show that the wavelet analysis is worse at identifying actual muscle fascicle orientations than the radon transform because we do not know the accuracy of manually digitizing the sequences, and indeed the different researchers produced a surprising variability in their perceived fascicle directions (standard deviation of 1.41°). It may be expected that the radon transform generates similar values to the manually determined ones because it is likely they follow similar principles. The radon transform identifies the dominant orientation within the image that would correspond to the most prominent and visible fascicles that draw the eye when being digitized manually. Furthermore, the radon transform projects parallel straight lines across the image and so would be particularly suitable when identifying linear approximations to the muscle fascicles. These features are particularly useful if the purpose is to identify a "representative" fascicle within the image for determining its linear length, as has been the case for many previous studies.

By contrast, the wavelet transform identifies the mean orientation of the fascicular structures within the space of the kernel. Within the kernel the energy of the wavelet is concentrated within a circular region of radius 11 pixels, corresponding to 1.3 mm in the muscle. Thus the wavelet transform can identify local orientations with a 1.3 mm spatial resolution throughout the ultrasound image. The mean orientations calculated across the image, for validation purposes, contained information about all fascicle orientations within the muscle. Where some fascicles were not in the ultrasound plane their projected segments in the image would be at different orientations to the fascicles that were in the ultrasound plane; thus, the mean orientations identified by the wavelet analysis would be different from the orientations obtained from fascicles that were visualized as entirely within the scanning plane. Nonetheless, the mean orientations determined from the wavelet analysis were within the range of those

manually digitized and thus this method could be used to automatically track whole fascicles for the purposes of determining their linear length.

The wavelet transform not only provides the information needed to estimate linear fascicle length, but it additionally resolves the local orientations that can be used to quantify variations in fascicle orientation across an image and variation in orientation along the length of a fascicle such as when the fascicles are curved. It has been shown that muscle fascicles must follow curved trajectories within a muscle in order to be mechanically stable, particularly for the case of unipennate muscles (van Leeuwen and Spoor, 1992). Fascicle curvatures have previously been determined by manual digitization (Muramatsu et al., 2002), and have been predicted to contribute to the non-uniform strain patterns that are observed along fascicles (Ahn et al., 2003; Drost et al., 2003; Pappas et al., 2002). Fascicle curvature is thus an important aspect of muscle architecture that is commonly overlooked for the ease of assuming and digitizing linear fascicles within a muscle. We have recently developed automated methods to quantify the fascicle curvature in 2D ultrasound images (Namburete et al., 2011). The combined multiscale vessel enhancement and wavelet analysis methods presented here provide an automatic and objective method for quantifying local fascicle orientations and thus the non-linear trajectories of fascicles through muscles. These methods are extended to quantify the 3D muscle fascicle orientation as explained in chapter 3.

Both the wavelet analysis and radon transform methods assessed in this study can be applied to an image with no prior manual digitization or algorithm training, and they can be applied to a single frame as easily as to a sequence to obtain fascicle orientation. The study by Loram and co-workers (2006) and Darby and co-workers (2011) involved tracking of features in image sequence to track the motion of the selected features. The methods presented in this study are independent of the other images obtained in a sequence and extract orientation of the underlying pattern in the image region. The study by Darby and co-workers (2011) quantified movement in different regions of the image and related it to the activation of the muscle regions (Darby et al., 2011), this can potentially be combined with the fascicle orientation determined by the methods presented in this study to relate the change in fascicle orientation with the activation of the respective region. The radon transform can be used to identify the dominant fascicular orientation within an image, and thus can be used to estimate the representative muscle fascicle

lengths. The wavelet analysis additionally provides information on the local fascicle orientations and can be used to quantify fascicle curvatures and regional differences with fascicle orientation across and image.

3. In vivo determination of 3D muscle architecture of human muscle using free hand ultrasound

3.1. Introduction

Muscle fascicle orientation is an important architectural parameter affecting the muscle properties. Previous studies in different species have shown regionalization of fascicle architecture in muscle and these differences in architecture have been related to differential activation patterns and function of muscles (Blazevich et al., 2006; Herring et al., 1979; Wakeling and Horn, 2009).

From the last two decades, brightness mode (B mode) ultrasonography has been used to study muscle architecture in two dimensions (Kawakami et al., 1993; Kuno and Fukunaga, 1995). Muscle fascicle architecture can be quantified non-invasively using B-mode ultrasound for both dynamic and isometric relative torques (Fukunaga et al., 1997a; Fukunaga et al., 1997b; Ito et al., 1998; Kawakami et al., 1998; Maganaris et al., 1998c). Ultrasound probes are typically less than 60 mm and so B-mode ultrasound scans do not image the whole muscle. Additionally each scan represents a 2D slice through the muscle, and hence information in the third dimension is lost. Because of this, studies using 2D ultrasound usually image the muscle belly and implicitly assume that the 2D information from the belly is representative of the whole muscle. 3D trajectories of the muscle fascicles must be quantified in order to test the assumption that the whole muscle properties can be explained from the 2D ultrasound images of muscle belly. In order to do so, we need to develop reliable and validated methods to quantify the 3D muscle architecture across the whole muscle. Muscle fascicle structure is visible in ultrasound images for a range of probe orientations; however, the optimal alignment of the probe for 2D studies is for the muscle fascicles to lie within the scanning plane. An error of up to 23% has been reported in fascicle angles for probe orientations that do not align the fascicles with the scanning plane (Benard et al., 2009). Thus, it is also important to develop robust methods that are not sensitive

to the probe orientation. Studying the muscle fascicle architecture in 3D will help to alleviate this problem.

3D muscle fascicle orientation has previously been reported as the angle between a few manually digitized fascicles and either the aponeurosis (Malaiya et al., 2007) or the internal tendon of a muscle (Hiblar et al., 2003). To date, no studies have quantified a complete set of 3D fascicle orientations in the whole muscle, based on ultrasound images; this is largely due to lack of the appropriate methods.

The purpose of this study was to develop and validate methods to study fascicle orientation in 3D across the whole muscle using B-mode ultrasound. Based on the automated methods to determine fascicle orientation in 2D image planes (described in chapter 2), we have developed methods to obtain 3D fascicle orientations from 2D ultrasound and a 3D motion tracker system.

3.2. Methods

In order to obtain 3D muscle fascicle orientation, 2D images were collected using a linear ultrasound probe (Echoblaster, Telemed, LT) in B-mode and a rigid body set-up made up of a cluster of three optical markers (Certus, Optotrak, NDI, Ontario) was attached to the probe to obtain its position and orientation in 3D. One optotrak position sensor was mounted in horizontal position to capture the rigid body markers. The motion capture system returned the position and orientation of the cluster of markers in terms of three translations and three rotations relative to the lab coordinate system.

The calf muscles of one male subject (height 1.83 m, weight 80 kg) were imaged using a sweeping motion of the ultrasound probe across the right leg while the subject was kneeling in a water tank. The scanning was done for passive state of muscle with knee angle maintained at 110° and ankle at 90° (Figure 3.1). The leg was scanned in water immersion as this allowed the probe to be kept away from surface of skin and, hence, avoid probe pressure artifacts.

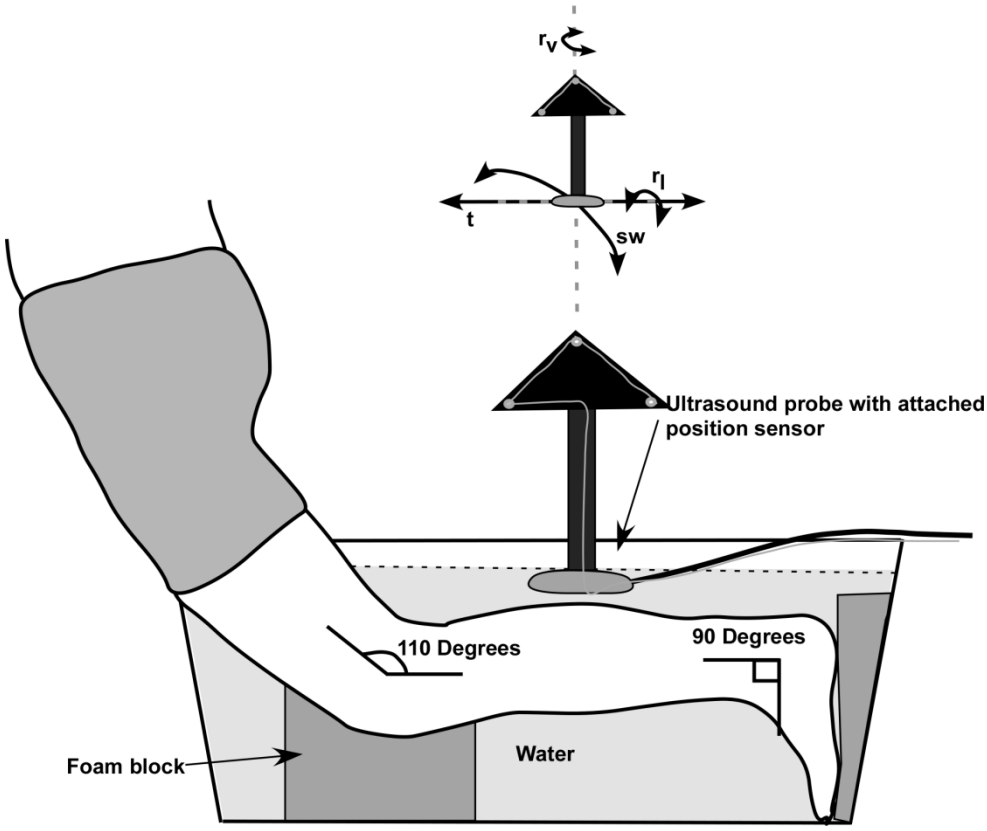

Figure 3.1 ***Experimental set-up showing the position of leg during scanning. Knee angle was maintained at 110 degrees with the help of foam block and ankle angle at 90 degrees. The diagram on the top represents the probe motion during scanning; translation along the muscle length (t), sweeping across width of muscle (sw), rotation along the longitudinal (rl) and the vertical (rv) axis the probe.***

During the scanning process the probe was kept within a range of ±15° along the longitudinal axis of the muscle to capture the muscle fascicles from different angles (Figure 3.1) and was kept 1-2 cm away from the skin surface. In order to ensure that the whole muscle was covered, a grid was drawn over the skin surface prior to scanning. The scan time depends on frame rate, speed of moving the probe and probe length. The scan time can be decreased by using a longer probe, increasing the ultrasound frame frequency or the speed of moving the probe. For a given probe, scan times can be decreased by making probe movements more rapid; however, this causes flow in the water that affects the accuracy of the ultrasound image. A frame frequency of 20 Hz and a probe of length of 5 cm was used in this study and this resulted in scan

times of between 90-120 s to image all three muscles of the triceps surae, or a more rapid 40–60 s to image the soleus and lateral gastrocnemius.

The ultrasound images were filtered using multiscale vessel enhancement filtering in order to enhance the line-like structures in the images and then convolved with polarized spatial wavelets to obtain local 2D orientations in the image plane (as described in chapter 2). 2D orientations within the image were then combined with the 3D position and orientation information from the optical system to obtain 3D fascicle orientations in lab space.

3.2.1. 3D orientations of muscle fascicles

3D orientations of the muscle fascicles were determined by (A) calibrating the probe relative to the rigid body, (B) relating points in the image plane (pixels) to points in 3D space (voxels), (C) transforming the orientation from 2D image plane to direction cosines in the 3D lab coordinate system, and (D) selecting among multiple pixels from different images belonging to same voxel in space.

The ultrasound probe was calibrated with respect to the rigid body in order to determine the position of each point in the image relative to the rigid body (Dandekar et al., 2005; Prager et al., 1998). Calibration was done by scanning two parallel wires set at a constant distance z_0 from a horizontal surface (Dandekar et al., 2005). Images were taken along the cross-section of the wires and along length of the wires (Figure 3.2). Two points were digitized in each image to locate the position of each of the wire in the image plane or the line formed by imaging along the length of the wires (Figures 3.2). These points were transformed from the image frame of reference to the rigid body frame of reference using six unknown values (three translations and three rotations), and then from the rigid body frame to the lab coordinate system using the following transformations with the parameters from the optical motion capture.

$$C(x, y, z_0) = T_p^c T_i^p (Pu, Pv, 0),$$

where $C(x, y, z_0)$ is a point on the wire in the lab coordinate system, (u, v) is the corresponding point in the image plane, P represents the scale between pixels and the actual distance. T_p^c is calculated using the position and orientation information of the rigid body from

frame of reference relative to the lab coordinate system and T_i^p is the unknown transformation matrix from the image to the rigid body. This can be solved for T_i^p as problem of minimization using the $z_0 = constant\ value$, because the points on the wires had a constant z coordinate in the lab coordinate system.

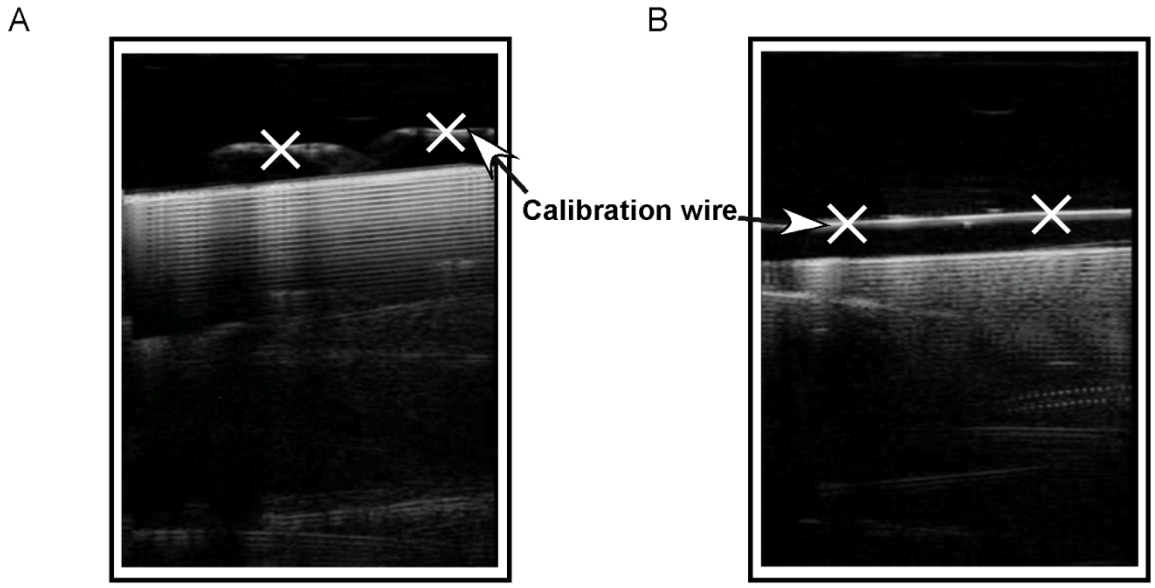

Figure 3.2 ***Images obtained during calibration .Ultrasound images of the two wires imaged along the cross-section (A) and ultrasound image of a wire imaged along length of the wire (B). The cross signs represent the points digitized on images.***

Once the calibration was known, any pixel in the image could be related to a particular voxel in lab space using the above equation. For fascicle orientations, 2D unit vectors were constructed in the image plane using the orientation values from the wavelet analysis (chapter 2) and transformed to 3D vectors in lab space. Voxels were chosen to contain pixels from a 5×5×5 mm region. Due to the nature of the scanning, multiple pixels correspond to each voxel, and thus there is an over-determined series of solutions. The correct 3D fascicle orientation occurs when the fascicle lies within the image plane of the ultrasound image, and so it is defined by its 2D orientation in the image, and the orientation of that image plane. When the fascicles are in the image plane they appear as more continuous line-like structures, and this can be characterized by a high convolution value from the wavelet analysis. The best solution to the 3D orientation at

each voxel can thus be determined from the pixel with greatest convolution. We have represented the 3D fascicle orientations in terms of the direction cosines of the vectors obtained.

3.2.2. Validation

The methods to determine 3D muscle fascicle orientation were validated by testing them on a physical phantom (Figure 3.3). The phantom was made with horse-hair stacked together in ten layers. The horse-hairs were arranged parallel to each other with the distance between adjacent hairs less than 2 mm. The hair ends were digitized using a stylus with the motion capture system to determine the orientation of hair in space. The phantom was immersed in water and scanned with a range of probe positions and orientations. A sample image from the phantom is shown in Figure 3.3. The images were processed using the musltiscale vessel enhancement filtering and wavelet analysis to obtain local 2D orientations of lines in the image planes. The 2D orientations were then converted to 3D direction cosines using the above methods. In order to identify the 3D solution to the orientations and validate the methods with the phantom we used information from the convolution value of the wavelets to constrain the problem of multiple pixels representing each voxel. The error of each calculated direction cosine from the digitized direction cosines was calculated.

In order to compare the results from these 3D methods with the architectural parameters calculated with 2D studies, pennation angle and fascicle length were calculated for the LG of one subject. The mean pennation angle (β) in the muscle belly was measured as the mean of the angle of the local fascicle orientations in the muscle belly region relative to the deep aponeurosis. The mean fascicle length was calculates as the mean of the fascicle length (L_f) over all the voxels in the belly region obtained from the pennation angle (β) and thickness (L_t) using the following

relation$L_f = {}^{L_t}/_{\sin\beta}$.

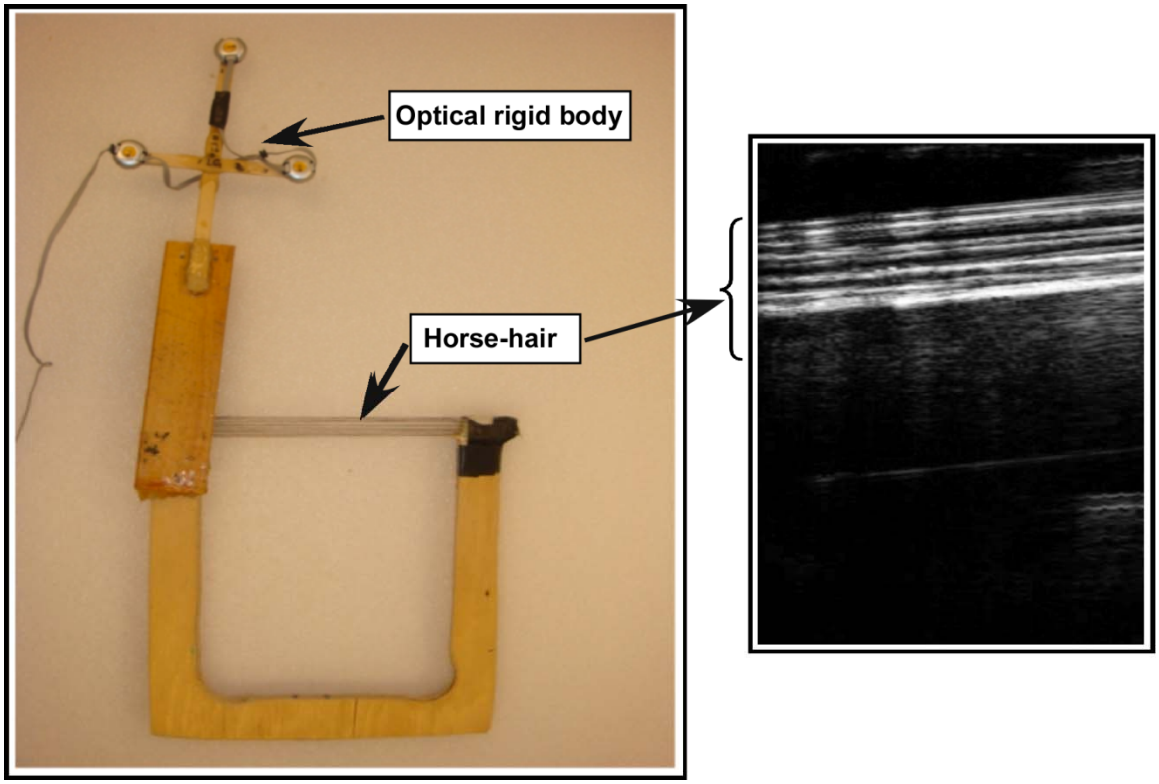

Figure 3.3 ***Horse-hair phantom used for validation of methods and ultrasound image of the phantom. The optical rigid body was attached to the phantom to track the position of phantom while scanning.***

3.3. Results

The mean errors in the *yz*, *xz* and *xy* planes are shown in Table 1. The error was calculated as the angle between the projection vectors in the three coordinate planes (*xy*, *yz* and *xz*) obtained from direction cosines determined by the image processing with the direction cosines from digitizing the hair stands in the phantom. The histograms for errors in the three planes spread on both sides of the zero value with peak values close to zero for the *xz* and *yz* planes and a more distributed pattern for the vertical *xy* plane (Figure 3.4). The mean (± s.e.m.) pennation angle in the muscle belly was 12.27 ± 0.25 ^{o} and the fascicle length (L_f) was 50.4 ± 1.8 mm.

Table 3.1 Error in direction cosines in the three coordinate planes.

Coordinate Plane	Mean error (°)	Standard Deviation (°)
yz	-0.32	2.81
xz	-0.41	2.21
xy	0.05	2.11

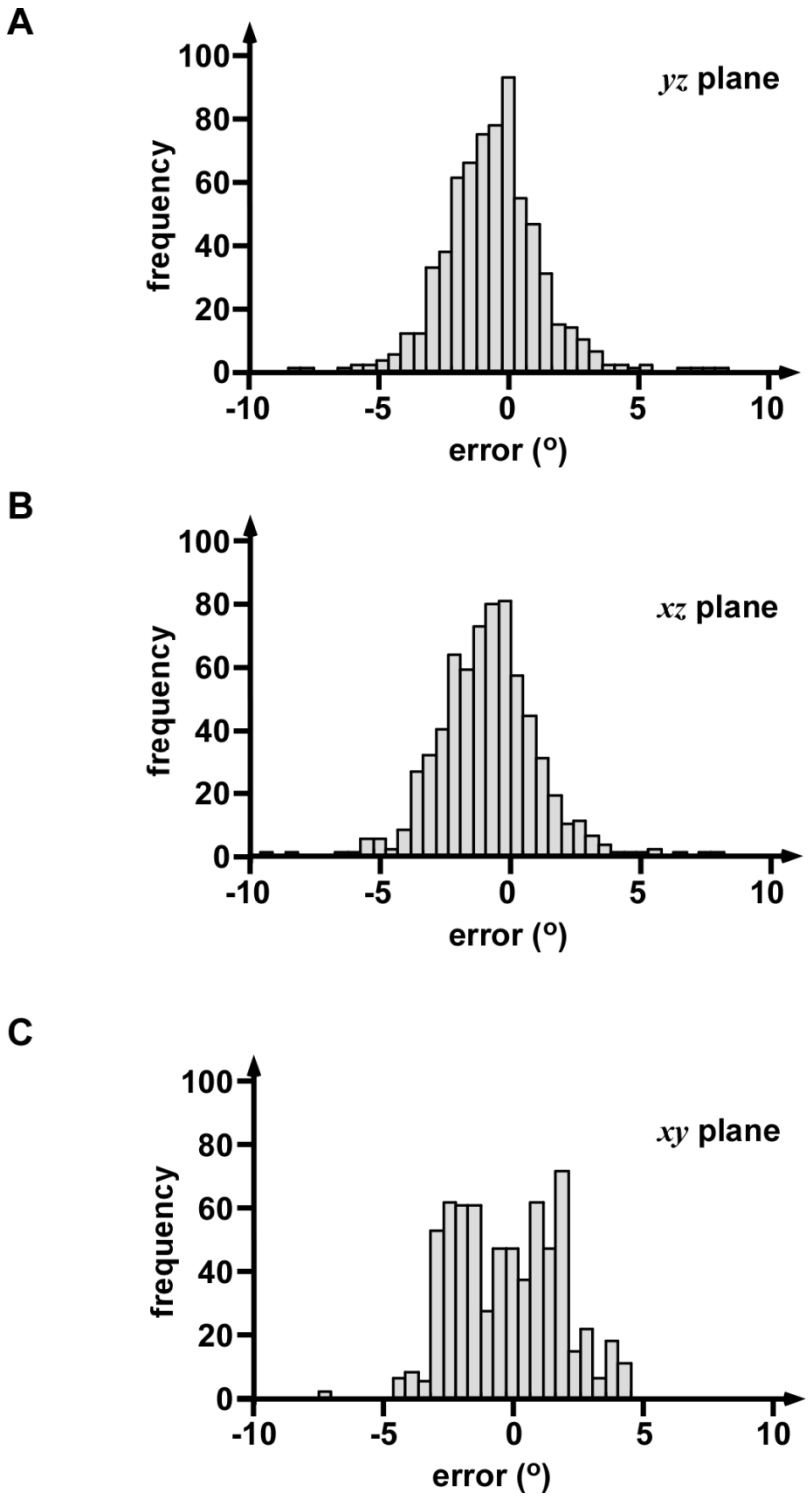

Figure 3.4 ***Histograms for between the calculated and measured direction cosines for the strands of hair in the phantom in the three coordinate planes.***

3.4. Discussion

The methods described in this chapter can be used to quantify the muscle fascicle architecture in three dimensions. The methods to study the fascicle orientation in 3D were developed on images from the lateral gastrocnemius muscle and the results indicate that the methods can be used to study the *in-vivo* muscle fascicle orientation in 3D.

The mean error in predicting the orientation value is less than 0.5^{o} in the three coordinate planes for the physical phantom. This error is not solely from the automated methods described above but additionally includes error due to the phantom digitization. Of note is that the hairs in the phantom bowed slightly in the vertical plane, however were assumed to lie in a straight line. Thus the actual local hair orientation varied by a couple of degrees (both positive and negative) in the *xy* plane. This effect can be seen by the more distributed range of errors in this plane (Figure 3.4), and show that the methods are sufficiently sensitive to detect non-linearities in the physical phantom used for validation.

The resolution of this analysis is limited by the size of the Gauss filter for the vessel enhancement filtering and the wavelet for the wavelet analysis, and both these dictate the kernel size used for the analysis. The kernels were 39x39 pixels, corresponding to 5.8x5.8 mm region in the scale of ultrasound images. The voxel size selected for this analysis (5x5x5 mm) was thus close to the limit that can be resolved by this technique. Larger voxels may result in greater accuracy for angle determination, but at the cost of reduced resolution. Nevertheless, the small errors found with this technique of less than 0.5^{o} (Table 1) mean that voxels can be kept small to combine good accuracy and resolution.

The methods were used to calculate pennation angle and fascicle length in the belly region of the muscle. The values reported for pennation angle and fascicle length for passive muscle in previous *in vivo* ultrasound studies are 11.3-16.7 ^{o} and 41.6–74.0 mm (Chow et al., 2000; Kawakami et al., 1998; Maganaris et al., 1998c; Martin et al., 2001) respectively. The calculated pennation angle (12.27 ^{o}) and fascicle length (50.4 mm) in this study lie within the range of previously reported values. It should be noted that fascicles may curve during relative torque (Maganaris et al., 2002; Muramatsu et al., 2002; Wang et al., 2009), and the methods in this chapter will also allow the local fascicle orientations and thus curvature to be quantified in

3D. However, in order to compare results from these methods with previous studies, we have assumed the fascicles to be linear. The purpose of the calculations in this chapter is to illustrate the application of these methods to study muscle architecture and are used to study 3D muscle architectural properties in the following chapters.

Previous studies on determination of muscle fascicle length or orientation from ultrasound have involved manual selection of fascicles in 3D muscle image to find fascicle length (Kurihara et al., 2005; Malaiya et al., 2007) and angle of fascicles relative to internal tendon (Hiblar et al., 2003). Manual digitization can be subjective and time consuming for studying the whole muscle architecture. All the processing for determination of 3D fascicle orientation in our methods is automated. This makes it possible to study architecture in whole muscle and also to compare the orientation changes in muscle with different relative torque levels.

This protocol has reduced some of the difficulties to studying 3D architecture *in vivo*. Data collection in water allows the sweeping motion of probe but may prohibit studies that involve simultaneous electrical stimulation or EMG collection. The short scan times of less than two minutes will enable sub-maximal relative torques to be studied, but are still too long to study non-isometric relative torques or maximum voluntary relative torque. These methods were used to quantify the 3D architecture in triceps surae muscle for different force levels and ankle angles, and these data are reported in chapter 4 and chapter 5. Since the fascicle orientations are initially determined in 2D and then converted to 3D, these methods can be only be used to study the 3D architecture in muscles whose fascicle structure is visible in 2D ultrasound scans.

Our methods can be used to determine *in-vivo* muscle fascicle orientation in 3D. The methods provide a tool to quantify the regionalization of fascicle orientation in the muscle and study the changes in 3D fascicle architecture in isometrically contracting muscle. Having reliable methods to quantify the architecture in 3D will enable future studies to test the importance of the third dimension in the relation between muscle architecture and function.

4. 3D fascicle orientations in triceps surae

4.1. Introduction

In-vivo muscle fascicle architecture has been extensively studied using B-mode ultrasound in 2D. Fascicle orientation is typically measured as the pennation angle that has been defined as the angle between the fascicles and the aponeurosis (Chow et al., 2000; Fukunaga et al., 1997a; Wakeling and Liphardt, 2006). Pennation angle depends on the muscle length and relative torque levels (Fukunaga et al., 1997a; Maganaris et al., 1998c; Narici et al., 1996a). In the gastrocnemii the pennation angle increases with decrease in muscle length and increase in force level and changes with an interaction between the two factors (Maganaris et al., 1998c; Narici et al., 1996a). Fukunaga and co-workers (1997a) found that in the vastus lateralis when the knee was extending, the pennation angle increased from 14° to 18° degrees in relaxed state and from 14° to 21° in tensed state (10% of maximum relative torque), and a greater increase in the pennation angle was observed in the tensed than in the relaxed condition when the knee was close to extension (>140°).

Pennation angle has been measured by using different methods in previous studies (Figure 4.1): as the angle the fascicles make with the superficial aponeurosis (Lichtwark and Wilson, 2005; Wakeling et al., 2006), angle between fascicle and deep aponeurosis (Narici et al., 1996a), angle between the tangent to the fascicle and deep aponeurosis (Kawakami et al., 1998) and as the mean of the modified insertion angle of fascicle on the superficial and deep aponeurosis (figure 4.1 C). Table 4.1 represents the angles reported in some of the studies on isometric relative torques in triceps surae.

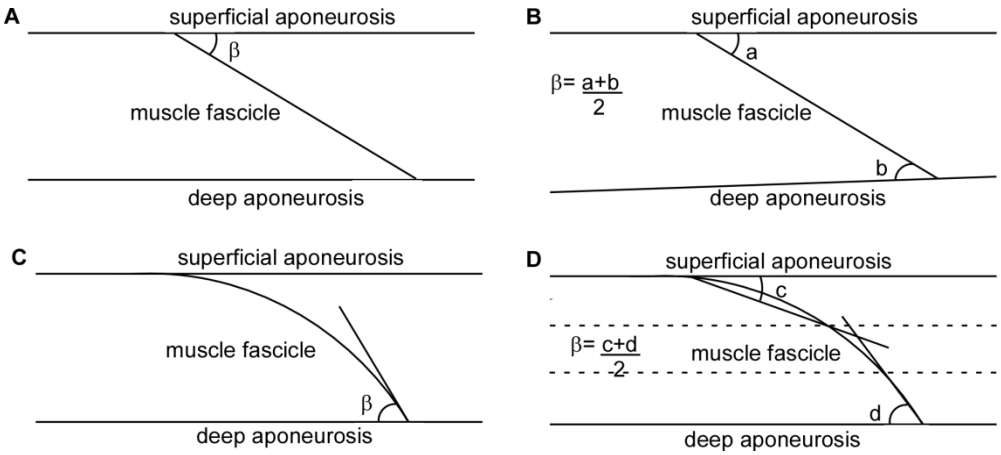

Figure 4.1 ***Schematic drawing of muscle fascicle describing the measurement of pennation angle in the literature. Pennation angle measured as (A) the angle of insertion of fascicle on superficial aponeurosis (B) the mean of the angle of insertion of fascicle on superficial and deep aponeurosis (C) the angle the tangent to fascicle makes with aponeurosis at the intersection of the fascicle with deep aponeurosis (D) the angle between the straight line obtained by joining the point of intersection of fascicle with aponeurosis and the line parallel to aponeurosis and at a distance of* $1/3^{rd}$ *of muscle thickness from aponeurosis. Modified from Kawakami et al., 1998; Maganaris et al., 1998c; Narici et al., 1996 a; Wakeling et al., 2006.***

Table 4.1 ***Pennation angles (β) from medial gastrocnemius (MG), lateral gastrocnemius (LG), and soleus as reported in previous 2D ultrasound studies for isometric relative torques (values are reported as mean ± s.e.m.). A fully extended leg is represented by a knee angle of 180° Negative ankle angles represent plantar flexion, 0° represents neutral ankle angle and positive ankle angles represent dorsi flexion.***

Paper	Muscle	Knee Angle, (°)	Ankle Angle, (°)	β (rest), (°)	β (MVC), (°)
(Kawakami et al., 1998)	MG	135	-15	26 ± 1.6	44 ± 3.2
			0	29 ± 1.6	51 ± 2.4
			15	34 ± 1.6	55 ± 2.0
			30	38 ± 2.0	58 ± 1.6
	LG		-15	13 ± 0.4	21 ± 0.8
			0	14 ± 0.8	25 ± 1.2
			15	15 ± 0.4	29 ± 1.6
			30	16 ± 0.8	34 ± 2.0
	Soleus		-15	19 ± 0.8	33 ± 1.2
			0	22 ± 0.8	39 ± 1.2
			15	25 ± 1.2	45 ± 1.6
			30	29 ± 1.2	49 ± 1.2
(Maganaris et al., 1998c)	MG	90	0	22.3 ± 0.8	42.5 ± 0.9
	LG		0	11.3 ± 0.5	35.0 ± 1.0
	Sol		0	25.0 ± 1.1	40.0 ± 1.3
(Narici et al., 1996a)	MG	180	0	15.8 ± 0.8	-
			60	27.7 ± 0.9	-
			22	17.3 ± 1.1	35.3 ± 1.7

Muscle is a 3D entity and changes shape in 3D in the form of muscle bulging. Muscle thickness has been shown to depend on the relative torque states of the muscle in experimental studies (Maganaris et al., 1998c; Wakeling et al., 2011) and has also been predicted to change with relative torque levels in modeling studies (Azizi et al., 2008; Lichtwark and Barclay, 2010; Otten, 1988; van Leeuwen and Spoor, 1992). Further, the change in thickness is not observed in

all muscles. For example, LG shows an increase up to 40% with relative torque while MG does not show a significant increase in thickness with relative torque (Maganaris et al., 1998c; Narici et al., 1996a). The change in shape of a muscle can change the orientation of the fascicles (Azizi et al., 2008; Wakeling et al., 2011). In 2D ultrasound studies muscle thickness is reported as the distance between aponeurosis in the 2D image plane (aligned with the fascicle plane). However, muscles can change shape in the direction perpendicular to the scanning plane and thus cannot be captured by 2D imaging modality. Muscle can bulge in the direction perpendicular to the fascicle plane, keeping the muscle thickness constant in the fascicle plane despite the changes in muscle belly length. This out-of-plane bulging is predicted to counteract the fascicle rotation (Azizi et al., 2008). Along with bulging, muscles are predicted to undergo 3D changes in shape involving twisting during shortening (Böl et al., 2011), which may further affect the 3D fascicle orientation.

In 2D muscle architecture studies muscle fascicles are considered to be arranged as planes that are called fascicle planes (Kawakami et al., 1998; Lichtwark et al., 2007; Maganaris et al., 1998c; van Leeuwen and Spoor, 1992; 1996). In previous 3D ultrasound studies it has been important to align the imaging plane with the fascicle planes in order to image complete fascicles (Kawakami et al., 1998; Lichtwark et al., 2007; Maganaris et al., 1998c; Benard et al., 2009). However, muscle fascicles may not be aligned in planes, particularly in a muscle with a non-uniform shape. Instead, fascicles may be arranged in non-planar sheets with different sheet orientations occurring across the muscle. These sheets may be considered as a 2D surfaces curved in 3D space, like a bent sheet of paper. This idea is supported by the observation of fascicles arranged in curved sheets in human vastus lateralis (Sejersted et al., 1984). Sejersted and co-workers (1984) referred to this sheet arrangement as fascicle layers and suggested that the fascicle sheets had an onion-like arrangement and observed that the outer sheets were more curved. As discussed above, the muscles may bulge during relative torque in a direction that is perpendicular to the fascicle sheets and so the sheets may bulge leading to a change in the local sheets' orientations. With the arrangement of fascicles in curved sheets, the orientations of fascicles may not lie in one plane and therefore cannot be fully explained in 2D. The fascicles are arranged in sheets in a muscle and it is important to quantify the orientation of the fascicle sheets as this will help understand the 3D function of the fascicles as a group. Huijing and co-workers (1998) have shown that the fascicles transmit force not only to the muscle tendon junction and

aponeurosis but also to alternate pathways involving the neighbouring fascicles. Determination of fascicle sheet orientations along with the fascicle orientations will help in understanding the alternate pathways of force transmission.

Numerous studies on muscle architecture and function have used 2D ultrasound to study the in-vivo changes in fascicle length, pennation angles and curvatures (Fukunaga et al., 1997a; Kawakami et al., 2000; Lichtwark et al., 2007; Maganaris et al., 1998c; Muramatsu et al., 2002; Namburete et al., 2011; Wakeling et al., 2006). Compared to other muscle imaging modalities, ultrasound is portable, less expensive, easier to maintain and use, and there is a potential for it to be used even more in future. In order to obtain accurate measures of pennation angle and fascicle lengths from 2D ultrasound studies it is important to match the orientation of the scanning plane with the fascicle planes (Lichtwark et al., 2007; Kawakami et al., 1998). A typical way of achieving this is to place the probe perpendicular to the skin and find the fascicle plane orientation by rotating the probe until the imaged fascicles appear continuous between aponeuroses (Benard et al., 2009). Many ultrasound studies involve strapping the ultrasound probe onto the skin surface in order to obtain measurements during different relative torque states of muscle (Maganaris et al., 1998c; Namburete et al., 20011; Wakeling et al., 2006). It is important to quantify the changes in the measured pennation angles by keeping the probe orientation fixed relative to the skin or finding the scanning plane for each relative torque level and muscle length.

3D fascicle architecture from dissected rat soleus (Stark and Schilling, 2003) and equine longissimus dorsi (Ritruechai et al., 2008) have shown regional variations in the 3D architecture. Stark and co-workers tracked the fascicles in 3D and reported local pennation angles as the angles of the fascicles with the muscle line of action, while Ritruechai and co-workers reported local orientations of the fascicles in perpendicular planes to obtain a 3D representation of fascicle orientations. There has been a study on formalin-fixed soleus muscle to quantify the fascicle architecture in 3D by dissecting the muscle in different planes and taking photographs of pinned fascicles with spatially calibrated cameras (Agur et al., 2003). A few diffusion tensor magnetic resonance imaging (DT-MRI) and 3D ultrasound studies have also looked at the in-vivo fascicle orientation in 3D. Most of the DT-MRI studies focused on the measurement of the pennation angle from the fascicles tracked in passive muscle (Kan et al., 2008; Lansdown et al., 2007;

Sinha et al., 2006). The 3D ultrasound studies have quantified external muscle architecture features of muscle, such as: muscle length and volume and fascicle architecture from a few fascicles selected in passive muscle (Barber et al., 2009; Fry et al., 2003; Fry et al., 2004; Kurihara et al., 2005; Malaiya et al., 2007). None of the earlier studies have quantified complete set of in-vivo fascicle orientations in 3D for different relative torque levels and muscle lengths.

The purpose of this study was to (1) quantify the 3D fascicle orientation and orientation of fascicle planes across the triceps surae muscles in man, (2) measure changes in orientations for different ankle angles and torque levels, and (3) compare the estimated pennation angles that would be calculated with different selection of scanning planes.

The hypotheses of this study are (1) 3D fascicles orientations are regionalized in each of the triceps surae muscle and vary with change in relative torque level and ankle angle, and (2) pennation angle measurements are affected by the scanning plane orientations.

4.2. Methods

4.2.1. Data collection and experimental design

The purpose of this study was to identify the 3D orientations of fascicles and fascicle sheets in the triceps surae muscles at different ankle angles and torque levels. The muscles were imaged for a relaxed state and during isometric relative torques at a range of ankle angles and torques. Experimental data were obtained from six healthy, athletic male subjects, due to lower fat content in the tissues (than females) which provides better image quality for the scans; subjects were athletic and experienced with specific sporting movements to ensure that stable and constant relative torques could be generated during imaging.

The scanning process was identical to that used in chapter 3 with ultrasound images obtained as video sequences recorded at 20 Hz. Two dimensional (2D) position and orientation information from ultrasound images were transformed to 3D information using the position and orientation of the position sensor attached to the ultrasound probe (chapter 3). Subjects were asked to perform a maximal voluntary contraction, MVC, for each ankle angle and the torque levels were determined relative to the MVC at each ankle angle. Muscles were then scanned for

a fixed knee angle (135°), four ankle angles (-15°, 0°, 15° and 30° relative to neutral) and three torque levels (0, 30%, 60% MVC). The data were not collected beyond 60% of MVC because the scanning times last for two minutes for each trial and it is not possible to sustain these relative torques for that duration. The position of the medial and lateral tibial condyles and the medial and lateral malleoli were obtained using an optical pointer, and later used to define the segmental coordinate system for the lower leg.

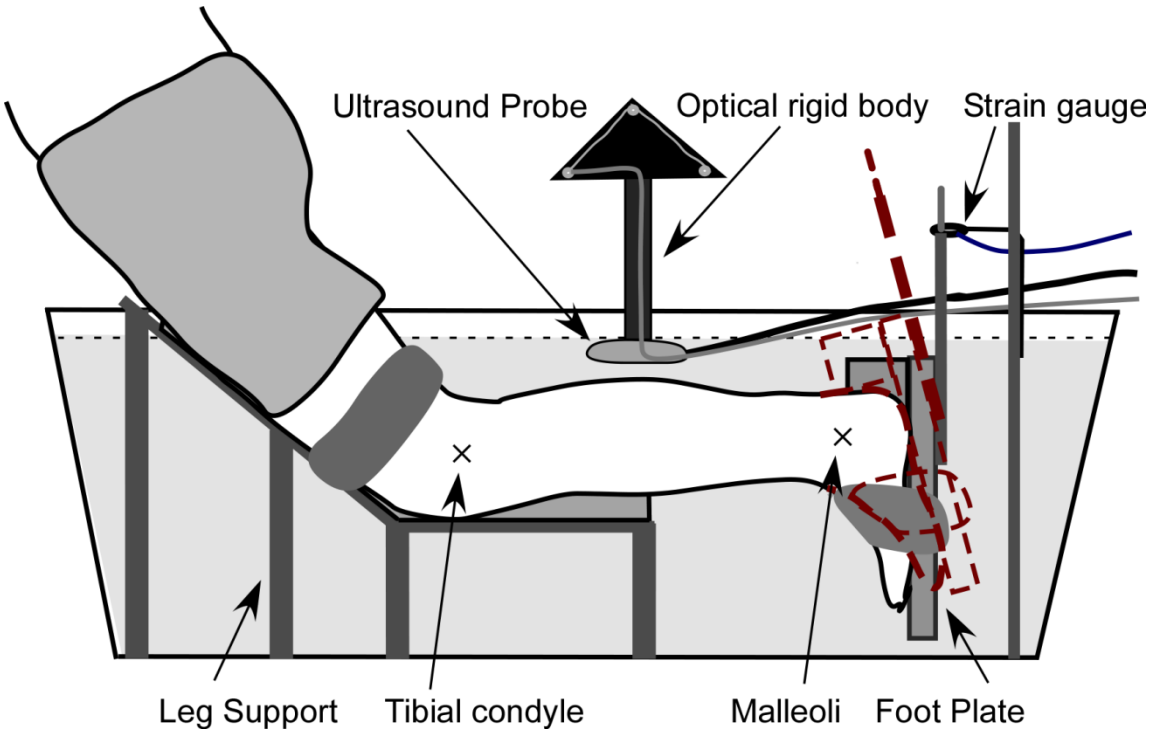

Figure 4.2 ***Schematic representation of experimental setup. Knee was fixed at 135° and ankle angles at -15°, 0°, 15° and 30°. The ankle is shown at neutral 0° position in the bold figure and plantar flexed at 30° in the dotted representation. The torque was measured using the strain gauge and visual feedback was given to the subjects to maintain the torque levels.***

A custom made frame was used to perform the isometric relative torques in a water tank (figure 4.2). The frame had two parts a foot plate to strap the right foot of the subject and a leg support to support the right thigh and maintain a fixed knee angle throughout the experiment. The leg support could be moved in relation to the foot plate in order to adjust to different leg lengths of the subjects. The foot plate was connected to a strain gauge to obtain the ankle torque and visual feedback for torque was provided to the subjects. The ankle torque data was collected

at 2000 Hz via a 16-bin A/D converter (USB-6210, National Instruments, Austin, TX) using LabView software environment (National Instruments, Austin, TX). When the ultrasound started to record it generated a 5V signal that terminated at the last recorded frame. The data from ultrasound, motion capture and strain gauge were synchronized by using this recording pulse generated by the ultrasound system. This recording pulse was later used to select the beginning and end of the data from the motion capture system and strain gauge to correspond these recordings with their time-matched ultrasound images.

4.2.2. Data Analysis

4.2.2.1. Determination of fascicle orientations

Images were processed using the methods described in chapter 2 and chapter 3 to obtain the muscle fascicle orientation in 3D. The muscle volume was divided into voxels of 5×5×5 mm^3 and then a representative fascicle orientation was chosen for each voxel. During the scanning process multiple scans of the calf muscles were obtained from different orientations of the ultrasound probe, resulting in imaged planes with different orientations of the same region. A voxel can contain multiple pixels which may belong to same or different scanning planes. The representative orientation in a voxel was obtained from the weighted mean of the orientations from all the pixels in that voxel. This step was slightly different from the chapter 3. Rather than taking the fascicle orientation from the pixel with the maximum convolution value, a weighted mean of fascicle orientation was considered. The weights were based on the convolution values obtained from the wavelet analysis for a particular pixel (chapter 2) and the distance of the pixel from the center of the voxel (figure 5.2). The weight function for the convolution (w_c) and for the distance (w_d) were given by

$$w_c = Exp\left(-\left(\frac{conv}{conv_0}\right)^2\right) - 1$$

$$w_d = Exp\left(-((x-x_0)^2+(y-y_0)^2+(z-z_0)^2)/_{2\sigma^2}\right)$$

where, $conv$ is the convolution value at a particular pixel, $conv_0$ is maximum convolution value over all the trials for a subject, $\{x, y, z\}$ is the location of the pixel in space, $\{x_0, y_0, z_0\}$ is the

voxel center and σ is the spread of an isotropic Gaussian distribution and was chosen to be 2.5 mm in this case (half-width of the isotropic voxel).

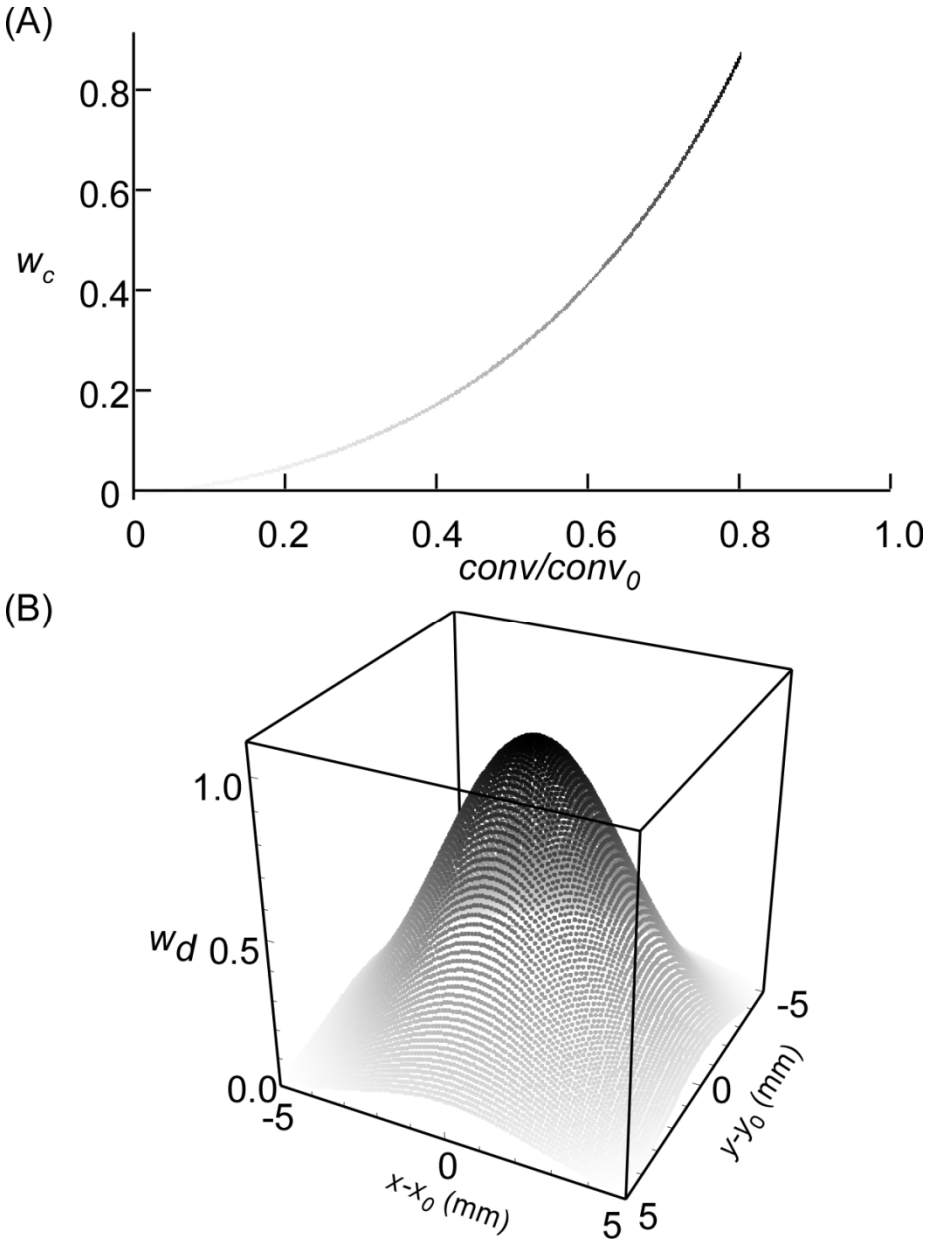

Figure 4.3 ***Functions used to determine the weight factor for convolution value (w_c) (A) and the distance of location of pixel from the voxel center {0,0}(w_d) (B). The intensities of the points represent the weight factors. The function for distance is shown for 2D locations for simplicity; the actual function was based on 3D locations.***

4.2.2.2. Determination of fascicle sheets orientations

The orientations of fascicle sheets were represented by the normal to the sheets. Fascicle sheets were considered to be made of small fascicle planes, contained in the voxels like a curved line and can be obtained by joining small segments of straight lines. As described in section 4.2.2.1, a voxel contained the image planes of different orientations .The ultrasound image represents the fascicle plane when the fascicles appear as long continuous lines in the image (Benard et al., 2009; Kawakami et al., 1998; Lichtwark et al., 2007; Maganaris et al., 1998b). This quality can be quantified by the convolution measures of the images and was used to select the fascicle plane orientation in each voxel (chapter 3). Analogous to the fascicle orientation, the representative orientation for each voxel was obtained as the weighted mean of the orientation of the normals to the fascicle planes lying in that region, with convolution being the weighting factor. The planes were defined to have constant orientation in a voxel region so the weight factor was only based on convolution value and not on the distance.

4.2.2.3. Determination of muscle-based coordinate system

In order to study the regionalization of the orientations, the 3D position for each voxel, the muscle fascicle orientations and the fascicle plane orientations were all transformed from the lab based coordinate system to the muscle based coordinate system as follows. Three major axes x, y and z were determined for the gastrocnemius muscles using eigenvalue decomposition. The major axes correspond to the major anatomical axes of the muscle: the z-axis approximates the length of the muscle, the y-axis approximates the width of the muscle (medial-lateral axis) and the x-axis approximates the depth (deep-superficial axis) of the muscle (figure 4.4 b). The origin of the muscle coordinate system was set at the mean point in the muscle. Due to the semi-cylindrical shape of the soleus (Augur et al., 2003), a different coordinate system was used with its z-axis as the vector joining the mean co-ordinate of the knee joint centers with the mean co-ordinate of the muscle-tendon junction markers, the y-axis along the width of the muscle and the x-axis along the depth of the muscle. The origin of the soleus was taken to be 60% of the total distance between the knee and the muscle tendon junction from the knee because this was almost in the middle of the muscle.

Both the local fascicle orientations and the local fascicle plane orientations were transformed from a Cartesian to a spherical coordinate system (figure 4.4). The 3D orientations that were represented by unit vectors $\{ux,uy,uz\}$ in Cartesian coordinates were transformed to a polar angle β_f $(= cos^{-1}(uz))$ that was the angle between the vector parallel to the local fascicle direction and the z- axis, and an azimuthal angle φ_f $(= tan^{-1}(uy/ux))$ that was the angle between the projection of fascicle in the x-y plane (transverse plane for the muscle) and the x-axis. The polar angle β_f can be considered as the pennation angle for a local segment of the muscle fascicles. The orientations of the normals to the fascicle sheets were similarly represented by β_{fp} and φ_{fp}.

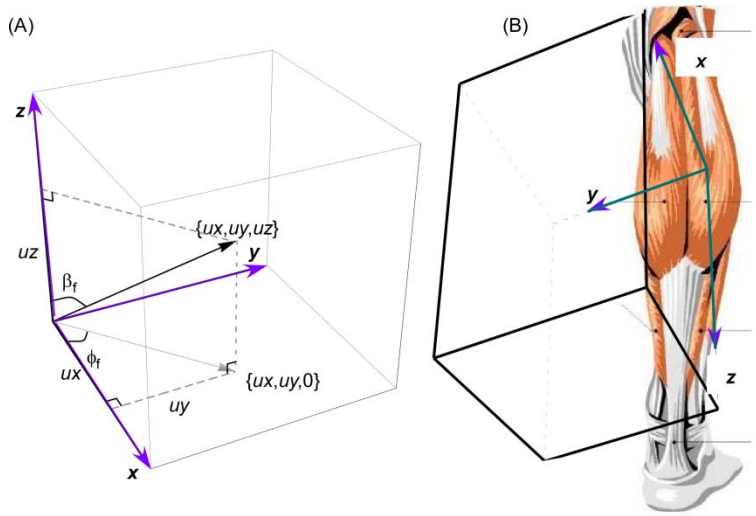

Figure 4.4 ***(A) Representation of the direction cosines of the fascicle orientations {ux,uy,uz} in a spherical coordinate system { β_f, φ_f}. (b) Alignment of the muscle based coordinate system shown for the LG.***

The orientations of the normals to the fascicle sheets were similarly represented by β_{fp} and φ_{fp}. A 90° value for β_{fp} and φ_{fp} represents a plane parallel to the y=0 plane, this plane is parallel to the long axis of the muscle and perpendicular to the width of the muscle. Any change in β_{fp} represents the change in rotation of the plane about the long axis of the muscle and a change in φ_{fp} represents the tilting of the plane.

4.2.2.4. Pennation angle representation

In this study the 3D orientations of fascicles and fascicle sheets were used to simulate the effect of 2D ultrasound scans along different directions in order to compare the pennation angles that would be obtained by different scanning protocols. Ultrasound takes a slice through 3D objects and the structures appearing in the slice represent sections through the 3D object. If ultrasound scans an infinitesimally thin wire, the image will contain a line when the scanning plane contains the wire (or a portion of it) and is parallel to the plane containing the wire. For any other orientation, a point will appear at the intersection of the imaging plane with the wire. If the wire has a finite thickness it can be considered as a thin cylinder. When scanned in a plane parallel to the plane containing the long axis of the cylinder the 3D cylinder will be images as a 2D line of certain thickness parallel to the long axis of the cylinder (figure 4.5 a). For any difference between the orientation of the plane containing the longitudinal axis of the cylinder and the scanning plane, the cylinder will be imaged as an elliptical structure with the major axis inclined to the longitudinal axis of the cylinder (figure 4.5 b,c). The elliptical structure will be line like for small deviations and the length of the imaged section will decrease for larger deviations (figure 4.5).

The ultrasound image contains fascicle structure with finite thickness. In chapter 2 the thickness of the fascicles was up to 5 pixels and hence can be considered as small cylinders in each voxel and the local regions in an image can be considered as the projections of the fascicles in the image plane. The locally projected fascicles are 2D representations of 3D fascicles and may result in a pennation angle different from that measured from the 3D fascicle depending on the position and orientation of the scanning plane.

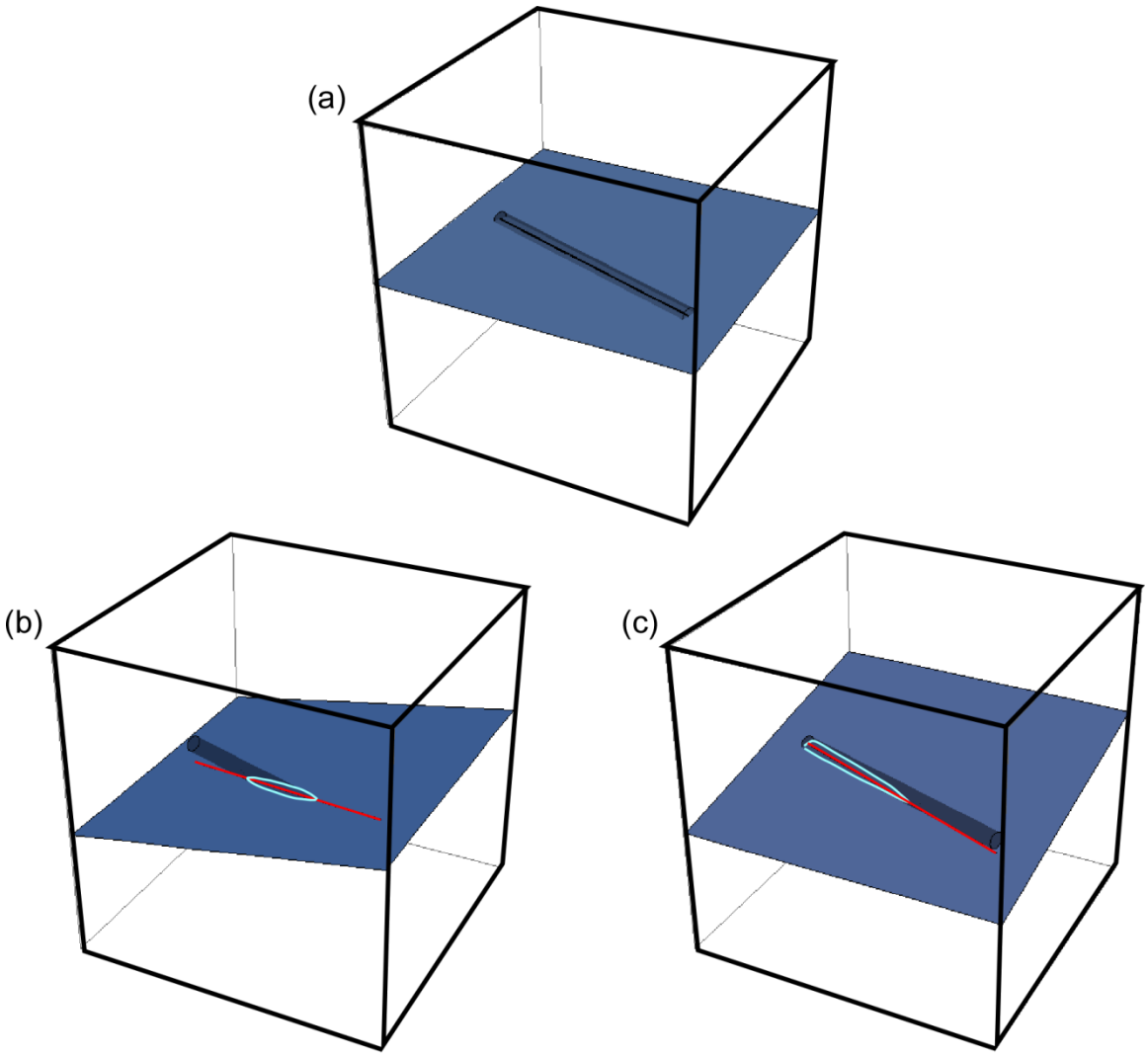

Figure 4.5 ***Representation of ultrasound images through long thin cylinders. The red line represents the orientation of the major axis of projected elliptical structure in 2D imaging plane. The intersection of the cylinder with the image plane is represented by the cyan ellipse. The line is parallel to the orientation of the section of the cylinder obtained in the image. The long axis of cylinder is contained in the z=0 plane. (a) Scanning plane parallel to z=0 plane (a). Scanning plane rotated about x-axis by 10° (b) and scanning planes rotated about y-axis by 10°(c).***

Pennation angle was calculated as the angle the fascicle makes with the z-axis of the muscle based coordinate system. β_f was measured as the angle the fascicle makes with the long axis of the muscle. In a typical 2D ultrasound scan the orientations are measured in the image plane, and in this thesis analogous calculations of the fascicle orientation were made by

projecting the fascicles in the mean fascicle plane. This was done in three different ways: (1) β_f was measured as described in section 4.2.2.1. (2) β_{cfp} was measured as the angle between the long axis of the muscle and the projection of the fascicle in the mean fascicle plane (calculated from the 0% torque level and 0^o ankle angle condition). This is analogous to collecting 2D ultrasound scans with the probe strapped in a fixed position over the muscle for all the trials. (3) β_{vfp} was measured as the angle between the long axis of the muscle and the projection of the fascicle when it was projected in the mean fascicle plane for each trial. This is analogous to adjusting the ultrasound probe to lie in the fascicle plane for each trial. Soleus was bigger in size and more complex in architecture (Agur et al., 2003) so the mean fascicle plane orientations were determined for medial and lateral sides of the soleus and the fascicle orientations were projected in the respective directions.

4.2.3. Statistical Analysis

The muscle was divided into the following regions (figure 4): three along the length of the muscle (z-axis) proximal, central and distal; two along the depth of the muscle (x-axis) deep and superficial; and two along the width of the muscle (y-axis) medial and lateral. General linear model ANOVA was used to test the effects of muscle region, ankle angle and relative torque level on fascicle orientation; with the polar angle and azimuthal angle as the dependent variables, subject identity as random factor, muscle region, ankle angle and relative torque level level as fixed factors. Post-hoc Tukey tests were performed to determine the effects of levels of regions, relative torque levels and ankle angles on the dependent variables. The results obtained were considered significant for p-value <0.05. Mean differences were calculated for the pennation angles calculated in section 4.2.2.4 using matched pair t-test to compare the effect of different scanning protocols.

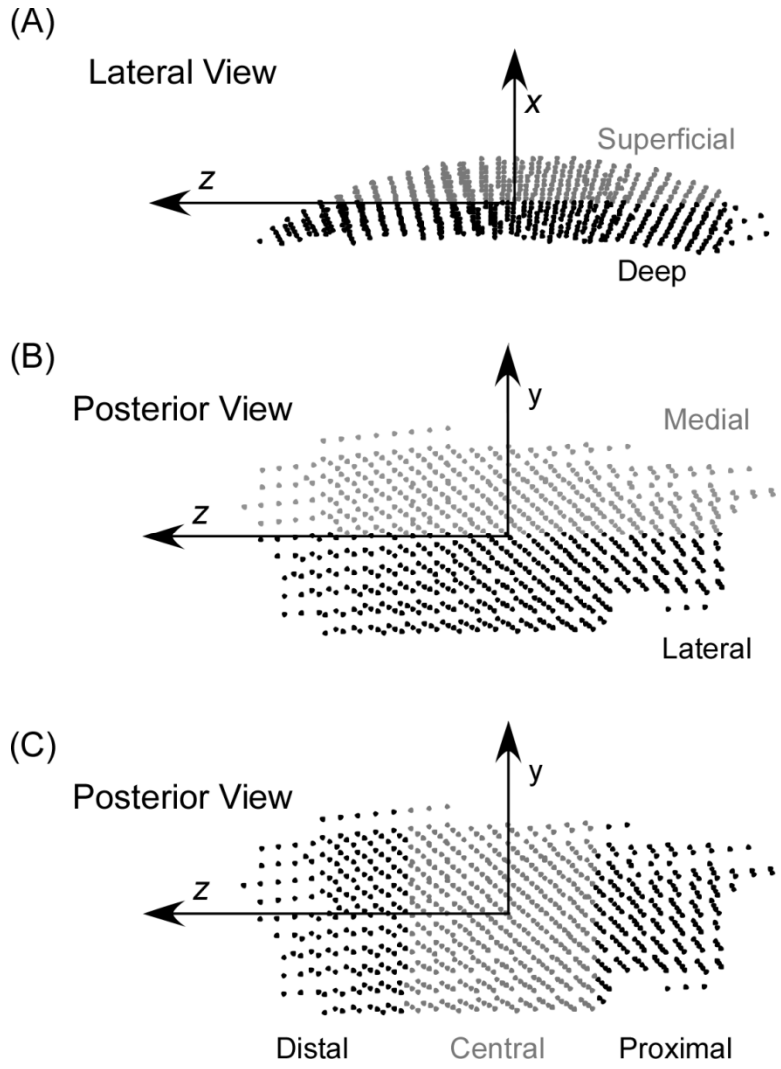

Figure 4.6 ***Representation of the regions into which the muscle was split, viewed from different viewpoints. The axes represent the muscle based co-ordinate system used to assign the positions in the muscle and the dots represent the voxel locations from the lateral gastrocnemius in one subject. The black and grey dots were used to differentiate the regions of the muscle. The lateral view shows the regions along the depth of the muscle (A). Posterior view shows the regions along the width (B) and length of the muscle (C).***

4.3. Results

4.3.1. Regionalization of fascicle orientation and fascicle plane orientation

Both the fascicle orientation and the fascicle plane orientation were regionalized in all three muscles (figure 4.7-4.9). Mean values with their standard errors are reported in table 4.2.

The results from LG are shown in figure 4.7. In LG, the maximum variations in β_f and φ_f were along the length of the muscle. β_f increased from 11.2° to 14.5° and φ_f increased from 96.3° to 99.2° from the proximal to distal end. The orientations of the normals to the fascicle planes changed across the muscle regions with maximum change along the muscle width and there was a greater variation in the φ_{fp} than β_{fp} (less than a degree change across different regions). φ_{fp} decreased from the lateral to medial sides of the muscle from 262.3° to 254.4°.

The results from MG are shown in figure 4.8. Similar to LG, the greatest variations in the fascicle orientations were along the length of the muscle. β_f increased from 11.3° to 19.0° and φ_f increased from 94.2° to 103.4°. The fascicle planes varied in both β_{fp} and φ_{fp}. The biggest variations in β_{fp} were along the length of the muscle with the increase from proximal to distal region from 93.2° to 98.5° and in φ_{fp} were along the width of muscle with the values decreasing from 226.0° to 218.7°.

The results from soleus are shown in figure 4.9. The changes β_f in soleus were similar in magnitude to that in the gastrocnemii muscle but the variation between lateral to medial sides from 12.0° to 7.3° was similar to the change from 10.3° to 7.6° from the proximal to distal ends. The φ_f changed from 95.6° to 124.0° from the lateral to medial region. Similar trends were reflected in the fascicle plane orientations. The φ_{fp} values changed from 70.2° to 111.2° which shows that the tilt in the two sides were such that the planes were almost the mirror-like reflections in the two halves.

Table 4.2 ***Regionalization of fascicle orientation and fascicle plane orientation in the triceps surae muscles. The values reported are mean ± standard error of mean of the orientations of the fascicles (β_f, φ_f) and normal to the fascicle planes (β_{fp}, φ_{fp}) across all the torque levels and ankle angle torques. Approximately 40,000 points were used to calculate the mean and standard error of mean values.***

	Depth		Width		Length		
	Lateral	Medial	Deep	Super	Proximal	Central	Distal
LG							
$ß_{f,}°$	12.41 ± 0.02	12.64 ± 0.02	12.71 ± 0.02	12.33 ± 0.02	11.25 ± 0.02	12.14 ± 0.02	14.54 ± 0.03
$f_{f,}°$	97.85 ± 0.02	96.67 ± 0.02	97.49 ± 0.02	96.97 ± 0.02	96.34 ± 0.02	96.65 ± 0.02	99.22 ± 0.03
$ß_{fp,}°$	93.10 ± 0.03	94.34 ± 0.02	93.73 ± 0.03	93.74 ± 0.02	93.46 ± 0.03	93.58 ± 0.02	94.32 ± 0.04
$f_{fp,}°$	262.27 ± 0.03	254.36 ± 0.06	257.21 ± 0.06	259.25 ± 0.05	257.29 ± 0.09	258.17 ± 0.05	259.14 ± 0.07
MG							
$ß_{f,}°$	14.34 ± 0.02	15.19 ± 0.03	14.90 ± 0.02	14.62 ± 0.02	11.37 ± 0.03	14.14 ± 0.02	19.01 ± 0.03
$f_{f,}°$	98.34 ± 0.02	97.76 ± 0.02	98.42 ± 0.02	97.65 ± 0.02	94.24 ± 0.02	96.93 ± 0.02	103.40 ± 0.02
$ß_{fp,}°$	95.14 ± 0.02	95.09 ± 0.02	95.54 ± 0.02	95.70 ± 0.02	93.16 ± 0.03	95.32 ± 0.02	98.47 ± 0.03
$f_{fp,}°$	226.02 ± 0.05	218.67 ± 0.04	222.42 ± 0.05	222.24 ± 0.04	221.78 ± 0.06	222.53 ± 0.05	222.61 ± 0.06
Sol							
$ß_{f,}°$	12.02 ± 0.02	7.31 ± 0.01	9.43 ± 0.03	8.93 ± 0.01	10.34 ± 0.02	8.73 ± 0.02	7.55 ± 0.02
$f_{f,}°$	95.6 ± 0.12	124.07 ± 0.19	112.20 ± 0.27	113.65 ± 0.15	117.81 ± 0.81	109.60 ± 0.21	111.26 ± 0.25
$ß_{fp,}°$	95.73 ± 0.12	103.93 ± 0.10	94.84 ± 0.13	102.90 ± 0.09	99.17 ± 0.12	103.08 ± 0.14	100.61 ± 0.14
$f_{fp,}°$	70.19 ± 0.09	111.19 ± 0.12	83.50 ± 0.16	100.16 ± 0.11	99.22 ± 0.16	94.84 ± 0.16	92.28 ± 0.17

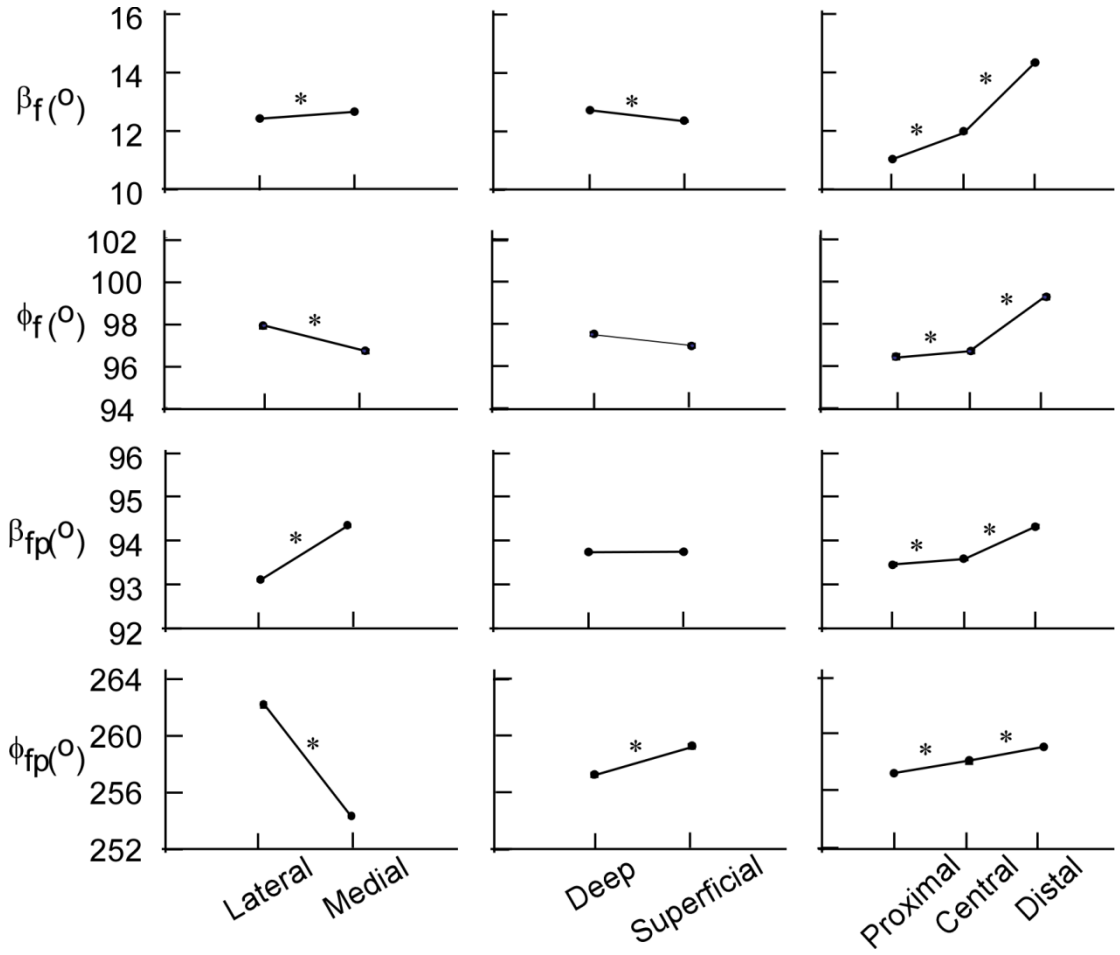

Figure 4.7 ***Regionalization of fascicle orientation and fascicle plane orientation in LG. The dots reported are mean values of the orientations of the fascicle (β_f, φ_f) and normal to the fascicle planes (β_{fp}, φ_{fp}) across all the torque levels and ankle angle torques. Error bars representing standard error of mean are drawn but are not visible in the figures where the error bars are smaller than the dot size. The "*" represents a significant difference between the levels. Approximately 40,000 points were used to calculate the mean and standard error of mean value.***

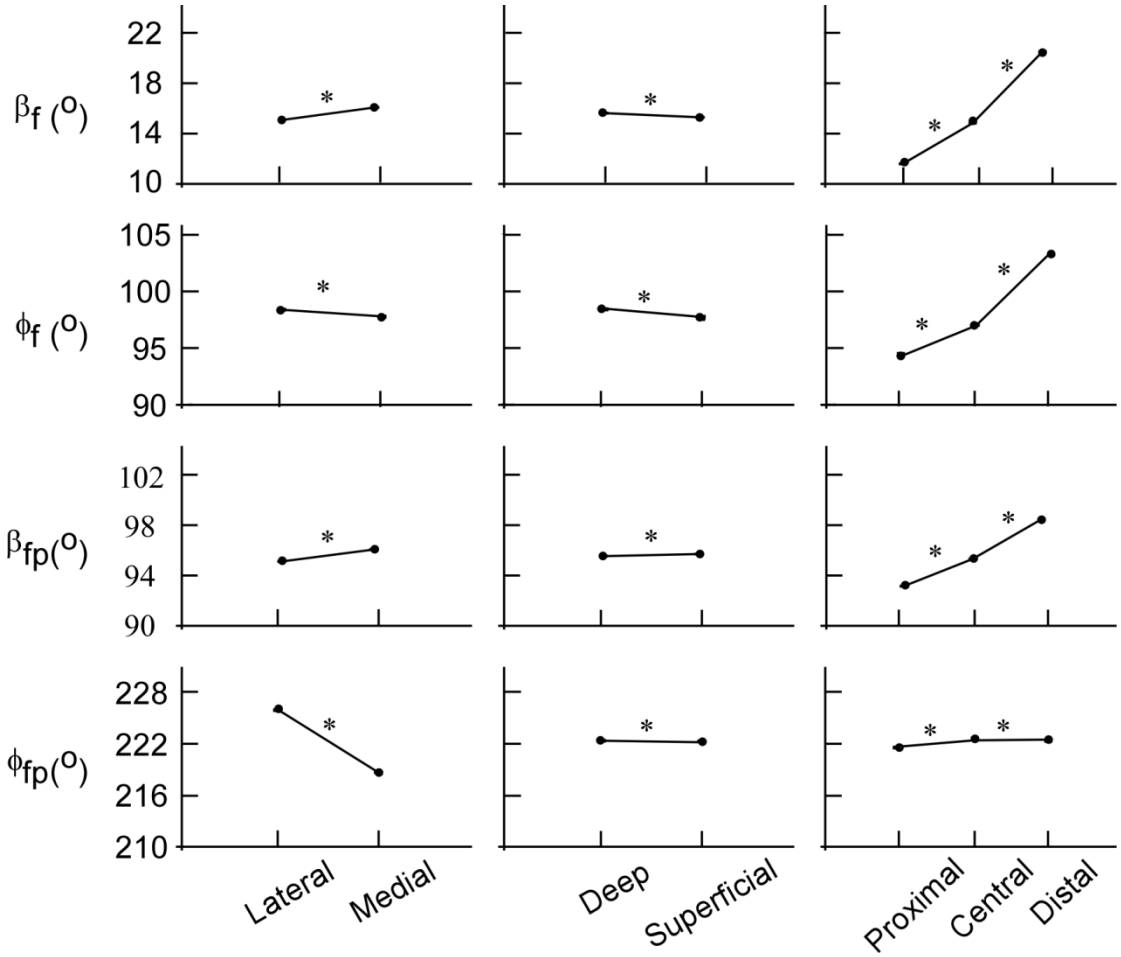

Figure 4.8 ***Regionalization of fascicle orientation and fascicle plane orientation in MG. The dots reported are mean values of the orientations of the fascicle (β_f, φ_f) and normal to the fascicle planes (β_{fp}, φ_{fp}) across all the torque levels and ankle angle torques. Error bars representing standard error of mean are drawn but are not visible in the figures where the error bars are smaller than the dot size. The "*" represents a significant difference between the levels. Approximately 40,000 points were used to calculate the mean and standard error of mean value.***

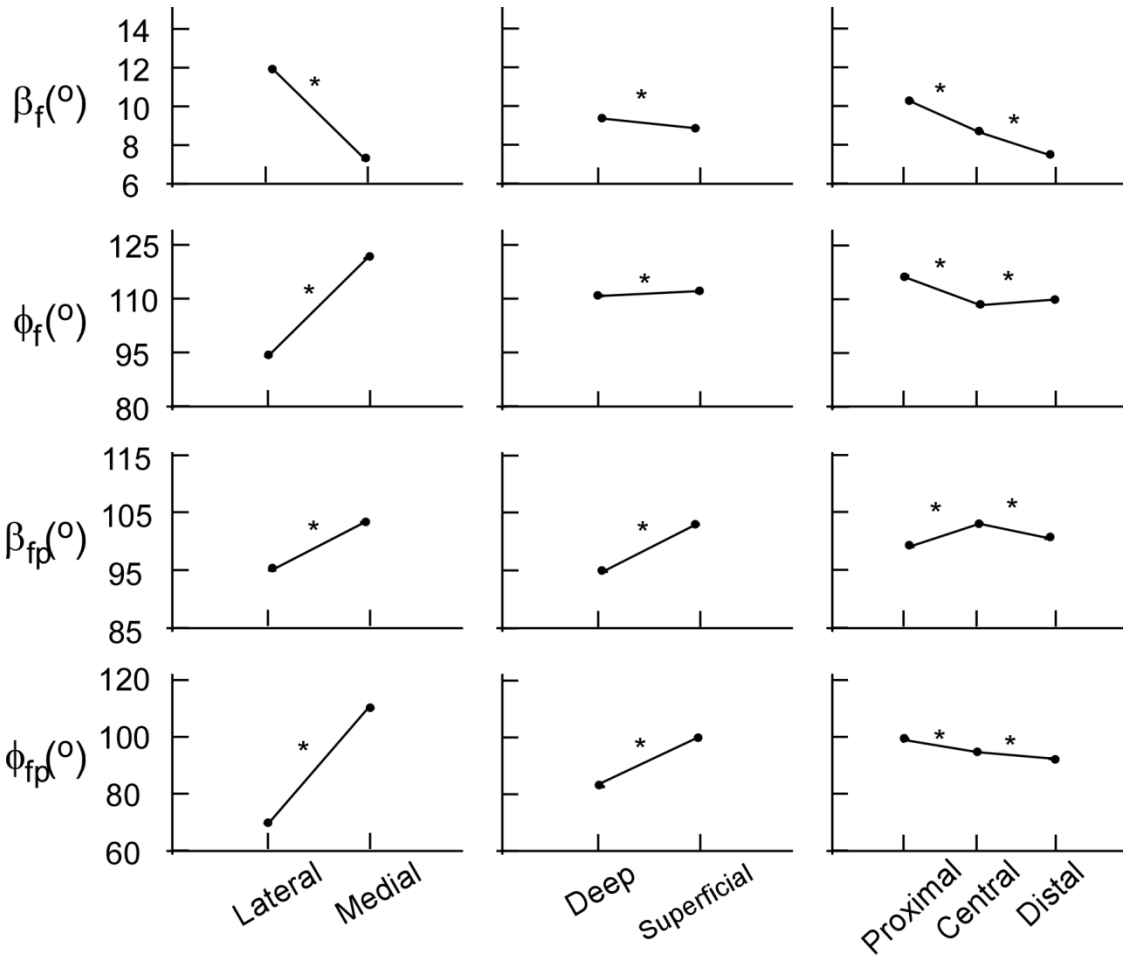

Figure 4.9 ***Regionalization of fascicle orientation and fascicle plane orientation in soleus. The dots reported are mean values of the orientations of the fascicle (β_f, φ_f) and normal to the fascicle planes (β_{fp}, φ_{fp}) across all the torque levels and ankle angle torques. Error bars representing standard error of mean are drawn but are not visible in the figures where the error bars are smaller than the dot size. The "*" represents a significant difference between the levels. Approximately 40000 points were used to calculate the mean and stand error value.***

4.3.2. Effect of torque level and ankle angle on fascicle orientations and fascicle plane orientation

There was a significant effect of the torque level and the ankle angle on LG architecture (figure 4.10). β_f decreased from 13.1° to 11.8° and φ_f decreased from 98.5° to 96.5° with the increase in ankle angle -15° to 0°. β_{fp} increased slightly with increase in ankle angle and φ_{fp}

decreased from ankle angles of -15° to 0° and then increased from 0° to 30°. β_f and φ_f increased slightly (less than a degree) with the increase in torque and φ_f decreased. β_{fp} and φ_{fp} changed less than 0.5° with increases in torque from 0% to 60% MVC.

There was a significant effect of the torque level and the ankle angle on MG architecture (figure 4.11). As the ankle angle increased from -15° to 30° β_f increased from 14.2° to 16.9° and φ_f decreased from 99.1° to 97.9°. β_{fp} increased with increase in ankle angle while φ_{fp} increased from ankle angles of -15° to 15° and decreased from 15° to 30°. With the increase in torque β_f, φ_f β_{fp} and φ_{fp} changed slightly.

There was a significant effect of the torque level and the ankle angle on soleus architecture (figure 4.12). β_f decreased from 9.4° to 8.5° with increase in ankle angle from -15° to 0° followed by an increase from 8.5° to 9.8° with the increase in ankle angle to 30°. φ_f increased from 111.6° to 117.3° with increase in ankle angle from -15° to 0° followed by a decrease to 110.9° with the increase in ankle angle to 30°. β_{fp} increased from 96.2° to 105.3° with increase in ankle angle from -15° to 15° followed by a decrease to 98.7 ° with increase in ankle angle to 30°. φ_{fp} showed statistically significant but very small changes.

There was a significant interaction between ankle angles and torque levels on the fascicle orientation. As shown in figure 4.13, the relation between ankle angle and orientation is altered by torque level. In LG β_f decreased as the ankle angle increased for 0% MVC but for higher torque levels this trend gradually vanished. Furthermore, in MG and soleus there was a greater increase in β_f with ankle angle at higher torque levels. In LG φ_{fp} had an opposite trend with increasing ankle angles for 0% and 60% torque levels.

Table 4.3 ***Mean fascicle orientations and fascicle plane orientations for different ankle angles and torque levels in the triceps surae. The values reported are mean ± standard error of mean of the orientations of the fascicles (β_f, φ_f) and normal to the fascicle planes (β_{fp}, φ_{fp}). Approximately 40,000 points were used to calculate the mean and standard error value.***

	Ankle Angle				Relative Torque		
	-15°	0°	15°	30°	0%	30%	60%
LG							
β_f,°	13.12±0.03	13.08±0.02	12.12±0.03	11.8±0.03	12.45±0.02	12.26±0.02	12.86±0.02
f_f,°	98.58±0.03	97.85±0.03	96.53±0.03	96.05±0.03	97.29±0.03	96.87±0.03	97.54±0.02
β_{fp},°	92.98±0.04	93.00±0.03	93.78±0.04	93.17±0.03	93.86±0.02	93.64±0.03	93.71±0.03
f_{fp},°	258.25±0.07	256.41±0.32	258.41±0.34	259.67±0.07	258.06±0.07	258.57±0.07	257.95±0.06
MG							
β_f,°	14.26±0.03	13.47±0.03	14.52±0.03	16.92±0.04	14.42±0.03	14.71±0.03	15.13±0.03
f_f,°	99.05±0.03	98.37±0.03	97.88±0.03	96.44±0.03	98.17±0.03	97.46±0.03	98.49±0.03
β_{fp},°	94.32±0.03	93.75±0.03	95.59±0.03	99.05±0.03	95.10±0.03	95.30±0.03	96.40±0.03
f_{fp},°	222.51±0.06	220.44±0.06	220.85±0.07	225.66±0.06	221.62±0.05	222.31±0.06	223.03±0.06
Sol							
β_f,°	9.40±0.02	8.49±0.02	8.66±0.02	9.79±0.02	9.30±0.02	8.77±0.02	9.19±0.02
f_f,°	111.65±0.23	117.34±0.26	113.02±0.25	110.87±0.20	108.48±0.21	113.6±0.21	118.18±0.22
β_{fp},°	96.22±0.13	103.13±0.16	105.33±0.16	98.69±0.16	102.58±0.14	101.21±0.13	98.69±0.13
f_{fp},°	91.11±14	103.15±0.24	94.96±0.17	94.98±0.18	93.75±0.15	96.45±0.17	97.86±0.17

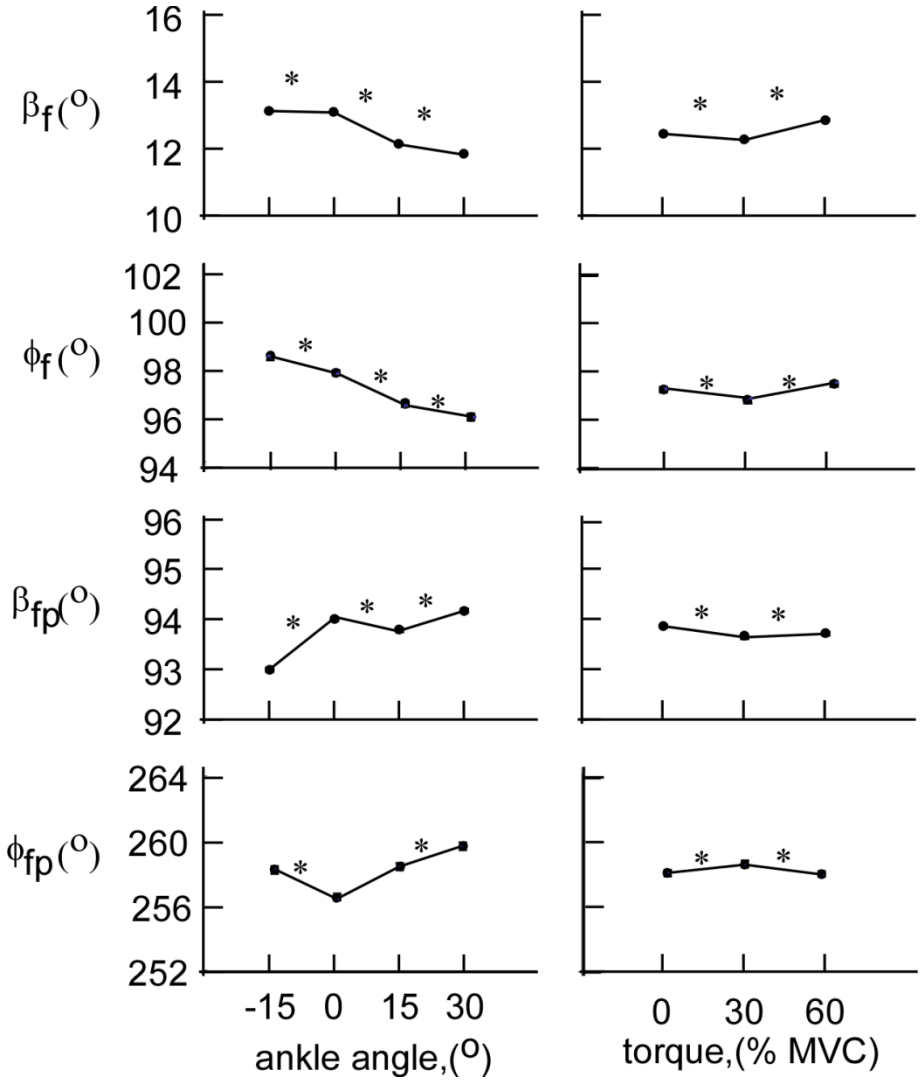

Figure 4.10 ***Effect of ankle angle and torque level on LG fascicle orientation and fascicle plane orientation. The dots reported are mean values of the orientations of the fascicle (β_f, φ_f) and normal to the fascicle planes (β_{fp}, φ_{fp}). Error bars representing standard error of mean are drawn but are not visible in the figures where the error bars are smaller than the dot size. The "*" represents a significant difference between the levels. Approximately 40000 points were used to calculate each value.***

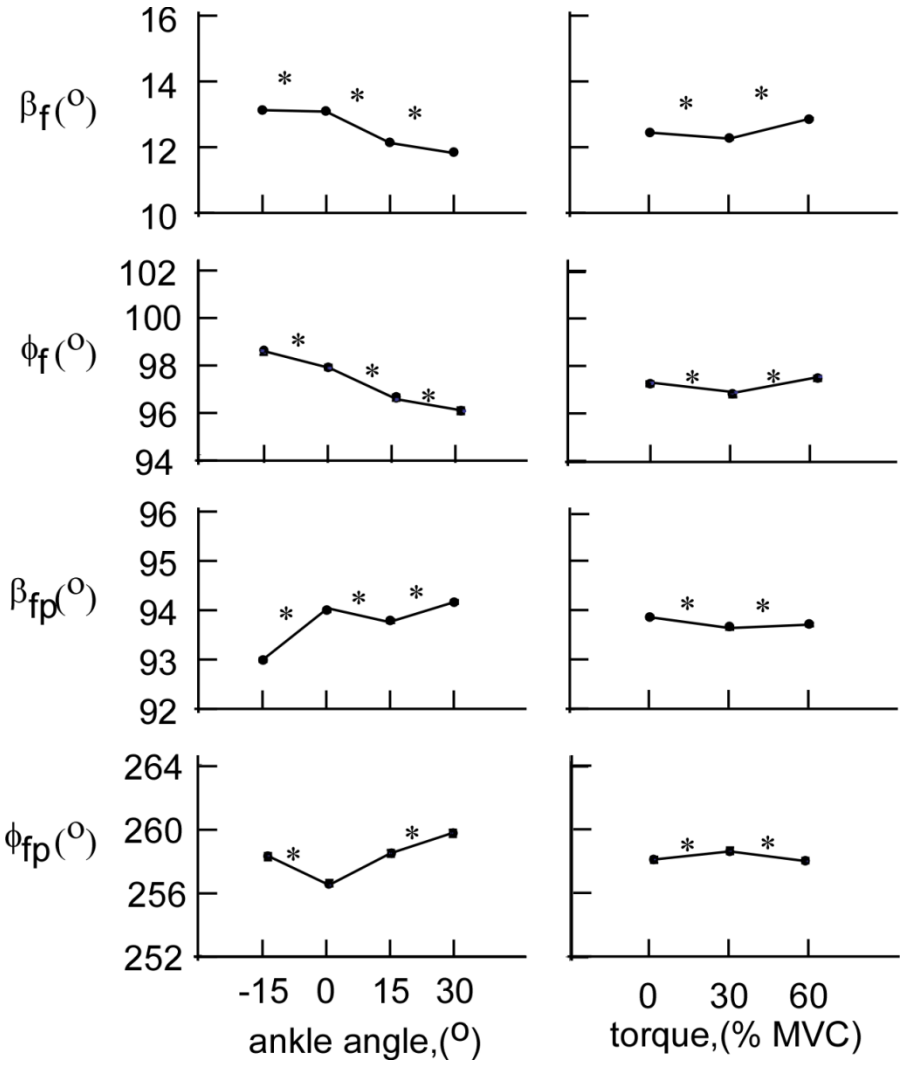

Figure 4.11 ***Effect of ankle angle and torque levels on MG fascicle orientation and fascicle plane orientation. The dots reported are mean values of the orientations of the fascicle*** **(β_f, φ_f)** ***and normal to the fascicle planes*** **(β_{fp}, φ_{fp})**. ***Error bars representing standard error of mean are drawn but are not visible in the figures where the error bars are smaller than the dot size. The "*" represents a significant difference between the levels. Approximately 40000 points were used to calculate the mean and standard error values.***

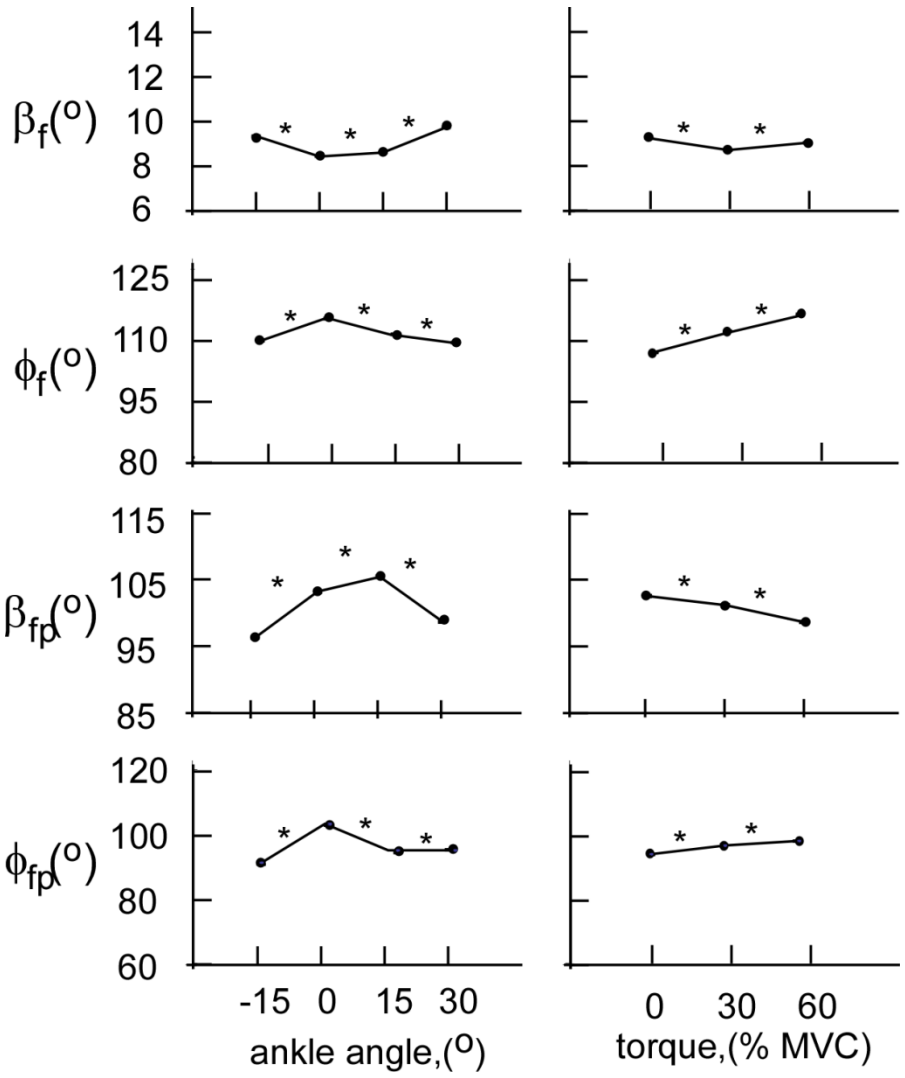

Figure 4.12 ***Effect of ankle angle and torque level on soleus fascicle orientation and fascicle plane orientation. The dots reported are mean values of the orientations of the fascicle (β_f, φ_f) and normal to the fascicle planes (β_{fp}, φ_{fp}). Error bars representing standard error of mean are drawn but are not visible in the figures where the error bars are smaller than the dot size. The "*" represents a significant difference between the levels. Approximately 40000 points were used to calculate the mean and standard error of mean value.***

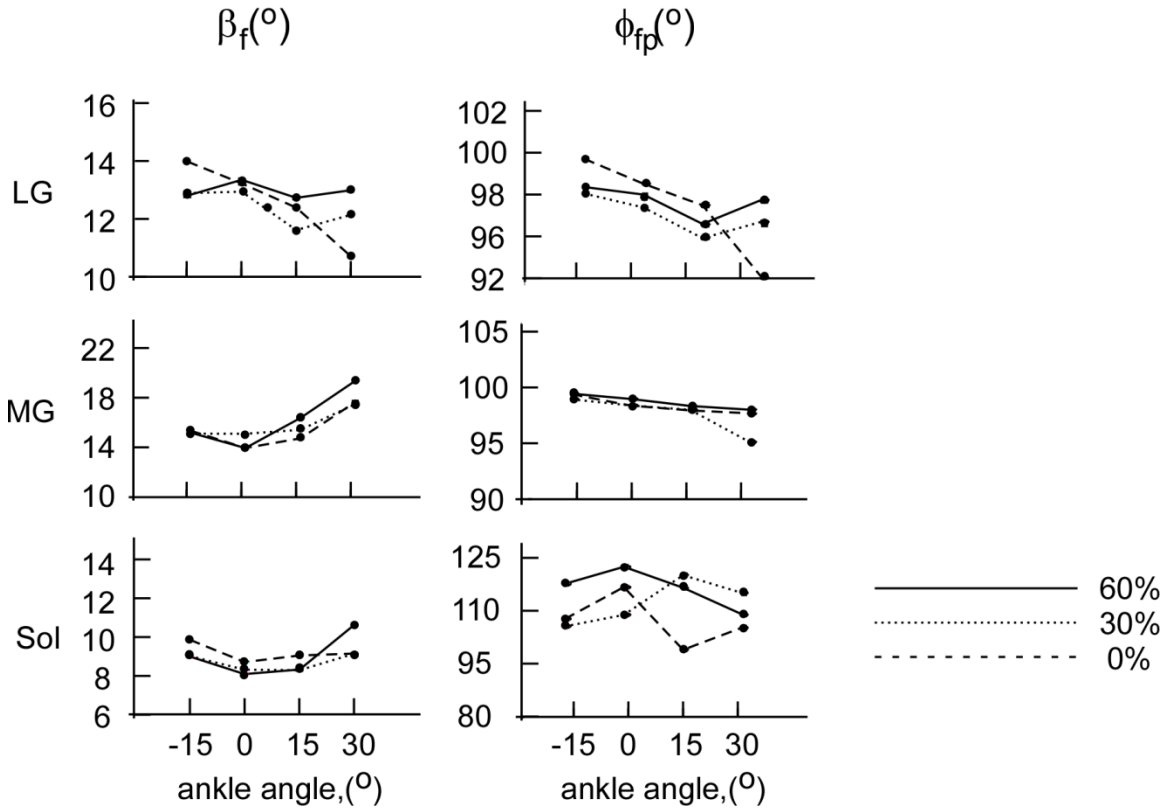

Figure 4.13 ***Effect of torque levels on fascicle orientation and ankle angle relation in triceps surae. The dots reported are mean values of the orientations of the fascicle (β_f, φ_f). Error bars representing standard error of mean are drown but are not visible in the figures where the error bars are smaller than the dot size. Approximately 25,000 were used to calculate the mean and standard error of mean values.***

4.3.3. Effect of orientation of scanning planning on the measured pennation angles

Pennation angle measured from the fascicles (β_f), projected fascicles in a constant fascicle plane (β_{fcp}) and projected fascicles in a variable fascicle plane (β_{fvp}) were different in the three muscles (figure 4.14). The planes of projection are similar to the scanning planes in 2D ultrasound scanning. Both β_{fcp} and β_{fvp} were underestimated in LG and MG compared to β_f by a small value of less than 1°. However, in soleus the mean difference between β_{fcp} and β_{fvp} was 4.5°, β_{fcp} and β_f was 10°, and β_{fvp} and β_f was 14°. The

differences were of similar magnitude across different relative torque levels and ankle angles.

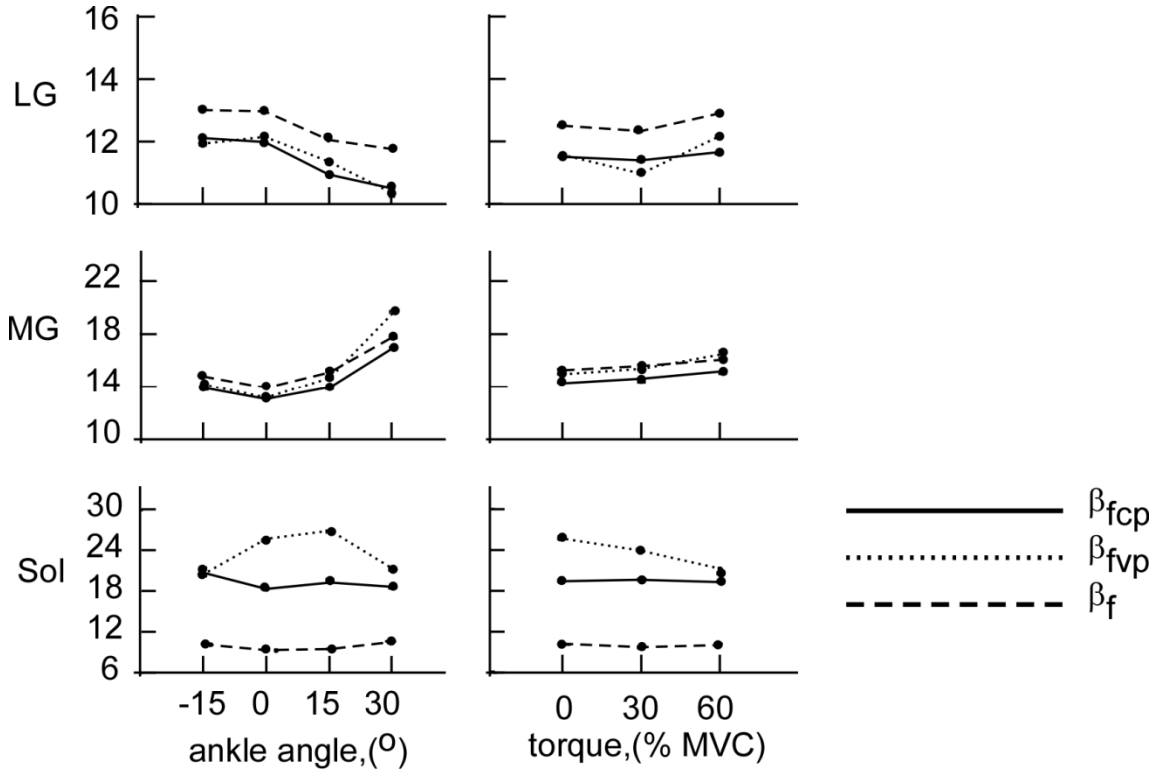

Figure 4.14 ***Effect of scanning plane on the measured pennation angle calculated from 3D fascicle*** **(β_f)**, ***from fascicle projected in a constant fascicle plane*** **(β_{fcp})**, ***and from the fascicle projected in the variable fascicle plane*** **(β_{fvp})**, ***as obtained in each trial corresponding to torque level and ankle angle.***

4.4. Discussion

None of the studies have quantified in-vivo muscle architecture in 3D for different relative torque states of the muscle. Most of the work on in-vivo fascicle architecture has been done using 2D ultrasound (Chow et al., 2000; Fukunaga et al., 1997a; Kawakami et al., 1998; Maganaris et al., 1998a). In this thesis, the 3D quantification was made possible by the novel data collection protocol and the automated processing methods. The major

findings of this study were: (1) muscle fascicle orientations and fascicle plane orientations are regionalized in each of the three muscles of triceps surae, (2) muscle fascicle orientation and the fascicle plane orientation depend on the relative torque level and muscle length, and (3) pennation angle estimates based on 2D ultrasound studies are affected by the orientation of scanning plane.

4.4.1. 3D fascicle orientation

Regionalisation of architecture has been related to regional changes in activation patterns in the pig masseter muscle (Herring et al., 1979). Herring and co-workers had shown a varying line of action of the muscle with a phasic activity pattern and this was co-related to the change in fascicle orientation in the muscle. Regionalisation of activation patterns has previously been reported in cycling studies in the gastrocnemii in man (Wakeling, 2009). There were distal to proximal and medial to lateral changes in activation patterns observed in the muscles and similar patterns have been observed in this study for fascicle orientations (figure 4.7-4.9). Wakeling (2009) had reported greater intensity of electromyography (EMG) in the distal region of LG and MG for high cadence than the proximal region. β_f is greater in the distal region of the muscle (figure 4.7 and 4.8) with a greater increase in β_f at higher torque levels in the distal region compared to that in the proximal region (figure 4.15). A greater value of pennation angle (β_f) allows for greater rotation of fascicles leading to a smaller change in fascicle length (greater gearing) facilitating the high velocity relative torques in an active muscle (Azizi et al., 2008; Wakeling et al., 2011).

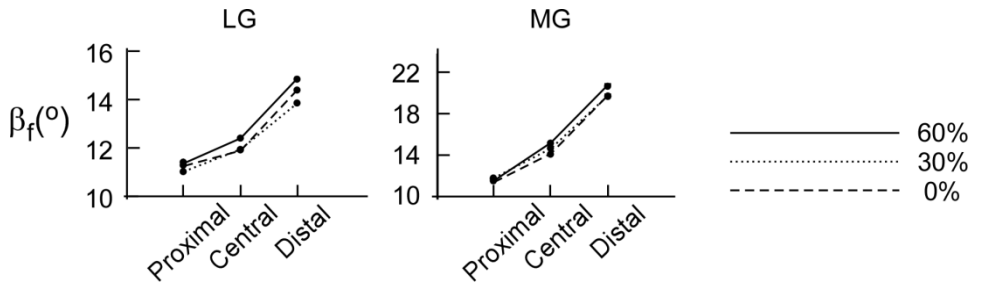

Figure 4.15 Regional differences increase in β_f at different torque levels in LG and MG. Greater β_f was obtained in the distal ends of the muscle.

The fascicle orientation depends on joint angle and relative torque level. Both in MG and soleus β_f increased with increase in joint angle while β_f decreased with increased ankle angle in LG. The decrease in β_f for LG was prominent at 0% relative torque level but was not observed at 60% MVC (figure 4.8). Pennation angle has been shown to increase with increase in joint angle in 2D studies. However, the increase in LG was small with a standard error of similar magnitude compared to a greater increase in MG and soleus. (Fukunaga et al., 1997a; Kawakami et al., 1998; Maganaris et al., 1998c). Further, it has also been shown in some studies that the pennation angle depends on the relative torque level with a greater pennation angles occurring at higher relative torque levels (Kawakami et al., 1998; Maganaris et al., 1998c). β_f increased significantly at greater angles in all three muscles with increasing torque level but not at the lower angles (figure 4.8). A similar trend has been shown for submaximal relative torques in the vastus lateralis, with a significantly greater pennation angle at greater knee angles compared to no change for smaller knee angles (Fukunaga et al., 1997a; Fukunaga et al., 1997b). The changes in β_f may seem different from the previous study in which the pennation angle increased with torque level (Maganaris et al., 1998c), but it has to be noted here that Maganaris and co-workers tested at MVC while in this study the maximum torque level was 60% MVC.

The pennation angle (β_f) has been studied extensively using 2D ultrasound but the azimuthal angle (φ_f) is an important component to describe the 3D orientation of the fascicles and has not been described before. The 3D orientation of muscle fiber

architecture has been quantified in fish muscles and its importance in transmission of force in fish swimming and maintenance of optimal strain rates has been discussed (Gemballa and Vogel, 2002; Kashin and Smolyaniow, 1969). During the very fast startle response in fish, the helical arrangement of white fibers enables optimal strain rates during shortening during startle response compared to extremely large strain rates in longitudinal red fibers (Alexander, 1969; Rome et al., 1988). Helical arrangement can be obtained for a constant polar angle (pennation angle in this study) but varying azimuthal angle. Regional variations in azimuthal angle of fascicles as observed in this study may be due to the partial helical arrangement of fascicles in the muscle and can possibly affect the strain rates of the fascicles.

As has been indicated in previous studies, 3D architecture information is important for 3D muscles models and to understand the force generation in healthy and diseased muscle (Huijing, 2003; Patel and Lieber, 1997). If the regional differences in the muscles are not considered, it will lead to errors in estimation of fascicle lengths and force transmission in the muscle. Muscle force is not just transmitted at the muscle tendon junction rather there are additional pathways for the force transmission (Huijing, 2003). It has been shown in experimental (Huijing et al., 1998) and modeling studies (Riewald and Delp, 1996) that, even after removing the tendon from a muscle, a significant fraction of the force can be transferred to the bone via non muscle-tendinous pathways. The non-tendinous pathways include lateral transmission of force to neighbouring fascicles, epimysium (the connective tissue surrounding the entire muscle) and to neighbouring muscles.

Pennation angle measurements are useful to study the transmission of force to aponeurosis or the muscle tendon junction while azimuthal angle will provide information for the lateral transmission of forces. 3D orientation will be helpful to understand the mechanism of this fascicular transmission of intramuscular force. This will also be important for clinical treatments involving manipulation of force transmission pathways like tendon transfer surgeries and aponeurotomy (cutting the aponeurosis of muscle perpendicular to longitudinal axis).

4.4.2. Fascicle plane orientations and effect of scanning plane on pennation angle measurements

Fascicle sheet orientations were represented by the orientation of the normal to the fascicle planes in each voxel. Fascicle plane orientations (β_{fp}, φ_{fp}) are architectural parameters which have not been explored in the past. Fascicle plane orientation is important to understand the arrangement of fascicles as a group and will have implications to the spread of force to the neighbouring fascicles. Larger variations were observed in φ_{fp} than β_{fp} in each of the three muscles, which means that the fascicle planes stay at a similar angle relative to the long axis of the muscle but the changes occur in the tilt direction of the sheets with the maximum change being observed along the width of the muscle (medial to lateral sides of the muscle).

Sejerested and co-workers (1984) have reported curved fascicle layers with higher curvature of the outer fascicle sheets in the human vastus lateralis and have suggested that all the layers would take up the curvature of the bone at high levels of relative torques. In this study, the fascicle plane orientations were not uniform across the muscle, which indicates that the fascicles may not be arranged in planar surfaces rather they were arranged in curved sheets. Further, in soleus, the φ_{fp} indicate that the fascicle plane orientations from the medial and lateral sides of the muscle are almost the mirror images of each other. Agur and co-workers (2003) had shown in human cadavers that the soleus is divided by a septum in the middle of the muscle and fascicles insert on the aponeurosis as well as the septum. The mirror image configuration of fascicle sheets further supports that observation. It is important that in 2D ultrasound scans of soleus that care is taken to scan the fascicles in the correct plane.

The fascicle plane orientations have implication to the 2D ultrasound scanning protocol. As has been identified in previous ultrasound studies, it is important to scan the fascicles in the fascicle planes (Benard et al., 2009; Kawakami et al., 1998). The pennation angles that would be estimated from different scanning planes differed by less than a degree in the gastrocnemii and the trends of change in pennation angle with force and ankle angle were same in spite of the small magnitude differences. It can be

concluded from these results that both scanning protocols, i.e. strapping the ultrasound over the muscle for different force and joint angle trials or finding a new fascicle plane for each trial, would result in similar results. However, larger differences in the estimated pennation were found between the different scanning planes in soleus: this can be attributed to a greater change in the fascicle plane orientations with ankle angle and torque levels in the soleus than in the gastrocnemii and greater variation in the architecture across the muscle. Due to larger variation in architecture across the muscle the errors obtained by projecting in a mean fascicle plane would be greater for the soleus. This is relevant to the 2D scanning studies because when a muscle contracts it bulges and this can change the position of the scanning plane relative to the muscle fascicles leading to errors in the pennation angles. It is thus important to optimize the ultrasound probe orientation for different relative torque levels in the muscles with complex architecture like the soleus.

4.5. Conclusions

In conclusion, this study quantified the 3D muscle architecture in the triceps surae and related the architectural properties to the ankle joint angle and joint torque. The determination of fascicle plane orientation has important implications not just in 3D muscle architecture and function but also in the way that 2D measurements of architectural parameters are made. The regionalisation of 3D architecture in both the fascicle orientations and the normals to the fascicle planes imply that the fascicles and fascicle sheets may be curved in 3D. Chapter 5 is based on the regional variations in 3D fascicle curvature in the triceps surae muscle.

5. 3D curvature in the triceps surae muscle

5.1. Introduction

Muscle fascicle curvature is an important architectural parameter related to the muscle function and is important to maintain the mechanical stability of the muscle (Muramatsu et al., 2002; Namburete, 2011; Otten, 1988; van Leeuwen and Spoor, 1996). Curvature is the measurement of the deviation of a structure from being flat. Curved fascicles exert pressure on the concave side and contribute to the intramuscular pressure when under tension and balance the pressure due to the aponeurosis (Otten, 1988; van Leeuwen and Spoor, 1992). Intramuscular pressure increases with the increase in force and is regionalized in the muscle (Sejersted et al., 1984). Sejersted and co-workers (1984) have shown that the curvature increases linearly with increase in distance from the fascia in the vastus lateralis muscle. Two dimensional (2D) modeling studies have shown that the whole muscle shape, the fascicle stress and the fascicle curvatures affect the pressure distributions in the muscle (van Leeuwen and Spoor, 1992 and 1996).

In 2D studies where the fascicles are considered linear for the purpose of estimating their length, ignoring the fascicle curvature can result in an underestimation of fascicle lengths by 6% (Muramatsu et al., 2002). The fascicle curvatures can also affect the transmission of force. The force transmitted by a linear fascicle along the main axis of the muscle is the product of the fascicle force and the cosine of the angle of attachment to the aponeurosis, and there would be no pressure differential across the fascicle. On the other hand, in a curved fascicle, a part of its tension contributes to the pressure development on the concave side of the curve (Heukelom et al., 1979).

Muscle fascicle curvature is related to the relative torque state of the muscle and the muscle length. In a 2D ultrasound study, Muramatsu and co-workers (2002) have shown increase in fascicle curvature at higher relative torque levels and with increase in ankle angle from a dorsiflexed to a plantarflexed state during MVC. The curved fascicles were considered as part of a circle and the curvature was measured as the inverse of the radius of that circle. Increases in fascicle curvature of up to 10 m^{-1} were found with increase of force from rest to MVC, however curvature did not change with joint angle for passive conditions. Further, the intramuscular pressure is related to the fascicle curvature. Intramuscular pressure increases with relative torque state of the muscle and depends on the muscle length. Three dimensional (3D) curvature may also change with the increase in relative torque state of the muscles and muscle length.

Muscle fascicle curvature has been studied in a rat model using muscle dissections (Stark and Schilling, 2003), 2D mathematical modeling (Otten, 1988; van Leeuwen and Spoor, 1992), and 2D ultrasound studies in man (Muramatsu et al., 2002; Namburete, 2011; Namburete et al., 2011; Wang et al., 2009). In the rat study, regional variations in curvature were reported in the muscles (Stark and Schilling, 2003). Similarly, in the studies in man, Muramatsu and co-workers (2002) reported fascicle curvature from each of the distal, central and proximal region of the muscle and have shown varying values of curvature with concave side towards the deep aponeurosis across the MG. Namburete and co-workers (2011) measured the curvature values across the muscle region in a scan and reported S-shaped fascicles with convex side up in the superficial region, convex side down in the deeper region and very small curvature in the central region. Not much work has been done on the 3D curvature of the fascicles except a DT-MRI study on passive tibialis anterior (Heemskerk et al., 2011). The curvature values increased from 2 to 5 m^{-1} with dorsiflexion from 30° to -15° in the superficial region of the muscle and the regional variations were of 1 m^{-1}. Stark and Schilling (2003), Namburete and co-workers (2011) and Heemskerk and co-workers (2011) used Frenet–Serret formulas to quantify the curvature from 2D ultrasound scans of dissected section of the muscle in rat, human gastrconemius, and DT-MRI images of human tibialis anterior results. Heemskerk and co-workers reported the curvature magnitudes but did not

report the direction of bending of curves. This latter parameter is important as it indicates the direction of the pressure gradient across the fascicles, with higher pressures on the concave side of the fascicles.

Three dimensional (3D) fascicle curvatures have not been quantified for contracting muscles before due to lack of adequate methods. The calculation of curvature requires the 3D orientations of segments fascicles in the muscle region. The orientation grids obtained in chapter 4 made it possible to track the segments of fascicles to obtain the regional curvature values.

The results in chapter 4 showed that the orientations of normals to the fascicle planes were not uniform across the muscle and this indicated that the fascicles may be arranged in curved sheets. This is also supported by the observation of curved fascicle sheets in the vastus lateralis muscle in man (Sejersted et al., 1984). Sejersted and co-workers (1984) reported that the fascicle sheets were more curved in the outer sheets and predicted that with an increase in muscle force the curvature of the fascicle sheets would increase leading to a uniform curvature that matched that of the underlying bone. This could lead to medial-to-lateral differences in the curvature values. This has never been quantified before due to lack of information on the structure of fascicle sheets. The 3D information on fascicle sheets orientations obtained from chapter 4 now makes it possible to quantify the curvature of the fascicle sheets.

The purpose of this study was to quantify (1) the 3D curvature of the fascicles across the muscle and study the changes in curvature at different relative torque states and muscle lengths, and (2) the curvature of the fascicle sheets in a transverse section through the center of the muscle.

The hypotheses of this study are (1) fascicles are curved in the muscle with non-uniform curvature across the muscle, (2) 3D fascicle curvatures increase with increase in contraction state of the muscle and the muscle length, and (3) fascicle sheets are curved in the muscle with a regionalization in the sheet curvature between the medial and lateral regions.

5.2. Methods

The data collected in chapter 4 were used to determine the curvature values in this study. Three dimensional (3D) voxel grids with voxel size 5×5×5 mm containing local 3D position and orientation of the fascicles and the fascicle sheets, as obtained in chapter 4, were used to calculate the local fascicle curvatures and fascicle sheet curvatures.

5.2.1. Determination of 3D fascicle curvature

The trajectories of the fascicle segments were tracked using the Fibre Assignment by Continuous Tracking (FACT) approach such that the fascicle segment would be propagated on a continuous coordinate system (Jiang et al. 2006; Mori & van Zijl 2002). The tracking started from the center p_0 of a particular voxel v_0 in the direction of the fascicle orientation at v_0 to obtain the p_1 at a distance of 9 mm p_0 (the point p_1 may not lie at the center of a voxel). At p_1, the tracking direction was changed to that of voxel v_1 and the same procedure was repeated to obtain the third point p_2 (figure 5.1). These local trajectories were defined by the coordinates of the points p_0, p_1 and p_2, and were equivalent to 18 mm of length. The distance between voxel centers of two diagonally adjacent voxels is 8.67 mm, and in order to make sure that the adjacent points were obtained in separate voxels, the tracked segment length was chosen to be 9 mm. The 5×5×5 mm voxel size was further based on the size of the spread of the wavelet used to calculate the local orientations in the 3D image (chapter 2).The wavelet grid size was 39×39 pixels equivalent to 6.09×6.09 mm, however the intensity of the wavelets in the grids falls to zero close to the edges (figure 2.3) so the voxel size was chosen to be 5×5×5 mm.

The coordinates of the points p_0, p_1 and p_2 were then parameterized to create a second order parametric function in 3D, $r(p)$. The curvature κ_c for the fascicle at the location p_1 in the middle of the tracked fascicle segment was calculated using Frenet-Serret formulas (Stark & Schilling 2010),

$$\kappa_c(p) = \frac{|\dot{r}(p) \times \ddot{r}(p)|}{|\dot{r}(p)|^3}$$

where $r(p)$ is a representation of the position vector of the fascicle trajectory in the Euclidean space as a function of pixel location (i.e. $r(p) = \{x(p), y(p), z(p)\}$) and $\dot{r}(p)$ and $\ddot{r}(p)$ were the first and second derivatives of this function. The direction of curvature is obtained as the normal to the curve ($N(p)$) at the point p_1, and is given by

$$N(p) = \frac{\ddot{r}(p)}{|\ddot{r}(p)|}$$

$N(p)$ was a 3D unit vector, and similar to the fascicle orientations (figure 4.2), was represented in spherical coordinates by polar angle (β_c) and azimuthal angle (φ_c).

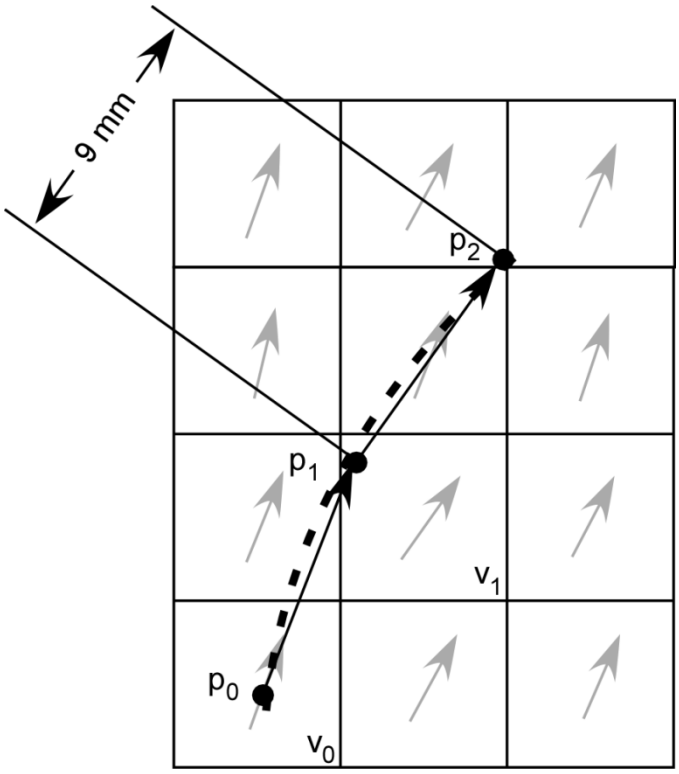

Figure 5.1 ***2D representation of a tracked fascicle segment with the squares representing the voxels in the grid and arrows represent the fascicle orientation in the voxels. The tracking started at p_o in the orientation at v_o to obtain p_1 at a distance of 9 mm from p_o. p_2 was obtained in the direction of orientation in v_1 and at a distance of 9 mm from p_1. The dotted line represents the second degree fit function. The tracking was perfomed in a 3D grid, the 2D drawing is for simplicity. (Figure modified from Mori & van Zijl 2002)***

5.2.2. Determination of fascicle sheet curvature

Muscle fascicles are arranged in sheets separated by connective tissue in the muscle. In 2D ultrasound and 2D modeling studies, the fascicles are assumed to be arranged in planes. However, due to the shape of the muscle, the fascicles may not be arranged in planes, rather they may exist in curved sheets. The curvature of the fascicle sheet in the longitudinal plane is reflected in the fascicle curvature. However, the curvature of the sheets in the transverse plane depends on the arrangement of the fascicles in fascicle sheets rather than the fascicle curvature. In order to study this, the fascicle

sheet curvature was obtained for a transverse plane through the muscle at the center of the belly (z = 0 in the muscle based co-ordinate system). When a transverse section is taken through the muscle it forms a 2D plane that intersects with the fascicle sheets. These intersections appear as lines in the plane (figure 5.2), with the lines being curved for curved fascicle sheets or straight for planar fascicle sheets.

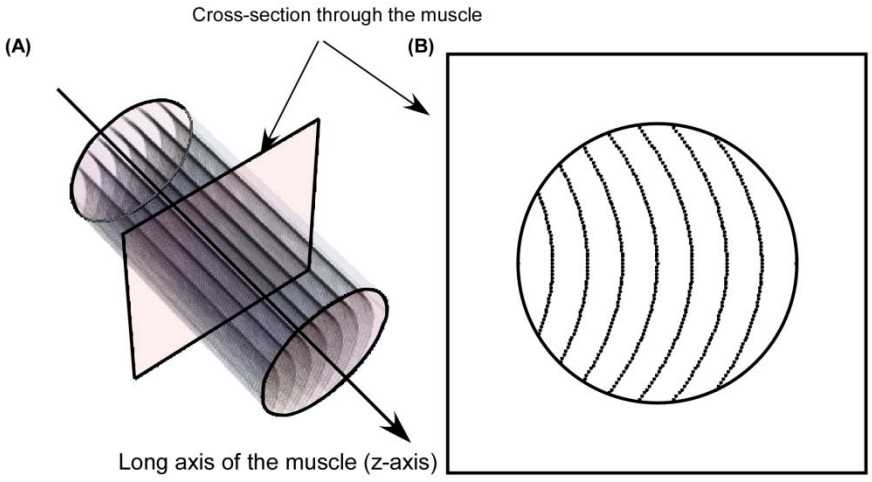

Figure 5.2 ***Schematic representation of curved fascicle sheets in a muscle (A) and a transverse plane containing edges of the fascicle sheets through the muscle (B).***

The transverse plane through the muscle contained the position and orientation information of fascicle sheets contained in the local 3D voxels. There were not many voxels with their center location exactly lying on z = 0 pane (figure 5.2 B) leading to insufficient points to track the boundaries of fascicle sheets. In order to resolve this problem, the orientation value at any point reached during tracking was obtained as the weighted average of the distance of the voxels from a required pixel in the transverse plane. Nearest neighbourhood was defined in terms of the voxels included by the weighting function with the center of the neighbourhood located at the point reached

during tracking. The weight factor (w_d) was a Gaussian interpolation function of a distance of the voxel center from the required pixel in the transverse plane:

$$w_d = exp\left(-((x-x_0)^2+(y-y_0)^2+(z-z_0)^2)/_{2\sigma^2}\right)$$

where $\{x, y, z\}$ is the location of pixel in space and $\{x_0, y_0, z_0\}$ is the voxel center and σ is the spread of a Gaussian kernel and was chosen to be 0.7 mm in this case.

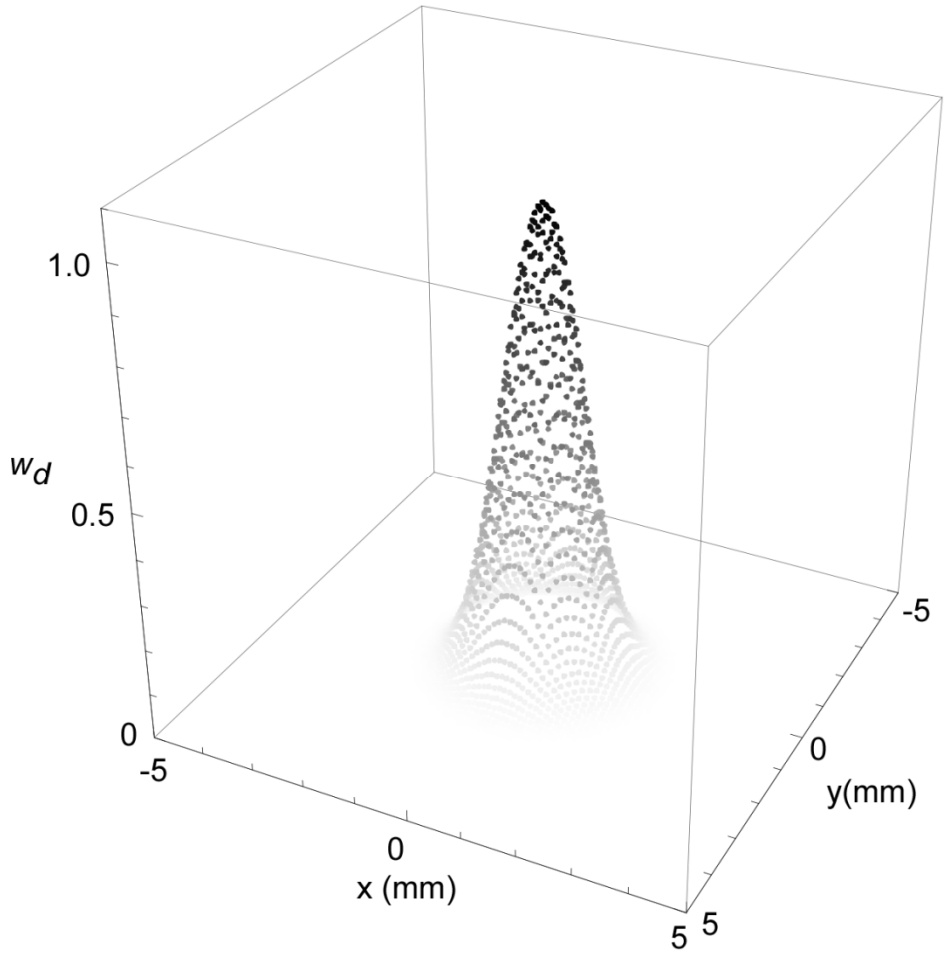

Figure 5.3 ***Weight factors used to obtain the orientation for a pixel located at (0,0). For simplification the weight factors are shown for 2D points. The same function was used to obtain the weight factors in 3D. The intensity of the points indicates the weight factors and the x and y axis represents the coordinate values in mm.***

The edges of the fascicle sheets in the transverse plane (z=0) were tracked using the methods similar to those described in section 5.2.1. The tracking of the fascicle sheet edges were not restricted to three points (as for fascicles) rather were tracked until the aponeuroses were reached. The tracked points were obtained at a distance of 5 mm from the initial point in the direction of the local fascicle plane orientation at the initial point. The local orientation at the new point reached was calculated as the weighted average of the orientation based on the nearest neighbourhood centered at that point. In order to quantify the curvature of fascicle sheets seed points were selected at x = 0 and fascicles were tracked in both directions from the seed point and the value of the curvature was reported at the middle of the tracked fascicle sheet edge. The curvature magnitude and direction were calculated by using the above methods. Since these measurements were made in 2D in the transverse plane, the fascicle sheet curvature was reported by magnitude of the curvature (κ_{fsc}) and azimuthal angle of the normal to the curve (φ_{fsc}).

5.2.3. Statistical Analysis

Muscle region was divided into the following regions: three along the length of the muscle (z-axis) proximal, central and distal, two along the depth of the muscle (x-axis) deep and superficial and two along the width of the muscle (y-axis) medial and lateral. General linear model ANOVA was used to test the effects of muscle region, ankle angle and relative torque level on fascicle curvature and orientation of the normal to the curve fascicle curvature, polar angle and azimuthal angle as the dependent variables, subject identity as random factor, muscle region, ankle angle and relative torque level as fixed factors. Post-hoc Tukey tests were performed to determine the effects of levels of regions, relative torque levels and ankle angles on the dependent variables. The results obtained were considered significant for p-value <0.05.

Fascicle sheet curvatures were obtained for the transverse plane at z = 0 and the plane was divided into medial and lateral regions to test the regional differences in fascicle sheet curvature. General linear model ANOVA was used to test the effects of muscle region, ankle angle and relative torque level on the fascicle sheet curvatures and the orientation of the normals to the curve; fascicle sheet curvature and azimuthal angle were the dependent variables, subject identity as random factor, muscle region, ankle angle and relative torque level as fixed factors. Post-hoc Tukey tests were performed to determine the effects of levels of regions, relative torque levels and ankle angles on the dependent variables. The results obtained were considered significant for p-value <0.05.

5.3. Results

5.3.1. Regionalization of fascicle curvature

Fascicle curvatures were distributed non-uniformly in each of the three muscles (figure 5.4-5.6). Mean values with their standard errors are reported in table 5.1. The regional variations in β_c were small compared to those in variations in φ_c in all the three muscles. The β_c values were close to 90° indicating that the normal to the fascicle curves were perpendicular to the long axis of the muscle.

The results from the lateral gastrocnemius are shown in figure 5.4.The largest variations in κ_c were along the length of the muscle and the depth of the muscle. Along the length of the muscle the central region had a lower κ_c (3.3 m^{-1}) than the proximal (4.6 m^{-1}) and distal ends (4.1 m^{-1}). Along the depth of the muscle κ_c was higher in the deeper layers (4.1 m^{-1}) than the superficial layers (3.5 m^{-1}) of the muscles. The largest variations in φ_c were along the long axis of the muscle with the values increasing from the proximal to the distal end from 163.5° to 214.0°. The φ_c values show that the curves were facing the medial side in the proximal end and the lateral side in the distal end.

The results for the medial gastrocnemius are shown in figure 5.5. The largest variations in κ_c were along the length of the muscle and the width of the muscle. κ_c increased from the medial to the lateral sides from 4.2 m^{-1} to 5.2 m^{-1}, decreased slightly from the proximal end (4.5 m^{-1}) to the central region (4.4 m^{-1}) followed by an increase in the distal end (5.2 m^{-1}) of muscle. φ_c was greater than 200° across the whole muscle indicating that the curves were facing the lateral side.

Results from soleus are shown in figure 5.6. The largest variations in κ_c were along the length of the muscle and the depth of the muscle. κ_c increased from the medial to the lateral sides from 4.1 m^{-1} to 5.7 m^{-1}, decreased slightly from the proximal end (4.3 m^{-1}) to the central region (4.0 m^{-1}) followed by an increase in the distal end (4.7 m^{-1}) of the muscle. The largest variations in φ_c were along the width of the muscle with 175.4° in the lateral side and 205.6° in the medial side, indicating that the curves were facing the medial side in the lateral side of the muscle and facing the lateral side in the medial side of the muscle.

Table 5.1 ***Regionalization of fascicle curvatures across the three muscles. The values reported are mean ± standard error of mean of curvature magnitude (κ_c) and direction of normals to the curve in terms of polar angle (β_c) and azimuthal angle (φ_c) across all the torque and ankle angle torques. Number of data points used to calculate the mean and standard error of mean values were approximately 40,000.***

	Width		Depth		Length		
	Lateral	Medial	Deep	Superficial	Proximal	Central	Distal
LG							
κ_c,m^{-1}	3.78 ± 0.02	3.83 ± 0.02	4.12 ± 0.25	3.51 ± 0.02	4.63 ± 0.04	3.28 ± 0.02	4.13 ± 0.03
ß$_c$,°	91.79 ± 0.06	92.33 ± 0.06	91.60 ± 0.06	92.55 ± 0.06	89.73 ± 0.08	92.04 ± 0.06	93.60 ± 0.08
f$_c$,°	193.10 ± 0.61	198.60 ± 0.58	190.88 ± 0.69	201.08 ± 0.59	163.49 ± 0.98	197.74 ± 0.59	213.96 ± 0.72
MG							
κ_c,m^{-1}	4.19 ± 0.02	5.23 ± 0.02	4.62 ± 0.02	4.77 ± 0.02	4.49 ± 0.03	4.41 ± 0.02	5.22 ± 0.03
ß$_c$,°	93.82 ± 0.05	92.75 ± 0.06	92.94 ± 0.05	93.07 ± 0.05	90.73 ± 0.06	93.43 ± 0.06	95.16 ± 0.08
f$_c$,°	215.05 ± 0.43	210.94 ± 0.45	210.04 ± 0.43	216.46 ± 0.45	198.45 ± 0.62	218.50 ± 0.48	217.38 ± 0.54
Sol							
κ_c,m^{-1}	4.13 ± 0.01	4.66 ± 0.02	4.56 ± 0.02	4.21 ± 0.01	4.33 ± 0.02	4.04 ± 0.02	4.74 ± 0.02
ß$_c$,°	90.03 ± 0.03	92.34 ± 0.04	9 0.69 ± 0.04	91.49 ± 0.04	90.55 ± 0.04	92.30 ± 0.04	90.39 ± 0.05
f$_c$,°	175.37 ± 0.32	205.56 ± 0.37	188.69 ± 0.36	190.50 ± 0.34	181.05 ± 0.47	204.25 ± 0.41	182.11 ± 0.40

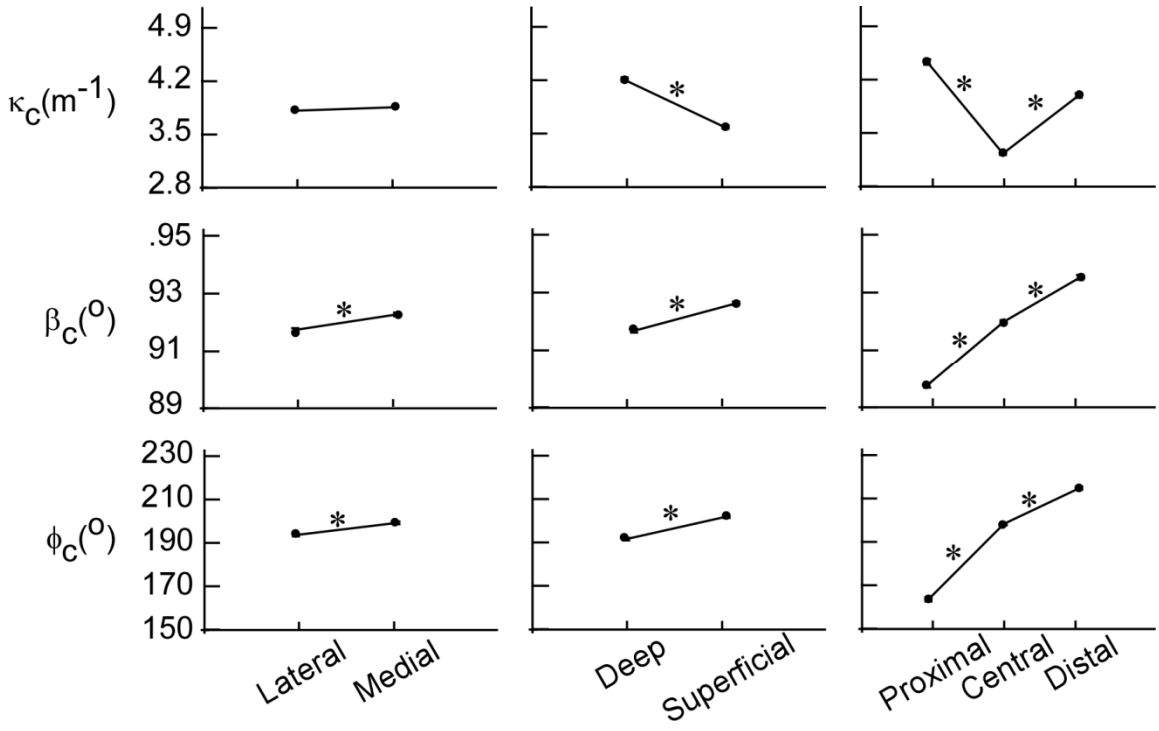

Figure 5.4 ***Regionalization of fascicle curvature in LG. The dots represent the mean values of fascicle curvature magnitude (κ_c) and direction of curvature in terms of polar angle (β_c) and azimuthal angle (φ_c) across all the torque and ankle angle trials. Error bars representing standard error of mean are drawn but are not visible in the figures where the error bars are smaller than the dot size. The "*" indicates a statistically significant change between adjacent regions. Approximately 40,000 points were used to calculate the mean and standard error of mean values.***

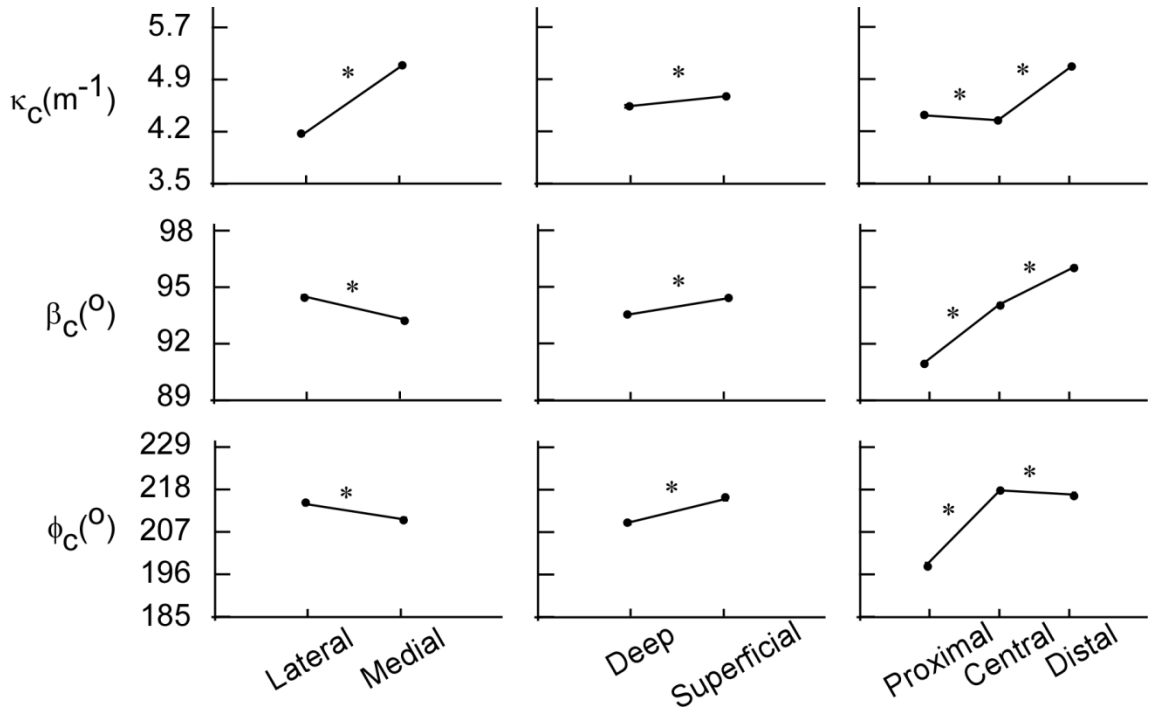

Figure 5.5 ***Regionalization of fascicle curvature in MG. The dots represent the mean values of fascicle curvature magnitude (κ_c) and direction of curvature in terms of polar angle (β_c) and azimuthal angle (φ_c) across all the torque and ankle angle trials. Error bars representing standard error of mean are drawn but are not visible in the figures where the error bars are smaller than the dot size.. The "*" indicates a statistically significant change between adjacent regions. Approximately 40,000 points were used to calculate the mean and standard error of mean values.***

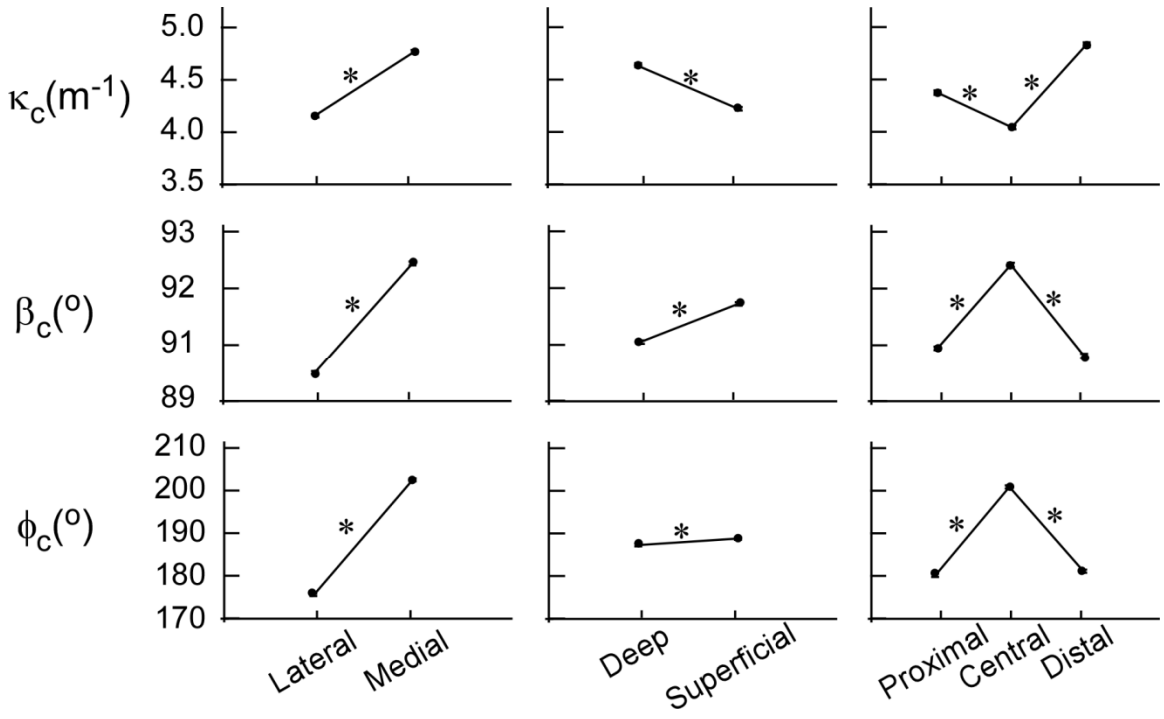

Figure 5.6 ***Regionalization of fascicle curvature in soleus. The dots represent the mean values of fascicle curvature magnitude (κ_c) and direction of curvature in terms of polar angle (β_c) and azimuthal angle (φ_c) across all the torque and ankle angle trials. Error bars representing standard error of mean are drawn but are not visible in the figures where the error bars are smaller than the dot size The "*" indicates a statistically significant change between adjacent regions. Approximately 40,000 points were used to calculate the mean and standard error of mean values.***

5.3.2. Effect of torque level and ankle angle on fascicle curvature

There was significant effect of ankle angle and relative torque level on the fascicle curvature in all three muscles (table 5.2, figures 5.7-5.9).

The general trend was a higher value of κ_c with decrease in ankle angle from 0° to -15° and an increase at greater dorsiflexion. κ_c was significantly greater at a relative torque level of 60% MVC than the lower relative torque levels. β_c changed significantly but with very small magnitude (less than 1° in each muscle) between the ankle angles and

relative torque levels for all three muscles. The changes in φ_c with change in angle (10°) and relative torque levels (4°) were small compared to that obtained across the muscle regions (50°).

There was a significant interaction between ankle angles and torque levels on the fascicle curvatures. As shown in figure 5.10 the increase in κ_c with increase in torque level was greater at 30° ankle angle the increase was lower at the -15° (figure 5.10).

Table 5.2 ***Effect of relative torque level and ankle angle on muscle fascicle curvature. The values reported are mean ± standard error of fascicle curvature magnitude (κ_c) and direction of normal to curve in terms of polar angle (β_c) and azimuthal angle (φ_c) across the whole muscle. Approximately 40,000 points were used to calculate the mean and standard error of mean values.***

	Ankle Angle				Relative Torque		
	-15°	0°	15°	30°	0%	30%	60%
LG							
κ_c,m^{-1}	3.93 ± 0.03	3.58 ± 0.03	4.02 ± 0.03	3.70 ± 0.03	3.72 ± 0.03	3.67 ± 0.03	4.01 ± 0.03
ß$_c$,°	91.81 ± 0.09	92.57 ± 0.09	92.55 ± 0.08	91.35 ± 0.08	92.04 ± 0.07	92.13 ± 0.07	92.05 ± 0.07
f $_c$,°	191.30 ± 0.85	196.79 ± 0.84	202.31 ± 0.85	193.06 ± 0.82	198.45 ± 0.75	195.44 ± 0.73	194.10 ± 0.71
MG							
κ_c,m^{-1}	4.69 ± 0.03	4.17 ± 0.02	4.99 ± 0.03	4.9 ± 0.03	4.56 ± 0.02	4.52 ± 0.02	4.97 ± 0.02
ß$_c$,°	93.35 ± 0.08	93.46 ± 0.07	92.97 ± 0.07	93.42 ± 0.08	93.47 ± 0.07	92.93 ± 0.07	93.49 ± 0.07
f $_c$,°	209.91 ± 0.60	216.14 ± 0.63	211.97 ± 0.64	214.63 ± 0.63	214.71 ± 0.55	210.73 ± 0.54	213.77 ± 0.53
Sol							
κ_c,m^{-1}	4.62 ± 0.02	4.06 ± 0.02	4.39 ± 0.02	4.41 ± 0.02	4.36 ± 0.02	4.26 ± 0.02	4.51 ± 0.02
ß$_c$,°	91.04 ± 0.05	91.04 ± 0.05	91.28 ± 0.05	90.58 ± 0.05	91.11 ± 0.04	91.21 ± 0.04	91.00 ± 0.05
f $_c$,°	194.77 ± 0.47	186.69 ± 0.50	189.42 ± 0.47	186.18 ± 0.54	191.34 ± 0.43	189.01 ± 0.43	188.60 ± 0.43

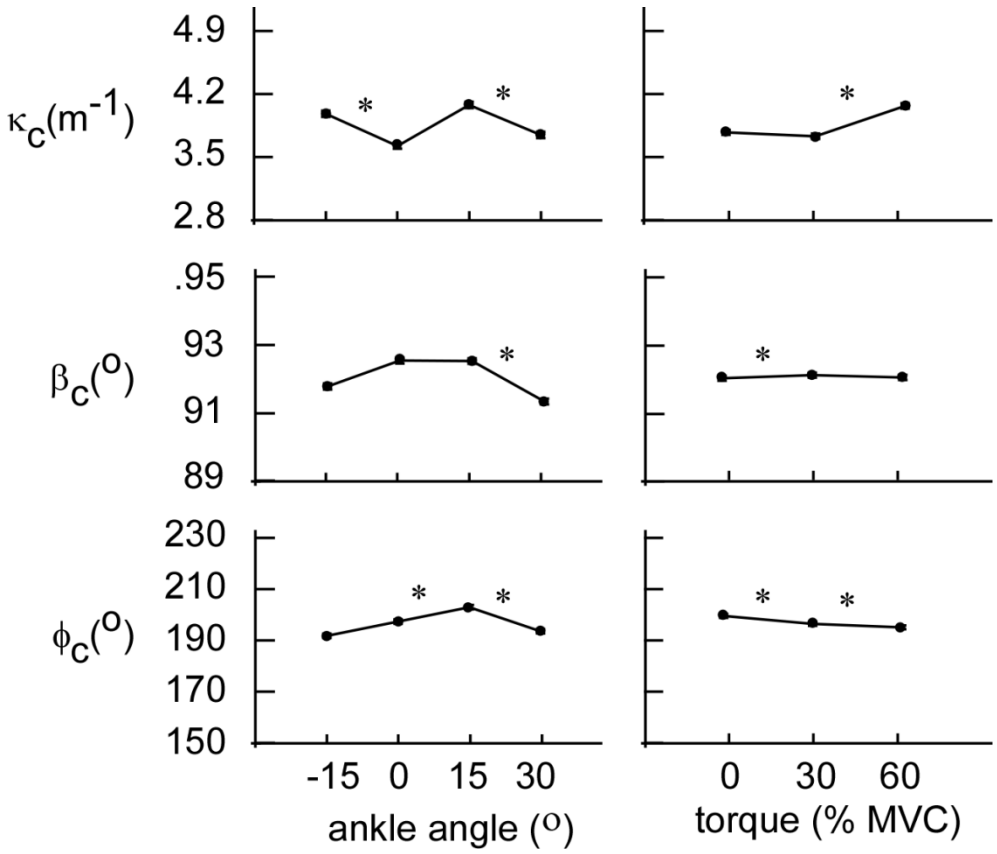

Figure 5.7 ***Effect of torque levels and ankle angle on muscle fascicle curvature in LG. The dots represent the mean values of fascicle curvature magnitude (κ_c) and direction of curvature in terms of polar angle (β_c) and azimuthal angle (φ_c) across the whole muscle. Error bars representing standard error of mean are drown but are not visible in the figures where the error bars are smaller than the dot size. The "*" indicates a statistically significant change between adjacent regions. Approximately 40,000 points were used to calculate the mean and standard error of mean values.***

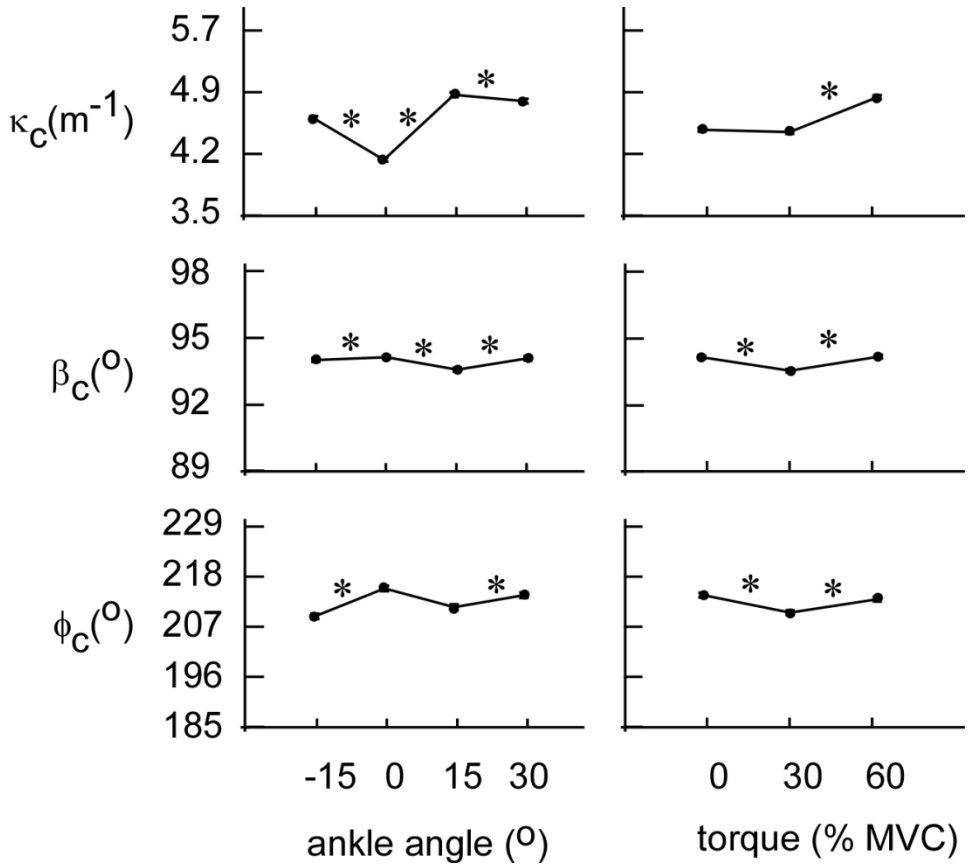

Figure 5.8 ***Effect of torque levels and ankle angle on muscle fascicle curvature in MG. The dots represent the mean values of fascicle curvature magnitude (κ_c) and direction of curvature in terms of polar angle (β_c) and azimuthal angle (φ_c) across the whole muscle. Error bars representing standard error of mean are drawn but are not visible in the figures where the error bars are smaller than the dot size. The "*" indicates a statistically significant change between adjacent regions. Approximately 40,000 points were used to calculate the mean and standard error of mean values.***

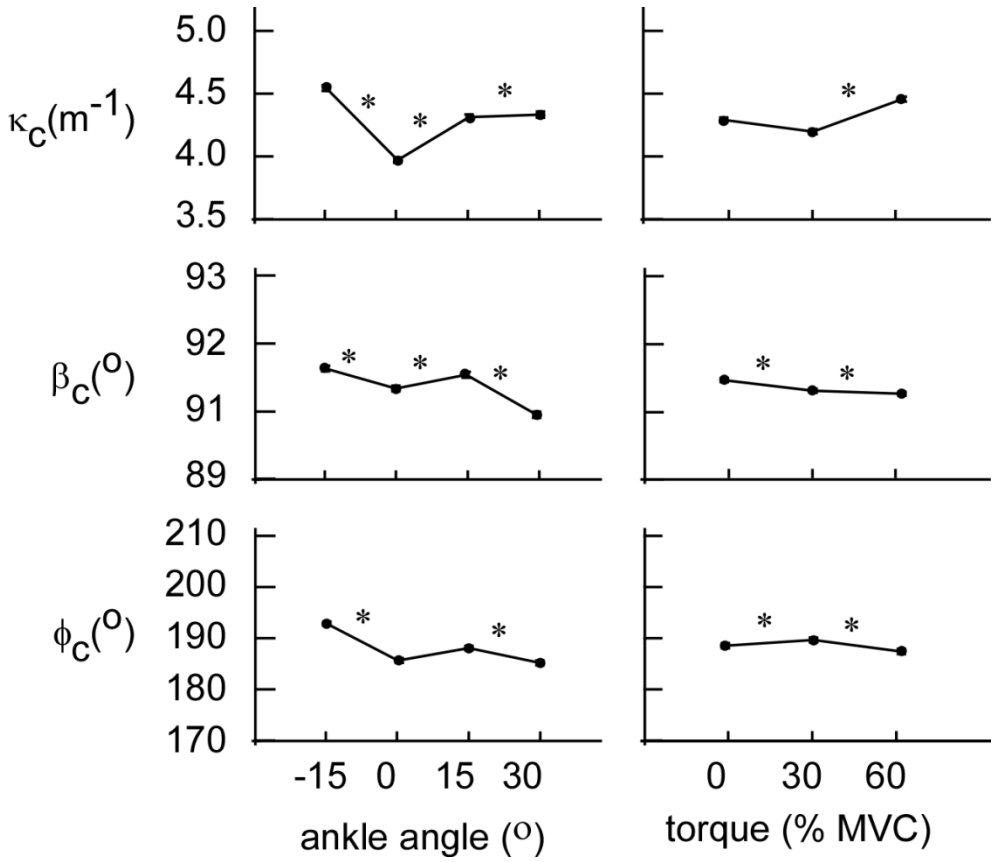

Figure 5.9 ***Effect of torque levels and ankle angle on muscle fascicle curvature in soleus. The dots represent the mean values of fascicle curvature magnitude (κ_c) and direction of curvature in terms of polar angle (β_c) and azimuthal angle (φ_c) across the whole muscle. Error bars representing standard error of mean are drawn but are not visible in the figures where the error bars are smaller than the dot size. Numbers of data points for each value were approximately 40,000. The "*" indicates statistically significant change between adjacent ankle angles and relative torque levels).***

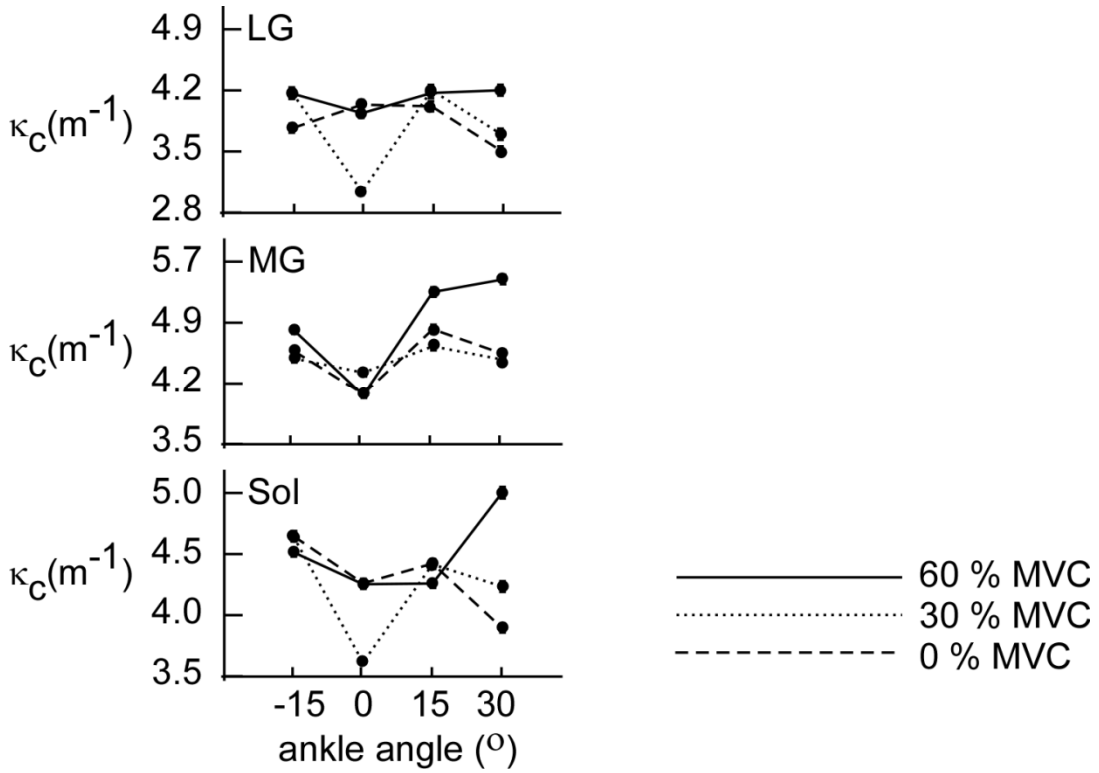

Figure 5.10 ***Effect of relative torque levels on fascicle curvature and ankle angle relation. The dots represent the mean values of fascicle curvature magnitude (κ_c). Error bars representing standard error of mean are drawn but are not visible in the figures where the error bars are smaller than the dot size. Numbers of data points for each value were approximately 10,000.***

5.3.3. Fascicle sheet curvature

The results for quantification of fascicle sheet curvature are shown in tables 5.3-5.4 and figure 5.10. Fascicle sheet curvatures (κ_{fsc}) varied between the medial and lateral region in all the three muscles. In LG κ_{fsc} increased from the lateral to the medial side and the concave side of curved sheet was facing the medial side of the muscle. In MG the curvature decreased from the lateral to the medial side and the concave side of the muscle was facing the medial side of the muscle. In soleus the κ_{fsc} increased slightly from the lateral to the medial side and the curves were facing the medial side of the muscle.

Table 5.3 ***Regionalisation of fascicle sheets curvature. The values reported are mean ± standard error of fascicle curvature magnitude (κ_{fsc}) and azimuthal angle (φ_{fsc}) of normal to across all the torque and ankle angle torques. Approximately 400 points were used to calculate the mean and standard error of mean values.***

	Width	
	Lateral	Medial
LG		
κ_{fsc},m^{-1}	2.11 ± 0.11	3.48 ± 0.23
φ_{fsc},°	86.60 ± 0.53	88.63 ± 0.97
MG		
κ_{fsc},m^{-1}	7.76 ± 0.37	3.61 ± 0.14
φ_{fsc},°	102.62 ± 1.59	105.26 ± 2.07
Sol		
κ_{fsc},m^{-1}	6.11 ± 0.51	6.26 ± 1.09
φ_{fsc},°	84.50 ± 1.73	93.03 ± 1.06

Table 5.4 ***Effect of relative torque level and ankle torque in fascicle sheet curvature. The values reported are mean ± standard error of fascicle curvature magnitude (κ_{fsc}) and direction of curvature in terms of angle with respect to deep-superficial axis of muscle polar angle (φ_{fsc}) across all the torque and ankle angle torques. Approximately 200 points were used to calculate the mean and standard error of mean values.***

	Ankle Angle				Relative torque level		
	-15°	0°	15°	30°	0%	30%	60%
LG							
κ_{fsc}	2.47 ± 0.17	2.18 ± 0.17	2.75 ± 0.22	3.43 ± 0.33	2.70 ± 0.20	2.87 ± 0.25	2.58 ± 0.17
f_{fsc}	86.16 ± 1.10	89.01± 1.16	97.65 ± 0.98	87.15 ± 0.93	88.86 ± 0.95	87.35 ± 0.89	86.35 ± 0.87
M							
κ_{fsc}	5.23 ± 0.37	5.06 ± 0.32	6.08 ± 0.44	6.54 ± 0.50	5.49 ± 0.32	5.88 ± 0.38	5.81 ± 0.39
f_{fsc}	110.77 ± 2.34	102.32 ± 2.78	101.87 ± 2.69	100.69 ± 2.56	105.46 ± 2.32	98.53 ± 2.34	107.66 ± 2.09
Sol							
κ_{fsc}	4.13 ± 0.30	5.92 ± 0.46	7.46 ± 1.31	7.43 ± 2.30	6.68 ± 0.89	4.78 ± 0.30	7.15 ± 1.85
f_{fsc}	91.28 ± 1.82	89.02 ± 1.96	88.80 ± 2.02	88.08 ± 1.91	89.41 ± 1.59	87.15 ± 1.87	92.00 ± 1.51

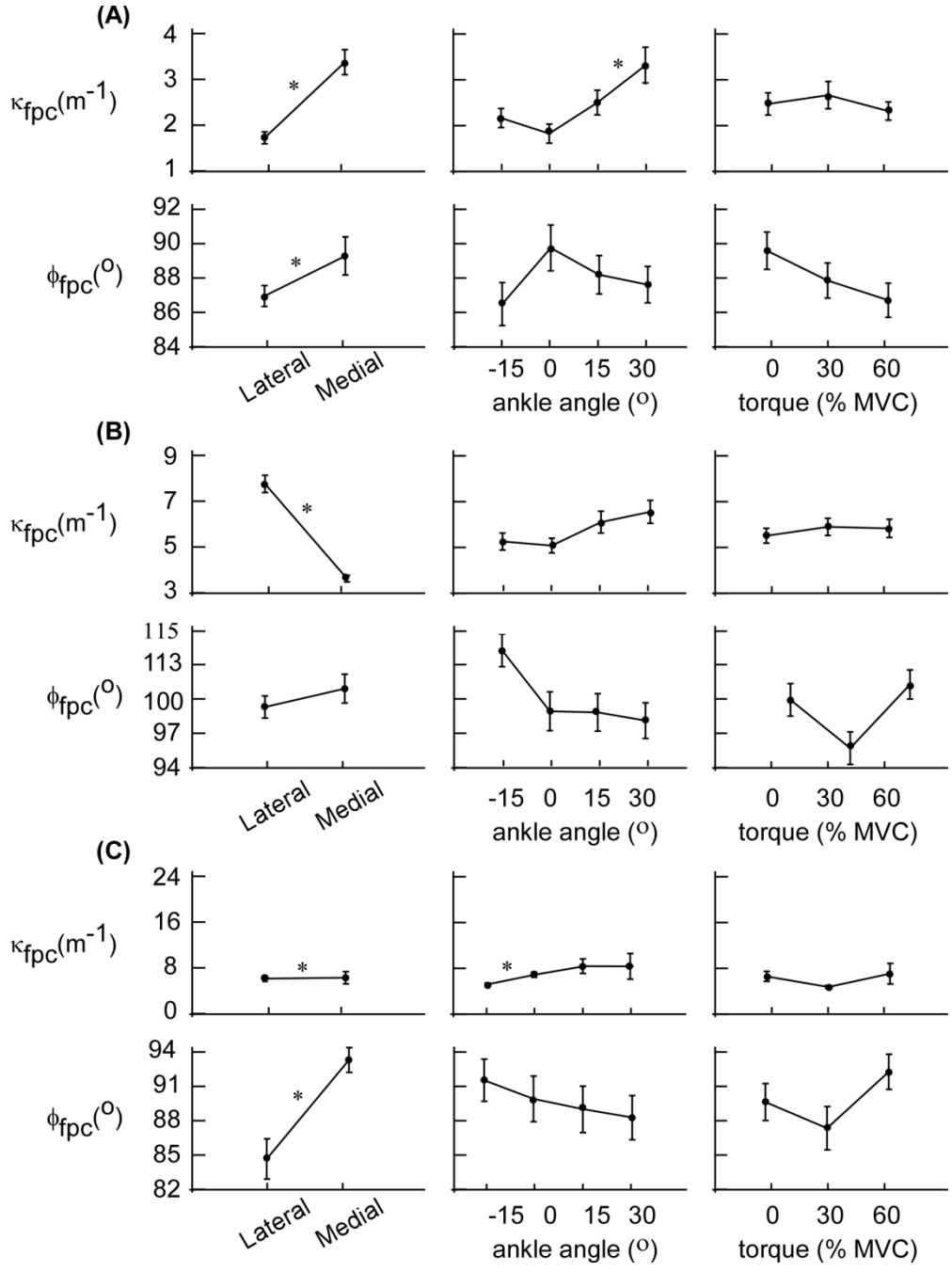
(A)
$\kappa_{fpc}(m^{-1})$
4
3
2
1
*
*
$\phi_{fpc}(^{o})$
92
90
88
86
84
*
Lateral
Medial
-15 0 15 30
ankle angle (^{o})
0 30 60
torque (% MVC)
(B)
$\kappa_{fpc}(m^{-1})$
9
7
5
3
*
$\phi_{fpc}(^{o})$
115
113
100
97
94
Lateral
Medial
-15 0 15 30
ankle angle (^{o})
0 30 60
torque (% MVC)
(C)
$\kappa_{fpc}(m^{-1})$
24
16
8
0
*
*
$\phi_{fpc}(^{o})$
94
91
88
85
82
*
Lateral
Medial
-15 0 15 30
ankle angle (^{o})
0 30 60
torque (% MVC)

Figure 5.11 ***Fascicle sheet curvature in LG (A), MG (B) and soleus (C). The dots represent the mean values of fascicle sheet curvature magnitude (κ_{fsc}) and direction as the angle relative to deep-superficial axis of muscle (φ_{fsc}). Error bars represent the standard error of mean. Approximately 400 points were used for region effect and 200 for ankle angle and torque level. The "*" indicates a statistically significant change.***

5.4. Discussion

This is the first time that the fascicle sheet curvatures and the 3D fascicle curvatures have been quantified in a muscle at different relative torque levels and muscle lengths. Previous studies have quantified fascicle curvatures in 2D with the values ranging from 0.5 m^{-1} at rest up to 20 m^{-1} during MVC. The curvature values reported in this study lie in the range of previously reported values (Muramatsu et al., 2002; Namburete et al., 2011). The curvature values reported in this study are lower than those reported by Namburete (2011) because that study involved a relative torque level up to 100% MVC and externally applied compressive bandages. Further, the greatest curvatures were measured from the superficial and deep layers of the muscle. The methods used to calculate the curvature values involved 18 mm segments compared to 7mm segments in the study by Namburete (2011). The 18 mm segment length used here was based on the voxel size (5×5×5 mm) in the 3D voxel grid and the segment was extended to points with each point in a different voxel to fit a second order polynomial for curvature calculations. The voxel size was further based on the wavelet grid size (39×39 pixels equivalent to 6×6 mm) as described in section 2.23. Namburete (2011) could calculate the curvature values closer to the aponeurosis compared to this study which may have contributed to the greater values of the curvatures. The resting curvature values from MG found in this study (mean 4.56±0.02 m^{-1}) are greater those reported by Muramatsu and co-workers (2002) (mean 0.53 m^{-1}). 2D curvature values measure the curvature only in 2D, ignoring the curvature in third dimension. Fascicles lie in the curved sheets (figure 5.12) which introduce curvature in the 3rd dimension leading to underestimation of curvature values in the 2D studies.

5.4.1. Fascicle curvature

Fascicle curvatures were regionalized in each of the three muscles and changed with change in muscle length and relative torque levels supporting hypotheses 1 and 2. In LG and soleus the curvatures were lowest in the central region of the muscle with greater curvatures values at the peripheral ends while in MG the curvatures gradually increased from the proximal to the distal end of the muscle. Intramuscular pressure depends on the fascicle curvature and tensile forces in the muscle fascicles. A curved fascicle generates a pressure difference between the convex and concave side with the pressure being greater on the concave side and the magnitude of the pressure differential increases with the increase in the curvature (Hill 1938, van Leeuwen and Spoor, 2002). Thus, the regionalization of fascicle curvature can be used to predict the intramuscular pressure distributions. The intramuscular pressure distributions are discussed in chapter 6.

5.4.2. Fascicle sheet curvature

The fascicle sheets were curved and the curvature was not uniform across the muscle. The fascicles sheets had a greater curvature in the lateral region in the LG than the medial region while it was greater in the medial region for MG. This result is similar to the greater fascicle sheet curvatures observed in the outer layers than inner layer in vastus lateralis (Sejersted et al., 1984). There was a small increase in the fascicle curvature with the increase in relative torque level but this was not observed in the fascicle sheet. The fascicle curvature had a greater component along the depth (x-axis) of the muscle than the width (y-axis) of the muscle (a value of 180° would represent the curvature entirely along the depth of the muscle) (table 5.2 and 5.3). The fascicle sheet curvature is a measure along the width of the muscle and the changes in the fascicle sheets curvature would be smaller than that in the fascicles.

5.4.3. Comparison with the 2D study on curvatures

Some superficial differences exist between the results in this study and that by Namburete (2011). Namburete reported S-shaped fascicles in a muscle with a positive

curvature at the superficial regions, negative curvature in the deep region and relatively straight fascicles in the middle region of the muscle resulting in S-shaped fascicles. Had this been the case the same would have been reflected in the different quadrants for φ_c in the deep and superficial region, but this was not the case in this thesis (figure 5.10- 5.12). This difference can be explained by considering a curved fascicle lying on a curved sheet as was found in this study. A 2D ultrasound image represents the local projections of a 3D entity in a 2D plane (section 4.2.2.4 and figure 4.5). In a 2D scan of the muscle a number of fascicles are scanned from the region lying in the plane. The image plane would contain local projections from the scanned region of the muscle. In order to visualize this problem a curved line was drawn on a curved surface (figure 5.12) and viewed it from different projection angles in order to compare with the 2D images. In this case only one fascicle was projected from different angles whereas in an actual image different regions of image will contain projections of fascicles form different regions of the muscle (figure 5.13).

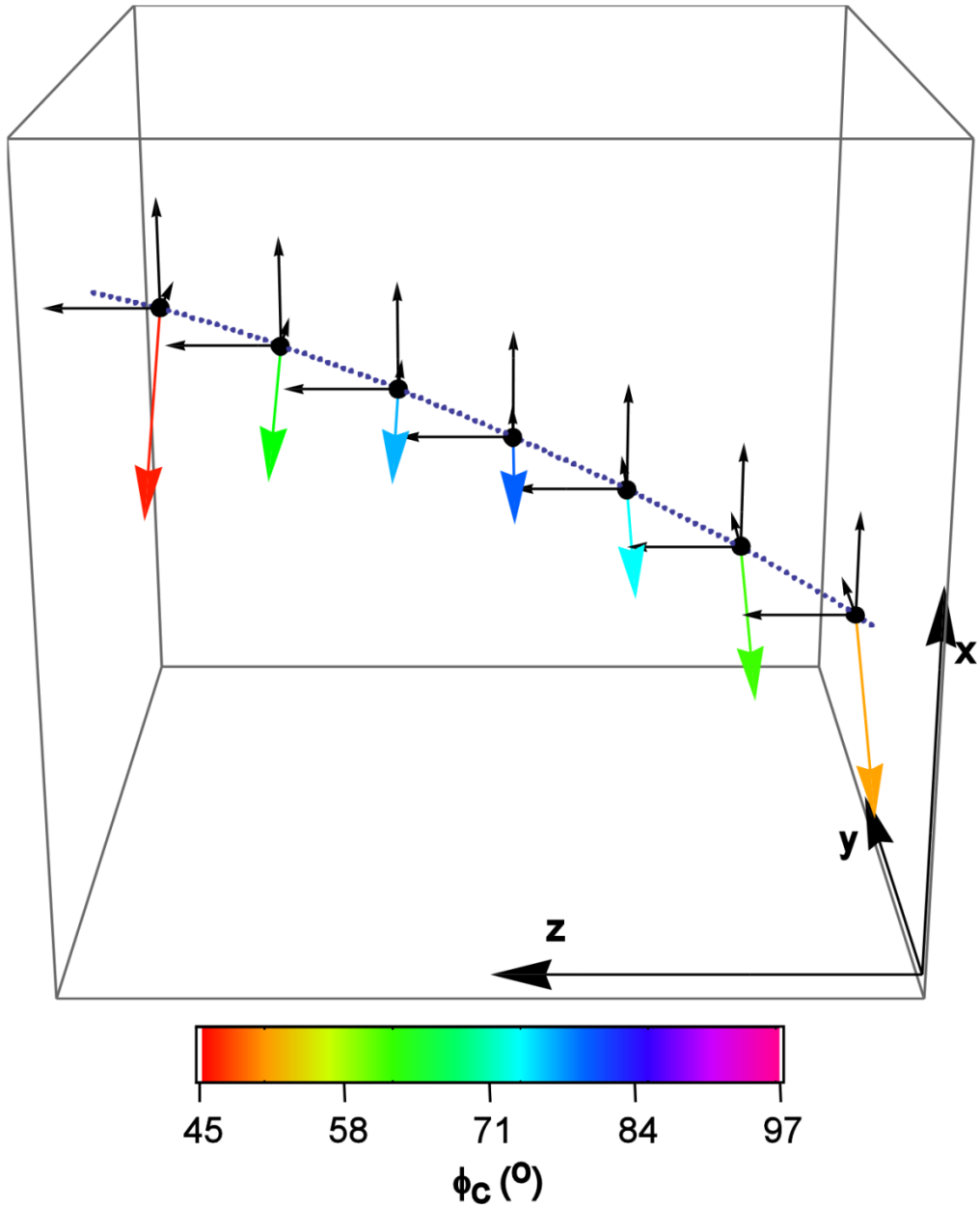

Figure 5.12 ***Schematic representation of the fascicle curvature in 3D. The path of the fascicle is shown by the blue dotted line. The curvature was represented by magnitude (represented by length of arrow) and azimuthal angle (represented by color of arrow). Polar angle (β_c) was constant in this case at 90°***

The figures were drawn for slightly greater curvature values than the values obtained in this study in order to enhance the visualization. The figures clearly demonstrated that the curved sheet changed the perceived curvature of the fascicles based

on the view points (figure 5.13). The view points were changed to replicate the effect of rotating the ultrasound probe on the leg surface as is typically done to get a good muscle image (Kawakami et al., 1998; Maganaris et al., 1998c). Different curvatures would be visualized for a straight fascicle on a curved sheet from a rotated view point compared to the front view (figure 5.13 C,D) and S-shaped fascicle projections would be visualized for a curved fascicle on a curved sheet (figure 5,13 G, H). Further, Namburete (2011) reported an increase in the S-shape of the fascicles at higher muscle forces; this may be attributed to the increasing curvature of the fascicles with relative torque level as seen in this thesis. The fascicles appear S-shaped for curved fascicles from a rotated view point but not for straight fascicles (figures 5.3 D, H). It should be considered that the curved fascicle sheets do not lie in a single plane and hence the ultrasound probe has to be aligned at different angles to obtain a good image of the fascicles: these different alignments would change the perceived values of curvature obtained in a 2D study. The S-shape appearance should not be considered as a measurement error because in 2D it would provide the information that the fascicle is curved in 3D. Further, a 2D scan cannot capture the fascicle curvature due to the curved fascicle sheets and hence, the 2D measurements errors would be greater in muscles with higher values of fascicle sheet curvatures.

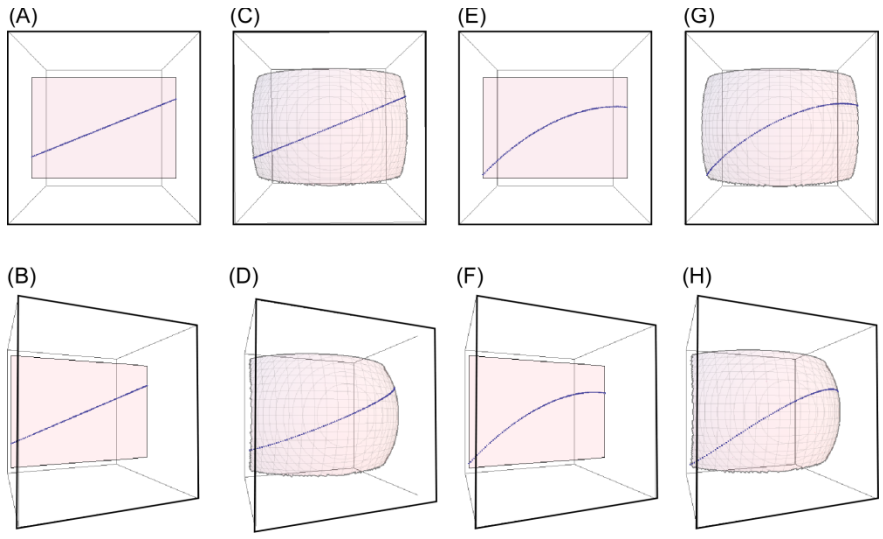

Figure 5.13 ***Visualization of a simulated straight fascicle on a planar sheet (A, B), a straight fascicle on a curved sheet (C, D), a curved fascicle on a planar sheet (E, F) and a curved fascicle on a curved sheet (G, H). The left column represents the front view and right column represents a rotated view point at an angle of 30°. The mean fascicle angle was 25° relative to the z-axis, mean curvature of 10 m^{-1} for E-H and fascicle sheet curvature was 15 m^{-1} for C, D, G and H and 0 for A, B E and F.***

5.5. Conclusions

In conclusion, this study quantified the 3D fascicle curvature and fascicle sheet curvature in the triceps surae. Changes in the curvature agree with the changes in intramuscular pressure reported in the past studies. The fascicles are arranged in non-planar sheets in the muscle. The 3D nature of the curvatures may affect the curvature values reported in 2D studies. The 3D fascicle curvature and fascicle sheets orientation are important parameters to understand the pressure development in the muscle which further affects the net function of the muscle and parameters involved in 3D muscle modeling.

6. General Discussion

This thesis describes methods to quantify muscle fascicle architecture in 3D, and provides a detailed description of the in–vivo muscle fascicle architecture in the triceps surae muscles. Previous in-vivo studies have considered the 2D architecture in contracting muscle using 2D ultrasound and a few studies have studied the 3D architecture in passive muscles using DT-MRI methods. The fascicle architectural parameters studied in the past were the pennation angle, fascicle length and curvature. The methods developed in this thesis now make it possible to quantify 3D properties of the muscle fascicles during relative torque. This study provides advances to previous architectural studies by now providing orientation and curvature values for the fascicles and the fascicle sheets.

The 3D fascicle orientations were represented by the pennation angle (β_f) and azimuthal angle (φ_f). The orientations of the fascicle sheets were represented by the normal to the fascicle planes in each of the voxels in terms of polar angle (β_{fp}) and azimuthal angle (φ_{fp}). 3D curvature values of the fascicles were represented by the magnitude of the curvature (κ_c) and direction of the normal to the curve (β_c, φ_c). Fascicle sheet curvatures were calculated in the transverse plane through the center of the muscle and were represented by the magnitude of curvature (κ_{fpc}) and direction of the normal to the curve in the sheets ($\varphi_{fpc)}$. Since the fascicle sheet curvatures were calculated in a plane their direction could be specified by only one angle. These parameters were tested for regionalization of in each of the triceps surae muscles, different relative torque states and different muscle lengths. The 3D information was also used to test the accuracy of different 2D ultrasound scanning methods for estimating the fascicle pennation angles.

The major findings of the thesis were that the fascicle orientations and curvatures were regionalized in the muscles. Fascicle sheet orientations were regionalized in the muscle and the fascicles sheets were curved which has important implications for the transmission of forces and the optimal 2D ultrasound scanning protocol. The soleus had a greater variation of the orientations of its fascicle sheets than the gastrocnemii across the muscle and at different lengths and torque levels. This greater variation would result in larger errors occurring in estimated pennation angle in a 2D study if the ultrasound probe was not correctly aligned. The fascicle curvatures are related to the intramuscular pressure which is further related to the relative torque state of the muscle. The curvature values increased with increase in torque level and the increase was the greatest at the short muscle lengths.

6.1. Methods for analyzing 3D muscle architecture

The study of in-vivo 3D architecture has been made possible with the automated image processing methods developed in this thesis. The ultrasound images were first processed in 2D to obtain the regional values of fascicle orientations in the image plane, and this information was used to obtain the regional architectural parameters in 3D. The image processing methods developed in this thesis used multiscale vessel enhancement filtering (Frangi et al., 1998) and wavelet analysis that have both been used in the past for enhancing the vessel like structures and feature extraction from medical images (Lin and Qu, 2000; Qian et al., 1999; Rahmati et al., 2010). In this study the methods were adapted to determine the muscle fascicle orientations in the ultrasound images.

A few recent ultrasound studies have developed alternative methods to determine fascicle orientations in the image plane (Jun and Rui-Ling, 2010; Zhao and Zhang, 2011; Zhou and Zheng, 2011). Jun and Rui-Ling (2010) assumed the muscle fascicles to be linear and calculated the mean pennation angle in the image region and Zhao and Zhang (2011) used the localized Radon transform to determine the linear fascicular structure in the image. These linear approximations lose information on the fascicle curvature that

have been shown to be important in this thesis. Zhou and Zheng (2011) used a Gabor transform to enhance the line-like structure in the image. Their methods focused on visually enhancing the fascicle structures and resulted in better visualized images than the results obtained by multiscale vessel enhancement used in chapter 2. However, a direct comparison between the methods on the accuracy of determining the fascicle orientations is not available as the methods developed in this thesis involve a two-step process that additionally uses wavelet analysis to obtain the orientation values.

The 2D methods presented in Chapter 2 formed the basis for the automated methods to calculate fascicle curvatures in 2D (Namburete and co-workers, 2011) and fascicle architecture in 3D (Chapter 3). The methods to calculate 2D fascicle curvatures (Namburete et al. 2011) were used in a physiological study to obtain the relation between fascicle curvature and relative torque levels, muscle length and external pressure imposed on the muscle Namburete (2011). Within this thesis, the methods developed in chapters 2 and 3 were successfully used to determine the relation of the architectural parameters with the muscle length and relative torque levels. This shows that the ultrasound can be used to study the 3D fascicular structure in passive as well as active states of the muscle. Along with the image analysis and computational methods, the experimental scanning and the imaging protocol were very important to obtain the data for the 3D structure of contracting muscle. The free-hand scanning was done in water immersion which required a custom made frame to perform the isometric relative torques and test the muscles at different relative torques states. The scanning process is very important to capture the information across the whole muscle and orient the probe through different rotation and tilt angles.

Heemskerk and co-workers (2011) calculated fascicle curvature values in a DT-MRI study of passive tibialis anterior. The curvature values increased from 2 to 5 m^{-1} with dorsiflexion from 30° to -15° in the superficial region of the muscle and the regional variations were of 1 m^{-1}. The range of these values for the tibialis anterior are similar to those reported in chapter 5 of this thesis for the triceps surae muscles. The ultrasound methods, however, can be applied to contracting muscles due to shorter scan times, and

ultrasonography is less expensive and easier to operate than DT-MRI which makes it suitable to study the changes in 3D architecture parameters.

6.2. Implications to 2D scanning

2D ultrasound is typically used to study in-vivo fascicle architecture. It has been shown in previous studies that the scanning plane orientation affects the measured pennation angles. In this thesis it was shown that the fascicles are not arranged in planes but actually lie in curved sheets. Due to the curvature of the sheets a fascicle may not be completely imaged in a 2D scan, and this can lead to errors in the estimated fascicle lengths and curvatures. These errors were smaller in the gastrocnemii as the fascicle sheet orientation did not change much with torque level and angle compared to that of the soleus. It becomes particularly important to adjust the probe orientation for different relative torque levels and muscle lengths in more architecturally complex muscles such as the soleus in order to obtain accurate measures of the pennation angles.

6.3. 3D orientations of fascicles and fascicle sheets

The 3D fascicle orientations and fascicle sheet orientations are important to understand the transmission of force through a muscle. The pennation angle gives information about the transmission of the force to the tendon, however, it has been shown in the past that the muscle-tendon junction is not the sole pathway of force transmission. Force may also be transmitted to the neighboring fascicles, other parts of the muscle, adjacent connective tissue and neighboring muscles (Huijing et al., 1998; Huijing 1999). Huijing and co-workers (1998) have shown in rat digitorum longus (a multi-head muscle) that the force is transmitted between the muscle heads. Riewald and Delp (1996) have shown that the rectus femoris muscle was capable of acting as a knee extensor after distal tendon transfer to flexor sites in human patients. In order to understand the alternate pathways of force transmission it is important to quantify the azimuthal angle (φ_f) along with the pennation angle of the fascicles. In chapter 4 it was shown that the variations in

φ_f in the three muscles were of the same magnitude as for the variations in pennation angle. Further, the orientation and curvature of fascicle sheets is needed to understand the relative arrangement of fascicles in the muscle to describe the arrangement of the fascicles with respect to each other and potentially the transmission pathways for force.

Regional variations in the fascicle orientations indicate curved fascicles in the muscle with differences in curvatures for different relative torque levels and ankle angles. Curved fascicles have greater length than their linear approximations and their curvature results in the pressure difference across the fascicles.

6.4. Fascicle curvatures and their relation to intramuscular pressure

Fascicle curvature is related to the intramuscular pressure developed in the muscle. Hill (1948) suggested that curved fascicles generate pressure on the inward side resulting in a pressure difference between the concave and the convex side of the fascicles. The pressure gradient depends on the fascicle thickness, curvature of the fascicle and the fascicle stress. It has been shown in the modeling study by van Leeuwen and Spoor (1992) that the pressure distributions in a muscle are important for mechanical stability of the muscle and the intramuscular pressure balances the pressure due to the curvature of the internal tendon and aponeurosis. The pressure difference (Δp) across a curved fascicle (van Leeuvan and Spoor, 1992) is given by

$$\Delta p = \Delta r_f \sigma_f \kappa_c$$

where, Δr_f is the fascicle thickness, σ_f is the stress in the fascicle and κ_c is the fascicle curvature. The intramuscular pressure can be estimated from the pressure gradient and the number of fascicle layers. For a uniform stress across the muscle fibers the curvature magnitude (κ_c) and orientations of normals to the curves (β_c, φ_c) can be used to predict the high pressure regions in the muscle. β_c is the angle between the normal to curve and the z-axis of the muscle and φ_c is angle of the normal to curve in the z = 0

pane and the x-axis of the muscle . The normal to curve gives the direction of the concave surface of the curve and the angles are represented on a simulated curve with varying values of β_c and φ_c.

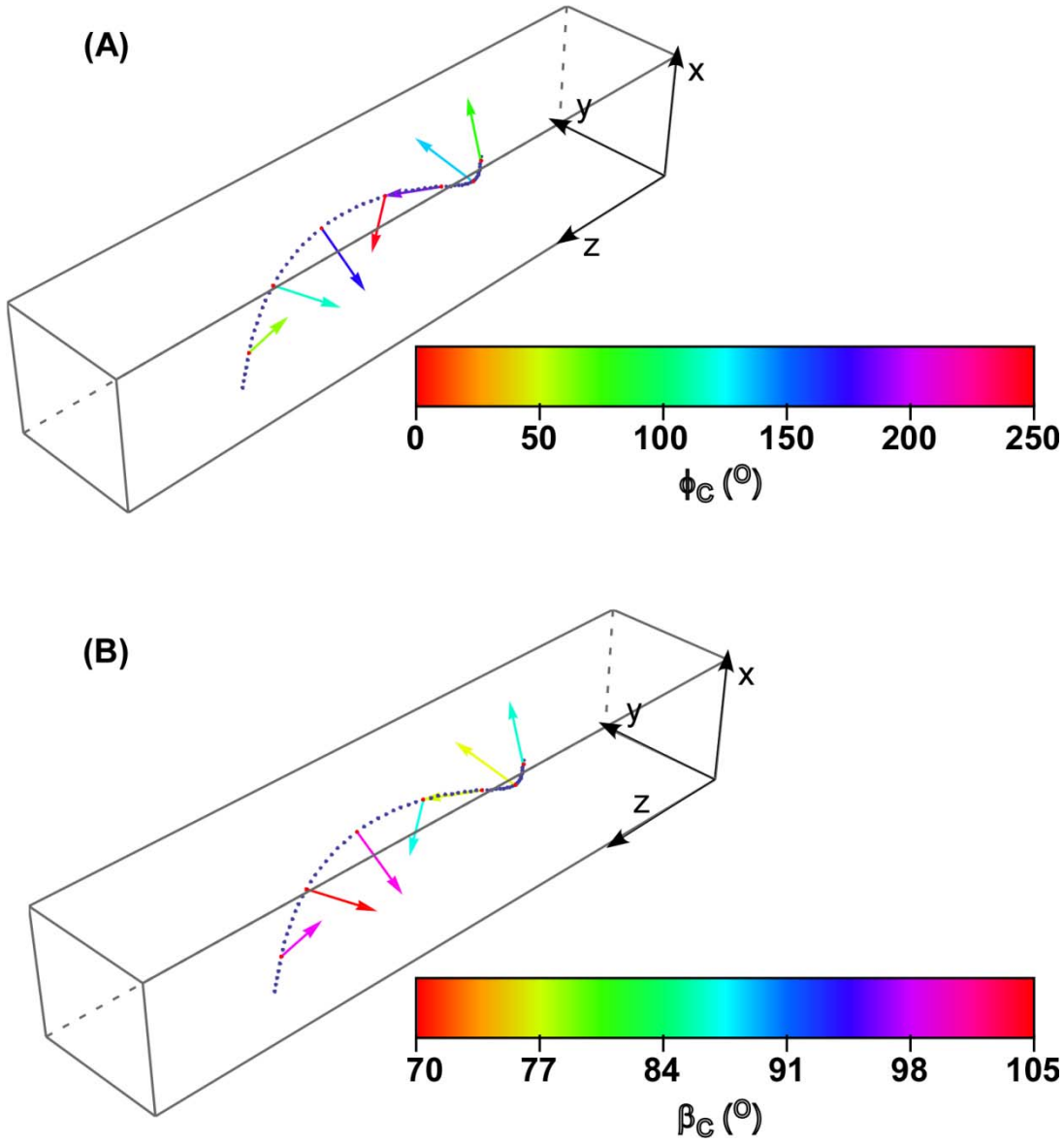

Figure 6.1. ***Representation of orientation of normal to the curve. A 3D curved line (shown as dotted blue line) was modeled with varying orientation angles for the normal to curve. The colors of the arrows represent φ_c (A) and β_c (B).***

In the lateral gastrocnemius the curvature was significantly higher in the deeper layers (4.12 m^{-1}) than the superficial layers (3.51 m^{-1}) indicating that the pressure

gradient would be greater in the deeper layers of the muscle. The normal to the fascicle curvatures shows that the concave side was facing the deeper layers of the muscles indicating a higher pressure in the deeper layers compared to the superficial layers. Along the length of the muscles the curvatures were greater in the proximal ends than the central region of the muscle. The curves were facing the deep-medial region ($\varphi_c = 163.5°$) in the proximal end and deep-lateral ($\varphi_c = 214.0°$) region in the distal end of the muscle indicating the pressure build up at the deeper layers of the muscle.

In the medial gastrocnemius the mean curvatures were greater in the superficial layers (4.77 m^{-1}) than the deeper layers (4.62 m^{-1}). The pressure gradients would be slightly higher in the superficial layers. The normals to the fascicle curvatures show that the concave side is facing the deeper layers leading to a greater pressure in the deeper layers of muscle. Along the length of the muscle the greatest curvatures were in the distal regions of the muscle leading to the greatest pressure gradients in the distal regions and further the curves were facing the deep-lateral direction throughout the muscle region ($\varphi_c >198°$) along with a small component of normal to curvature along the proximal end of the muscle ($\beta_c > 90°$) throughout the muscle region indicating a high pressure in the deep and slightly in the lateral and proximal regions of the muscle.

In soleus the mean curvatures were greater in the deeper regions (4.56 m^{-1}) than the superficial region (4.21 m^{-1}) and the curves faced the deeper regions indicating greater pressures in the deeper regions of the muscle. In soleus the curves on the medial sides were facing the deep-lateral direction ($\varphi_c = 205.6°$) and the curves on the lateral side were facing the deep-medial ($\varphi_c = 175.4°$) side of the muscle. This will lead to the high pressure in the middle of the muscle.

In all three muscles there was a greater pressure in the deeper layers of the muscle than the superficial layers which is supported by the experimental measures of greater pressures in the deeper layers of the muscle (Sejersted and co-workers, 1984).The soleus is a multipennate muscle with the fascicles inserting on a median septum as is indicated by the fascicle orientations in chapter 4 (that the fascicles sheets were the mirror image

on the two sides) and the insertion of fascicles on the median septum in anatomical dissection study by Augur and co-workers (2003). The median septum is a tendon-like structure that protrudes into the distal portion of the soleus and often reaches the anterior surface and divides the muscle into separate medial and lateral regions for a few centimeters (Oxorn et al., 1998). The higher pressure region in the middle of the muscle that can be predicted from this ultrasound study matches the prediction of a higher pressure around the internal tendon in bipennate muscles (van Leeuwen and Spoor,1992).

6.4.1. Application to compartment syndrome

Compartment syndrome is a condition involving high pressures in the muscle compartments, leading to damage in the nerve and blood vessels in the muscle. Blood vessels can rupture and this further increases the pressure in the muscle leading to a vicious cycle damaging the muscle tissue (Kostler et al., 2004). The condition is limb threatening and may be caused by impact injuries, burns in acute cases and repeated strenuous exercise in chronic cases. The treatment for the severe cases of compartment syndrome involves a cut in the fascia to relieve the pressure (fascicotomy) (Shadgan et al., 2008).

The methods used to diagnose compartment syndrome rely on the measurement of intramuscular pressure and are mostly invasive. A needle and catheter is inserted in different regions of the muscle to measure the intramuscular pressure. An exception to the invasive diagnostic methods is a recent study on non-invasive methods based on indirect measurements of intramuscular pressure in terms of the muscle fascia displacements using ultrasound images (Lynch et al., 2009).

The methods developed in this thesis to measure the fascicle curvatures can provide an alternative method to estimate the intramuscular pressure. A muscle can increase its intramuscular pressure by increasing the curvature of the fascicles (Otten 1988; Sejersted et al. 1984; van Leeuwen and Spoor 1992). A greater fascicle curvature

results in a higher pressure difference across the fascicles leading to an increase in the regional pressure. The fascicle curvatures not only predict the elevated pressures in a muscle but also estimate the regions of high pressure in a muscle. The estimation of high pressure regions can further help with deciding the site for fascicotomy.

6.5. Conclusions

The methods developed in this thesis lead to the study of the 3D architectural parameters of the muscle fascicles and the implication of the architectural parameters to the functional properties of the muscle. The thesis shows that B-mode ultrasound is a useful modality to study the detailed architectural properties of the muscle with optimal resolution and accuracy to study the functional importance of the muscle architecture. Furthermore, these methods for quantifying ultrasound images have potential to be used to study the pathological states of the muscle. In this thesis new parameters based on the 3D fascicle architecture were studied and were shown to have a significant effect on muscle function showing the importance of 3D architectural properties of the muscle. The 3D parameters were used to study the effects of typical 2D scanning protocols on the measured pennation angle (quantitatively) and curvatures (qualitatively). The quantification of parameters helped to explain the mechanical function of the muscle and has potential to explain the complex pathways of force transmission of in the muscle and the pressures generated in the muscle. Such 3D quantification of the architectural parameters in muscle will have important implications in understanding the fundamentals of its mechanical functions in the third dimension.

References

Agur AM, Ng-Thow-Hing V, Ball KA, Fiume E, McKee NH. 2003. Documentation and three-dimensional modelling of human soleus muscle architecture. Clin Anat 16(4):285-293.

Ahn AN, Monti RJ, Biewener AA. 2003. In vivo and in vitro heterogeneity of segment length changes in the semimembranosus muscle of the toad. J Physiol 549(Pt 3):877-888.

Alexander RM. 1968. Animal Mechanics. London: Sidgwick and Jackson.

Alexander RM. 1969. The orientation of msucle fibers in the myomers of fish. . Journal of the Marine Biological Association 49:263-290.

Azizi E, Brainerd EL, Roberts TJ. 2008. Variable gearing in pennate muscles. Proc Natl Acad Sci U S A 105(5):1745-1750.

Barber L, Barrett R, Lichtwark G. 2009. Validation of a freehand 3D ultrasound system for morphological measures of the medial gastrocnemius muscle. J Biomech 42(9):1313-1319.

Baskin RJ, Paolini PJ. 1967. Volume change and pressure development in muscle during contraction. Am J Physiol 213(4):1025-1030.

Benard MR, Becher JG, Harlaar J, Huijing PA, Jaspers RT. 2009. Anatomical information is needed in ultrasound imaging of muscle to avoid potentially substantial errors in measurement of muscle geometry. Muscle Nerve 39(5):652-665.

Benninghoff A, Rollhauser H. 1952. Zur inneren Mechanik des gefiederten Muskels. Pflugers Arch ges Physiol 254:527-548.

Bishop MJ, Hales P, Plank G, Gavaghan DJ, Scheider J, Grau V. 2009. Comparison of Rule-Based and DTMRI-Derived Fibre Architecture in a Whole Rat Ventricular Computational Model: Springer Berlin/ Heidelberg.

Blazevich AJ, Gill ND, Zhou S. 2006. Intra- and intermuscular variation in human quadriceps femoris architecture assessed in vivo. J Anat 209(3):289-310.

Böl M, Weikert R, Weichert C. 2011. A coupled electromechanical model for the excitation-dependent contraction of skeletal muscle. J Mech Behav Biomed Mater 4(7):1299-1310.

Budzik J.F. TVL, Demondion, X., Morel, M., Chechin, D. , Cotten, A. 2007. In vivo tractography of thigh muscles using diffusion imaging: intial results Eur Radiol 17:3079-3085.

Chow RS, Medri MK, Martin DC, Leekam RN, Agur AM, McKee NH. 2000. Sonographic studies of human soleus and gastrocnemius muscle architecture: gender variability. Eur J Appl Physiol 82(3):236-244.

Damon BM, Ding Z, Anderson AW, Freyer AS, Gore JC. 2002. Validation of diffusion tensor MRI-based muscle fiber tracking. Magn Reson Med 48(1):97-104.

Dandekar S, Li Y, Molloy J, Hossack J. 2005. A phantom with reduced complexity for spatial 3-D ultrasound calibration. Ultrasound Med Biol 31(8):1083-1093.

Darby J, Hodson-Tole EF, Costen N, Loram ID. 2011. Automated Regional Analysis of B-Mode Ultrasound Images of Skeletal Muscle Movement. J Appl Physiol.112(2):313-327

Drost MR, Maenhout M, Willems PJ, Oomens CW, Baaijens FP, Hesselink MK. 2003. Spatial and temporal heterogeneity of superficial muscle strain during in situ fixed-end contractions. J Biomech 36(7):1055-1063.

English AW. 1984. An electromyographic analysis of compartments in cat lateral gastrocnemius muscle during unrestrained locomotion. J Neurophysiol 52(1):114-125.

English AW, Letbetter WD. 1982. A histochemical analysis of identified compartments of cat lateral gastrocnemius muscle. Anat Rec 204(2):123-130.

Farr RF, Allisy-Roberts PJ. 1998. Physics for medical imaging.

Flitney FW, Hirst DG. 1978. Filament sliding and energy absorbed by the cross-bridge in active muscle subjected to cycical length changes. J Physiol 276:467-479.

Frangi AF, Niessen WJ, Vincken KL, Viergever MA. 1998. Multiscale vessel enhancement filtering. MICCAI 1496:130-137.

Friederich JA, Brand RA. 1990. Muscle fiber architecture in the human lower limb. J Biomech 23(1):91-95.

Fry NR, Childs CR, Eve LC, Gough M, Robinson RO, Shortland AP. 2003. Accurate measurement of muscle belly length in the motion analysis laboratory: potential for the assessment of contracture. Gait Posture 17(2):119-124.

Fry NR, Gough M, Shortland AP. 2004. Three-dimensional realisation of muscle morphology and architecture using ultrasound. Gait Posture 20(2):177-182.

Fukunaga T, Ichinose Y, Ito M, Kawakami Y, Fukashiro S. 1997a. Determination of fascicle length and pennation in a contracting human muscle in vivo. J Appl Physiol 82(1):354-358.

Fukunaga T, Kawakami Y, Kuno S, Funato K, Fukashiro S. 1997b. Muscle architecture and function in humans. J Biomech 30(5):457-463.

Gemballa S, Vogel F. 2002. Spatial arrangement of white muscle fibers and myoseptal tendons in fishes. Comp Biochem Physiol A Mol Integr Physiol 133(4):1013-1037.

Gordon AM, Huxley AF, Julian FJ. 1966. The variation in isometric tension with sarcomere length in vertebrate muscle fibres. J Physiol 184(1):170-192.

Hashemi RH, Bradley JWG. 1997. MRI: The Basics.

Haughton S. 1873. Principles of animal mechanics.

Heemskerk AM, Ding Z, Sinha T, Wilson KJ, Damon BM. 2011. In vivo muscle fiber curvature measurements using DT-MRI. The international society for magnetic resonance imaging in medicine. Montreal,Canada.

Heemskerk AM, Sinha TK, Wilson KJ, Ding Z, Damon BM. 2009. Quantitative assessment of DTI-based muscle fiber tracking and optimal tracking parameters. Magn Reson Med 61(2):467-472.

Herbert RD, Gandevia SC. 1995. Changes in pennation with joint angle and muscle torque: in vivo measurements in human brachialis muscle. J Physiol 484 (Pt 2):523-532.

Herring SW, Grimm AF, Grimm BR. 1979. Functional heterogeneity in a multipinnate muscle. Am J Anat 154(4):563-576.

Hiblar T, Bolson EL, Hubka M, Sheehan FH, Kushmerick MJ. 2003. Three dimensional ultrasound analysis of fascicle orientation in human tibialis anterior muscle enables analysis of macroscopic torque at the cellular level. Adv Exp Med Biol 538:635-644; discussion 645.

Higham TE, Biewener AA, Wakeling JM. 2008. Functional diversification within and between muscle synergists during locomotion. Biol Lett 4(1):41-44.

Hill AV. 1938. The heat of shortening and the dynamic constants of muscle. Proc R Soc London B Biol Sci 126:136-195.

Hodges PW, Pengel LH, Herbert RD, Gandevia SC. 2003. Measurement of muscle contraction with ultrasound imaging. Muscle Nerve 27(6):682-692.

Hoffer JA, Caputi AA, Pose IE, Griffiths RI. 1989. Roles of muscle activity and load on the relationship between muscle spindle length and whole muscle length in the freely walking cat. Prog Brain Res 80:75-85; discussion 57-60.

Hoffer JA, Loeb GE, Sugano N, Marks WB, O'Donovan MJ, Pratt CA. 1987. Cat hindlimb motoneurons during locomotion. III. Functional segregation in sartorius. J Neurophysiol 57(2):554-562.

Huijing PA. 1985. Architecture of the human gastrocnemius muscle and some functional consequences. Acta Anat (Basel) 123(2):101-107.

Huijing PA. 2003. Muscular force transmission necessitates a multilevel integrative approach to the analysis of function of skeletal muscle. Exerc Sport Sci Rev 31(4):167-175.

Huijing PA, Baan GC, Rebel GT. 1998. Non-myotendinous force transmission in rat extensor digitorum longus muscle. J Exp Biol 201(Pt 5):683-691.

Ichinose Y, Kawakami Y, Ito M, Kanehisa H, Fukunaga T. 2000. In vivo estimation of contraction velocity of human vastus lateralis muscle during "isokinetic" action. J Appl Physiol 88(3):851-856.

Ishikawa M, Finni T, Komi PV. 2003. Behaviour of vastus lateralis muscle-tendon during high intensity SSC exercises in vivo. Acta Physiol Scand 178(3):205-213.

Ito M, Kawakami Y, Ichinose Y, Fukashiro S, Fukunaga T. 1998. Nonisometric behavior of fascicles during isometric contractions of a human muscle. J Appl Physiol 85(4):1230-1235.

Jun S, Rui-Ling W. 2010. Estimation of msucle pennation angle in ultrsaound images using the beamlet transform. J Shanghai Univ (Engl Ed) 14(1):34-38.

Kan JH, Hernanz-Schulman M, Damon BM, Yu C, Connolly SA. 2008. MRI features of three paediatric intra-articular synovial lesions: a comparative study. Clin Radiol 63(7):805-812.

Kashin SM, Smolyaniow VV. 1969. Concerning the geometry of fish trunk muscles. J Icthyol (English translation of *Vopr Ikhtiol*) 9.

Kawakami Y, Abe T, Fukunaga T. 1993. Muscle-fiber pennation angles are greater in hypertrophied than in normal muscles. J Appl Physiol 74(6):2740-2744.

Kawakami Y, Amemiya K, Kanehisa H, Ikegawa S, Fukunaga T. 2000. Fatigue responses of human triceps surae muscles during repetitive maximal isometric contractions. J Appl Physiol 88(6):1969-1975.

Kawakami Y, Ichinose Y, Fukunaga T. 1998. Architectural and functional features of human triceps surae muscles during contraction. J Appl Physiol 85(2):398-404.

Kawakami Y, Muraoka T, Ito S, Kanehisa H, Fukunaga T. 2002. In vivo muscle fibre behaviour during counter-movement exercise in humans reveals a significant role for tendon elasticity. J Physiol 540(Pt 2):635-646.

Khouzani KJ, Zadeh HA. 2005. Radon transform orientation estimation for rotation invariant texture analysis. IEEE 27:1004-1008.

Kostler W, Strohm PC, Sudkamp NP. 2004. Acute compartment syndrome of the limb. Injury 35(12):1221-1227.

Kuno S, Fukunaga T. 1995. Measurement of muscle fibre displacement during contraction by real-time ultrasonography in humans. Eur J Appl Physiol Occup Physiol 70(1):45-48.

Kurihara T, Oda T, Chino K, Kanehisa H, Fukunaga T, Kawakami Y. 2005. Use of Three-Dimenionsal Ultrasonography for the Analysis of the Fasicle Length of Human Gastrocnemius Muscle During Contractions. International Journal of Sport and Health Science 3:226-234.

Kurokawa S, Fukunaga T, Fukashiro S. 2001. Behavior of fascicles and tendinous structures of human gastrocnemius during vertical jumping. J Appl Physiol 90(4):1349-1358.

Lansdown DA, Ding Z, Wadington M, Hornberger JL, Damon BM. 2007. Quantitative diffusion tensor MRI-based fiber tracking of human skeletal muscle. J Appl Physiol 103(2):673-681.

Levin DI, Gilles B, Madler B, Pai DK. 2011. Extracting skeletal muscle fiber fields from noisy diffusion tensor data. Med Image Anal 15(3):340-353.

Lichtwark GA, Barclay CJ. 2010. The influence of tendon compliance on muscle power output and efficiency during cyclic contractions. J Exp Biol 213(5):707-714.

Lichtwark GA, Bougoulias K, Wilson AM. 2007. Muscle fascicle and series elastic element length changes along the length of the human gastrocnemius during walking and running. J Biomech 40(1):157-164.

Lichtwark GA, Wilson AM. 2005. Effects of series elasticity and activation conditions on muscle power output and efficiency. J Exp Biol 208(Pt 15):2845-2853.

Lieber RL, Fridén J. 2000. Functional and clinical significance of skeletal muscle architecture. Muscle Nerve 23(11):1647-1666.

Lin J, Qu LS. 2000. Feature extraction based on Morlet wavelet and its application for mechanical fault diagnosis. Journal of Sound and Vibration 234(1):135-148.

Loram ID, Maganaris CN, Lakie M. 2006. Use of ultrasound to make noninvasive in vivo measurement of continuous changes in human muscle contractile length. J Appl Physiol 100(4):1311-1323.

Lynch JE, Lynch JK, Cole SL, Carter JA, Hargens AR. 2009. Noninvasive monitoring of elevated intramuscular pressure in a model compartment syndrome via quantitative fascial motion. J Orthop Res 27(4):489-494.

Maganaris CN, Baltzopoulos V, Sargeant AJ. 1998a. Changes in Achilles tendon moment arm from rest to maximum isometric plantarflexion: in vivo observations in man. J Physiol 510 (Pt 3):977-985.

Maganaris CN, Baltzopoulos V, Sargeant AJ. 1998b. Differences in human antagonistic ankle dorsiflexor coactivation between legs; can they explain the moment deficit in the weaker plantarflexor leg? Exp Physiol 83(6):843-855.

Maganaris CN, Baltzopoulos V, Sargeant AJ. 1998c. In vivo measurements of the triceps surae complex architecture in man: implications for muscle function. J Physiol 512 (Pt 2):603-614.

Maganaris CN, Baltzopoulos V, Sargeant AJ. 2002. Repeated contractions alter the geometry of human skeletal muscle. J Appl Physiol 93(6):2089-2094.

Magnusson SP, Hansen P, Aagaard P, Brond J, Dyhre-Poulsen P, Bojsen-Moller J, Kjaer M. 2003. Differential strain patterns of the human gastrocnemius aponeurosis and free tendon, in vivo. Acta Physiol Scand 177(2):185-195.

Malaiya R, McNee AE, Fry NR, Eve LC, Gough M, Shortland AP. 2007. The morphology of the medial gastrocnemius in typically developing children and children with spastic hemiplegic cerebral palsy. J Electromyogr Kinesiol 17(6):657-663.

Martin DC, Medri MK, Chow RS, Oxorn V, Leekam RN, Agur AM, McKee NH. 2001. Comparing human skeletal muscle architectural parameters of cadavers with in vivo ultrasonographic measurements. J Anat 199(Pt 4):429-434.

Mori S, Zang J. 2006. Principles of Diffusion Tensor Imagind and Its Applications to Basic Neuroscience. Neuron 51:527-539.

Muramatsu T, Muraoka T, Kawakami Y, Shibayama A, Fukunaga T. 2002. In vivo determination of fascicle curvature in contracting human skeletal muscles. J Appl Physiol 92(1):129-134.

Muraoka T, Kawakami Y, Tachi M, Fukunaga T. 2001. Muscle fiber and tendon length changes in the human vastus lateralis during slow pedaling. J Appl Physiol 91(5):2035-2040.

Namburete AI. 2011. Fascile curvature. Burnaby: Simon Fraser University.

Namburete AI, Rana M, Wakeling JM. 2011. Computational methods for quantifying in vivo muscle fascicle curvature from ultrasound images. J Biomech 44(14):2538-2543.

Narici MV, Binzoni T, Hiltbrand E, Fasel J, Terrier F, Cerretelli P. 1996a. In vivo human gastrocnemius architecture with changing joint angle at rest and during graded isometric contraction. J Physiol 496 (Pt 1):287-297.

Narici MV, Hoppeler H, Kayser B, Landoni L, Claassen H, Gavardi C, Conti M, Cerretelli P. 1996b. Human quadriceps cross-sectional area, torque and neural activation during 6 months strength training. Acta Physiol Scand 157(2):175-186.

Otten E. 1988. Concepts and models of functional architecture in skeletal muscle. Exerc Sport Sci Rev 16:89-137.

Oxorn VM, Agur AM, McKee NH. 1998. Resolving discrepancies in image research: the importance of direct observation in the illustration of the human soleus muscle. J Biocommun 25(1):16-26.

Pappas GP, Asakawa DS, Delp SL, Zajac FE, Drace JE. 2002. Nonuniform shortening in the biceps brachii during elbow flexion. J Appl Physiol 92(6):2381-2389.

Patel TJ, Lieber RL. 1997. Force transmission in skeletal muscle: from actomyosin to external tendons. Exerc Sport Sci Rev 25:321-363.

Powell PL, Roy RR, Kanim P, Bello MA, Edgerton VR. 1984. Predictability of skeletal muscle tension from architectural determinations in guinea pig hindlimbs. J Appl Physiol 57(6):1715-1721.

Prager RW, Rohling RN, Gee AH, Berman L. 1998. Rapid calibration for 3-D freehand ultrasound. Ultrasound Med Biol 24(6):855-869.

Qian W, Li LH, Clarke LP. 1999. Image feature extraction for mass detection in digital mammography: Influence of wavelet analysis. Medical Physics 26(3):402-408.

Rahmati P, Hamarneh G, Nussbaum D, Adler A. 2010. A New Preprocessing Filter for Digital Mammograms. Image and Signal Processing, Proceedings 6134:585-592.

Rana, M, Hamarneh G, Wakeling J.M., 2008. Automated tracking of muscle fascicle orientation in B-mode ultrasound images. J. Biomech. 42(13):2068-2073.

Rana, M, Wakeling J.M., 2011. In-vivo determination of 3D muscle architecture of human muscle using free hand ultrasound J. Biomech. 44(11):2129-2135.

Riewald SA, Delp SL. 1996. Rectus femoris knee moment and transfer. Dev Med child Neurol 39:99-105.

Ritruechai P, Weller R, Wakeling JM. 2008. Regional variations in muscle anatomy in the equine longissimus dorsi. Equine Veterinary Journal 40:246-251.

Roberts TJ, Marsh RL, Weyand PG, Taylor CR. 1997. Muscular force in running turkeys: the economy of minimizing work. Science 275(5303):1113-1115.

Rome LC, Funke RP, Alexander RM, Lutz G, Aldridge H, Scott F, Freadman M. 1988. Why animals have different muscle fibre types. Nature 335(6193):824-827.

Sejersted OM, Hargens AR, Kardel KR, Blom P, Jensen O, Hermansen L. 1984. Intramuscular fluid pressure during isometric contraction of human skeletal muscle. J Appl Physiol 56(2):287-295.

Shadgan B, Menon M, O'Brien PJ, Reid WD. 2008. Diagnostic techniques in acute compartment syndrome of the leg. J Orthop Trauma 22(8):581-587.

Sinha S, Sinha U, Edgerton VR. 2006. In vivo diffusion tensor imaging of the human calf muscle. J Magn Reson Imaging 24(1):182-190.

Soman A, Hedrick TL, Biewener AA. 2005. Regional patterns of pectoralis fascicle strain in the pigeon Columba livia during level flight. J Exp Biol 208(Pt 4):771-786.

Stark H, Schilling N. 2003. A novel method of studying fascicle architecture in relaxed and contracted muscles. J Biomech 43(15):2897-2903.

Stenosis NS, N.). 1667. Elementorum Myolgia Speciment, seu Musculi Descriptio Geometrica. Florence:Stellae 2(61-111).

van Leeuwen JL, Spoor CW. 1992. Modelling mechanically stable muscle architectures. Philos Trans R Soc Lond B Biol Sci 336(1277):275-292.

van Leeuwen JL, Spoor CW. 1996. A two dimensional model for the prediction of muscle shape and intramuscular pressure. Eur J Morphol 34(1):25-30.

Wakeling JM. 2009. The recruitment of different compartments within a muscle depends on the mechanics of the movement. Biol Lett 5(1):30-34.

Wakeling JM, Blake OM, Wong I, Rana M, Lee SS. 2011. Movement mechanics as a determinate of muscle structure, recruitment and coordination. Philos Trans R Soc Lond B Biol Sci 366(1570):1554-1564.

Wakeling JM, Horn T. 2009. Neuromechanics of muscle synergies during cycling. J Neurophysiol 101(2):843-854.

Wakeling JM, Liphardt AM. 2006. Task-specific recruitment of motor units for vibration damping. J Biomech 39(7):1342-1346.

Wakeling JM, Uehli K, Rozitis AI. 2006. Muscle fibre recruitment can respond to the mechanics of the muscle contraction. J R Soc Interface 3(9):533-544.

Wang HK, Wu YK, Lin KH, Shiang TY. 2009. Noninvasive analysis of fascicle curvature and mechanical hardness in calf muscle during contraction and relaxation. Man Ther 14(3):264-269.

Wang LC, Kernell D. 2000. Proximo-distal organization and fibre type regionalization in rat hindlimb muscles. J Muscle Res Cell Motil 21(6):587-598.

Wickiewicz TL, Roy RR, Powell PL, Edgerton VR. 1983. Muscle architecture of the human lower limb. Clin Orthop Relat Res(179):275-283.

Zhao H, Zhang LQ. 2011. Automatic tracking of muscle fascicles in ultrasound images using localized Radon transform. IEEE Trans Biomed Eng 58(7):2094-2101.

Zhou Y, Zheng YP. 2011. Longitudinal enhancement of the hyperechoic regions in ultrasonography of muscles using a Gabor filter bank approach: a preparation for semi-automatic muscle fiber orientation estimation. Ultrasound Med Biol 37(4):665-673.